KU LEUVEN

FACULTEIT INGENIEURSWETENSCHAPPEN

Intelligent control of green roofs as buffers in urban settings: a case study for Antwerp

Ewout Vereecke

Thesis voorgedragen tot het behalen van de graad van Master of Science in de ingenieurswetenschappen: bouwkunde, optie Civiele techniek

Promotor:
Prof. dr. ir. Patrick Willems

Assessor:
Em. prof. dr. ir. Jean Berlamont,
Prof. dr. ir. Jaak Monbaliu

Begeleider:
Dr. ir. Vincent Wolfs

Academiejaar 2018 – 2019

Preface

Flamenco, Flemish, Flamand, Flämisch... All these words can be traced back to the Germanic *flauma*. The latter signifies 'flooded territory'. This makes sense, since the Flemish coastal area was overrun by the North Sea twice a day from the 3rd until the 8th century. Is there a better place to study the effects of flooding than the region named after this phenomenon? I think not.
A friend from South-Africa once told me in 2017:

> I can't imagine a sound more beautiful than falling rain. It is the sound of rejuvenation, the song of life.

A year later, Cape Town was weeks away from a *day zero*, when it would run out of fresh water.
Flood, rain and drought. I chose to contribute to this research because of these three simple words which have an inconceivable impact on life on this planet.
When I say *contribute*, I say this in a very modest way. This master's thesis is not the work of one person, on the contrary. I am indebted to mention everybody who assisted me during this research, both directly and indirectly. Firstly, I would like to thank my promoter prof.dr.ir Patrick Willems. The interest in the water sector finds its roots in his classes. Like a river, the year passed at a merciless pace and contained obstacles below the calm surface. My supervisor, dr.ir. Vincent Wolfs was always available to help clear these obstacles in my path, and for this I am very grateful. I should also mention Daan and Xiaohan here, two researchers at the Hydraulics group who helped me out with more specific parts of the research. The test site, built with the help of the company Vegetal i.D., forms the foundation of this research project, and I would like to thank them for this. The Royal Meteorological Institute (RMI) in Belgium should also be mentioned here. The data I received was of paramount importance in this research. My family forms a well of energy and inspiration that will never run dry. For instance, my grandfather has been a cultivator of my love for nature, which drove me to this thesis subject. Most people also mention a sibling, a best friend, a cohabitant or a fellow student in the preface of their thesis. In my case, I can kill all these birds with one stone, since my twin brother Emiel plays all these roles simultaneously. During my entire university career, I could always fall back on my friends in Kortrijk and Leuven for some welcome distraction every now and then. You are the best. Last but not least, I would like to extend my gratitude to my girlfriend Annelies, who always had my back during this endeavour.

We are not alone in our need for water, but we have the ability to ensure the fresh waters of the world do flow, and we alone can determine how they are shared - *Sir David Attenborough (Our Planet)*

Ewout Vereecke

Contents

Abstract

In times of continuous urbanisation and climate change, the availability of water is expected to become a major concern for governments. The region of Flanders in Belgium can also be classified as dry based on the water availability per capita. Yet, although the expected trend is one of increasing drought in Flanders, the rainfall events are expected to become more intense. Sewer networks are designed to evacuate water as fast as possible, but intense rainfall can push the system to its limits and cause urban flooding. But even in the absence of floods, the situation should raise concerns. The urbanised environment leaves no time for infiltration in the soil. Instead, most of the valuable rainfall is discharged into rivers and lost.
To defend cities of the future, blue-green roofs are proposed as a solution. Like conventional green roofs, they intercept part of the rainfall and release it back to the atmosphere. The other part which flows through is slowed down, lowering the peak runoff in the sewer pipes. A blue-green roof adds an extra buffer layer under the soil, sharply increasing the amount of rainfall that can be captured. At the same time, the plants can access this water via capillary effects.
This research starts with the calibration and validation of a new (blue)-green roof model based on measurements in France and Belgium. Next, simulations of 100 years are conducted for Antwerp. A blue-green roof with a static buffer proves to be more beneficial for the health of the plants, as the soil only dries up for 8.1 days in an average year. On the other hand, a blue-green roof with a continuous outflow is most suited for flood reductions because the retention capacity stays higher.
To find a compromise between a discharging buffer which minimizes flood and a static buffer which minimizes vegetation stress, the effect of intelligent control is tested. The system generates different scenarios for the buffers and calculates the impact on an urban scale. The scenario leading to the smallest flood is then selected. If multiple scenarios are suited, the buffer chooses the most beneficial action for the plants. Lastly, this strategy is tested out with uncertain rainfall predictions. The method considers multiple possible rainfall fields, and calculates the flood risk rather than the actual flood. Simulations of the most recent extreme rainfall event in Antwerp show that intelligent control is a worthwhile strategy to effectively reduce flood volumes. Turning all green roofs in the city intelligent keeps another 45-50% of the already removed volume from the streets for this rainfall event. This result is found consistently for all considered degrees of green roof installation in Antwerp. Intelligent roofs could have reduced the most recent flood in Antwerp by 37%, by only converting all flat roofs in the centre, a mere 9.3% of the inner city surface.

Samenvatting

In tijden van sterke verstedelijking en klimaatverandering zullen overheden een prioriteit moeten maken van een doordacht waterbeheer. Zo ook in Vlaanderen, een regio die als 'zeer droog' geclassificeerd wordt volgens het beschikbare water. Samen met een trend van toenemende droogte geven studies aan dat de neerslag intenser zal voorkomen in de nabije toekomst. Riolen zijn ontworpen om water zo snel mogelijk te evacueren, maar intense buien kunnen tot overstromingen leiden. Bovendien laten de huidige rioleringen, in combinatie met de vele verharding in Vlaanderen niet toe dat regenwater de grondwaterpeilen aanvult. In plaats stroomt het regenwater af over asfalt en beton, en eindigt het meteen in de rivieren.
Om steden van de toekomst te wapenen tegen deze problematiek worden blauw-groene daken voorgesteld als oplossing. Zoals groendaken vangen ze de neerslag deels op, en vertragen ze de afstroming naar de riolen. Een blauw-groen dak voorziet een buffer onder de planten, wat de totale opvangcapaciteit sterk vergroot. Tegelijkertijd bevoorraadt deze buffer de planten in periodes van langdurige droogte.
Dit onderzoek beschrijft in de eerste plaats de kalibratie en validatie van een nieuw groendakmodel, gebaseerd op metingen in Frankrijk en België. Vervolgens worden simulaties over 100 jaar uitgevoerd voor de stad Antwerpen. Een statische buffer die nooit zijn inhoud loost blijkt meest aangewezen voor de planten. In een gemiddeld jaar vallen de planten slechts 8.1 dagen zonder water. Anderzijds kan een geleidelijke afvoer uit de buffer leiden tot minder schade tijdens overstromingen.
Intelligente controle van de buffers probeert de gulden middenweg te vinden tussen de betere overstromingsreductie via een continue afvoer en de betere beschikbaarheid van water via een statische buffer. Het sturingssysteem creëert een reeks mogelijke sturingen van de buffer en een rioleringsmodel berekent de impact van elke optie. Het scenario dat leidt tot de kleinste overstromingsvolumes wordt dan uitgevoerd.
Simulaties met onzekere neerslagvoorspellingen leiden nog steeds tot optimale reducties. In dat geval wordt de impact van elke sturing berekend voor verscheidene neerslagvoorspellingen. De optimale sturing garandeert een minimaal overstromingsrisico. Simulaties van de meest recente overstroming in Antwerpen tonen de meerwaarde aan. Intelligente sturing haalt 45-50% extra water weg van de straten bovenop wat conventionele groendaken reeds kunnen tegenhouden. Dit resultaat is bevestigd voor alle mogelijke gradaties van aanplanting. Intelligente blauw-groene daken hadden de recentste overstroming in Antwerpen kunnen reduceren met 37%. Dit resultaat wordt bekomen indien alle platte daken in het centrum zijn uitgerust met blauw-groene daken, wat slechts 9.3% bedraagt van de totale oppervlakte.

List of Figures

List of Tables

List of Abbreviations and Symbols

Abbreviations

UHI	Urban Heat Island effect
CIW	Coördinatiecommissie Integraal Waterbeleid
NBS	Nature Based Solutions
MSE	Mean Square Error
NSE	Nash-Sutcliffe efficiency index
ADWP	Antecedent Dry Weather Period
DUO1	Conventional green roof type (see Chapter 3)
DUO2	*Hydroventiv* roof type, a blue-green roof with a continuously emptying buffer (see Chapter 3)
DUO3	*Oasis* roof type, a blue-green roof with a static buffer (see Chapter 3)
DUO4	Reference roof
TBP	Tipping bucket pluviometer
PoT	Peak over Threshold method
CMD	Conceptual Model Developer
SC	Subcatchment
STEPS	Short-Term Ensemble Prediction System
GIS	Geographic Information System
SIC	Semi-intelligent Control
MPC	Model Predictive Control
MMPC	Multiple Model Predictive Control

Symbols

mm	Millimeter, equivalent to 1 litre on 1 square metre.
WL	Water level in buffer layer (mm)
P	Precipitation (mm/Δt)
RR	Rainfall Runoff (mm/Δt)
ET	Evapotranspiration (mm/Δt)
RSM	Relative Substrate Moisture (-)
FC	Relative Substrate Moisture at Field Capacity (-)
H_s	Substrate thickness (mm)
H_b	Buffer height (mm)
$H_{b,max}$	Overtopping height of buffer (mm)
$\Delta\theta$	Fraction of H_s that can be filled with water (mm/mm)
VOL	Temporary water in substrate layer (mm)

Chapter 1

Introduction

1.1 Problem statement

Urban water management is expected to face several challenges in the foreseeable future, both in Flanders and abroad. More and more people abandon the countryside and turn to urban settlements [1, Antrop et al., 2004]. This urban sprawl transforms an increasing amount of vegetated space into impervious surfaces [2, Qin et al., 2013]. Together with other human activities like agricultural expansion and deforestation, the residential development is an important driver of habitat loss [3, Veach et al., 2017]. Therefore urbanisation puts an enormous pressure on biodiversity in and around the cities [3, 4, Xu et al., 2018].
Moreover, impervious surfaces like asphalt and concrete typically possess a low albedo and a high heat capacity [5, Mohajerani et al., 2017]. Along with the heat from cooling installations and other anthropogenic heat production this results in what is referred to as the Urban Heat Island effect [5].
Thermal effects and high concentrations of aerosols have also been mentioned to induce more precipitation events over or downwind of large urban settlements [6, Shepherd et al., 2005][7, Han et al., 2014]. The asphalt and concrete in cities also hinder infiltration of this precipitation, leading to an increase of fast-forming rainfall runoff [2]. This effect in combination with the more frequent precipitation puts pressure on the present sewer network systems in many urban areas.

Climate change is another important factor that challenges the future liveability in cities. In Belgium, research showed that rainfall during the winter is expected to increase. Conversely, the summer will be drier according to predictions [8, Willems et al., 2010]. During these summer periods, the extreme precipitation events are said to become more frequent [9, De Niel et al., 2015] [10, Willems et al., 2011].
Since floods (pluvial, fluvial and coastal) are some of the economically most damaging events in Europe [11, Van Ootegem et al., 2018], mitigation measures become increasingly important for the future.
As mentioned above, climate models show that Belgium is likely to experience extremer rainfall events [10]. The lower periods of recurrence for these extreme rainfall

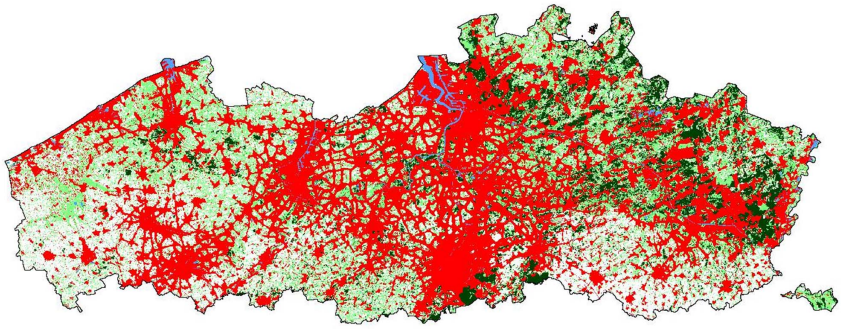

Figure 1.1: Prediction of land occupation in Flanders in 2050 under a business-as-usual scenario [14, Poelmans, 2010].

events along with continuing urbanisation, leads to the conclusion that pluvial urban flooding can occur more often in the coming years [12, Willems, 2011]. In Flanders for example, the impermeable surface is expected to reach values around 20% of the total area by 2050 [13] due to urbanisation, as shown in Figure 1.1. The following century is also said to experience more intense, more frequent, and longer-lasting heat waves [15, Gerald et al., 2004]. This increase in heat stress will be most prominently present in urban areas [16, Wouters et al., 2017].
So, although the prospect of more frequent urban flooding is often discussed, the periods of drought during the summer months could pose an even bigger challenge to growing cities. The sixth Sustainable Development Goal supports this claim and highlights the importance of water availability for all [17].
Several examples of periods of severe drought can already be found worldwide. The inhabitants of Madrid, Rome and Cape Town already faced such challenges in recent years.
However, this problem of dry spells is often overlooked by policy makers, also in the highly urbanised region of Flanders (Belgium) [18, De Waegemaeker, 2016]. In developing countries, the financial means are also missing sometimes [19, Ziervogel, 2010]. For the case of Cape Town, the potential economic loss of such water crises has already been described and it is found to be considerable [20, Viljoen, 2018]. Water availability and security even becomes the cause of conflict [21, Khalid, 2014]. In short, sustainable urban planning and good urban water management (e.g. rain-water collection) are needed to address this issue [22, Cameron, 2017].

Amidst all these challenges, several scientific publications have proven that green roofs are a viable solution that tackles several of the mentioned problems. The innovative installations are nowadays used to improve liveability in large cities, especially in temperate climates [23, Dvorak et al., 2010]. Apart from PV-panel installations, roof surfaces remain largely unused, while they can constitute up to 50% of the total impervious surface in urban settlements [24, Dunnet et al., 2008].
When it comes to temperature control, a green roof can serve a double purpose [25, Konasova, 2016]. Firstly, it serves as insulation for interior spaces during winter and

summer periods. Secondly, the evapotranspiration from the plants and the increased albedo succeed in cooling the direct exterior environment [26, Toparlar et al., 2018], both on a building scale and an urban scale [27, Susca et al., 2011]. Vegetated roofs are thus one of several effective strategies to lower the UHI effect [5].
Moreover, green roofs have been mentioned to tackle the problem of pollution [28, Rowe et al., 2011].
Among several other advantages (see Chapter 2) the hydrological performance of a green roof is the most important factor for the subject of this thesis. Plants and substrate succeed in retaining part of the incoming water [29, Stovin, 2015]. This volume can afterwards leave the roof as evapotranspiration. The other fraction that is not retained, arrives with a certain delay in the sewer network. This last process is commonly referred to as detention of rainfall [29]. In Flanders, recent legislation already mentions green roofs as a valid infiltration system for renovations and new constructions [30]. On a catchment scale, this practice of implementing Nature Based Solutions such as green roofs has proven to lower the runoff discharges and volumes [31, Qiu et al., 2018].
The installation of green roofs can even become more beneficial under climate change. However, increased water stress for vegetation will have to be taken into account in the design choices [32, Vanuytrecht et al., 2014]. Succulent plants are therefore often used in vegetated roofs [29, 32, 33, Cirkel, 2018].
In light of this problem of heat waves and drought, an interesting addition to conventional green roofs is a water buffer under the substrate (soil) layer. These so-called blue-green roofs are capable of retaining a larger volume of water. The retained volume both relieves the downstream sewer network, and provides more water to the plants during dry spells [33]. Moreover, a larger cooling effect is realised [33].
According to Stovin [29], it is widely acknowledged that the antecedent conditions of the substrate (and buffer) layer in a (blue-)green roof play an important role in its event-specific retention capacity. Intelligent control of blue-green roofs can be a way to assure optimal antecedent conditions. Before an extreme precipitation event, the full buffers underneath blue-green roofs can be emptied as a precautionary measure. This way, more rainfall can be intercepted by the buffer, relieving the downstream sewer network of high runoff peak values. Conversely, in dry periods, the water will be stored and can be used by plants (or households). Although this intelligent control strategy has already been mentioned before (see [34]), it is hardly applied.

1.2 Research objective

This research aims to assess the benefits of a weather-dependent operation of buffers on an urban scale. Hence, one could formulate the main goal of this project as follows:

> *To what extent can intelligent control of blue-green roofs help to solve the problem of urban flooding?*

In order to solve this main goal, several intermediate objectives should be met.

Objective 1: collect experimental data to build a reliable model.

First and foremost, research starts with a large and reliable set of data. Some of this data is publicly available. Other info is collected on specific test sites, both in Belgium and in France. This large amount of data needs to be collected, processed and analysed before new research can be conducted.

Objective 2: choose a suitable model structure, calibrate and validate it on existing data and assess the performance of different green roofs.

Secondly, an appropriate green roof model should be selected or built. Calibration of the model for several roof types is done relying on the previously acquired data. Validation is preferably executed with similar but independent time series. Afterwards, long term simulations can provide a more complete image of the performance of the different green roof types.

Objective 3: analyse the long-term hydrologic performance of wide-scale green roof application in an urban setting.

For this objective, the flood mitigation potential of green roofs is investigated on an urban scale. The earlier work of Bertels and Janssens [35] resulted in a conceptual model for the sewer network of Antwerp. For each of the five subcatchments, they already determined the surface suitable for green roofs. The new green roof model can be implemented in this model. This way, the conceptual model indicates to what extent wide-scale application of vegetated roofs can reduce pluvial flooding.

Objective 4: find a feasible intelligent control strategy for blue-green roofs, considering a certain future.

Next, intelligent control of the buffer volumes is added to the model. Based on weather data from the RMI (Royal Meteorological Institute in Belgium), the model becomes capable of deciding when to empty the buffer storage. By considering different control strategies and parameters, the advantages are weighed. To conclude, practical design recommendations for the test site in Antwerp and for blue-green roofs in general are given to the reader.

Objective 5: adapt the intelligent control strategy for blue-green roofs to make it robust to uncertain weather forecasts.

An intelligent control strategy might work well in theory, but an implementation in real-time is something else entirely. The most important challenge in real-time is that rainfall forecasts are inevitably subjected to uncertainty. An important, final objective is to see if the intelligent control is still viable when the decisions are based on (partly) incorrect information.

1.3 Reader's guide

Chapter 2 gives a summary of literature on the topics of green roof modelling, conceptual modelling of sewer networks, intelligent control strategies and forecast uncertainties.

Chapter 3 elaborates on the research site, the collected data, and available models and expertise in the deparment of Civil Engineering in the KU Leuven.

Chapter 4 contains the assembly, calibration and validation of an appropriate green roof model. Using this model, long-term simulations are done on an individual green roof and on an urban scale. Conclusions concerning drought stress and flooding mitigation are then drawn from these simulation results.

Chapter 5 describes the intelligent control strategies, implemented on the blue-green roofs.

Chapter 6 investigates if the intelligent control needs to be adapted to cope with uncertain weather forecasts.

Finally, the main conclusions of the research are summarized in Chapter 7. An answer to the main research objective is formulated, and the results from the intermediate goals are evaluated.

Chapter 2

Literature review

This chapter summarises acquired knowledge from earlier research on green roofs and water problems in cities. In order to conduct a thorough research on green roofs, basic knowledge of these vegetated roofs is necessary. Therefore, the first section gives an overview of different (blue-)green roof configurations that have been designed worldwide. Afterwards, the hydrologic performance is further elaborated. A last part sums up other advantages of green roofs that have been researched in several scientific publications.
The second section treats the different hydrological models, as a suitable green roof model needs to be build or selected for this research. A study of the available literature reveals a multitude of possible hydrological models to describe the rainfall-runoff relation of vegetated roofs. Each subdivision in this section is devoted to one of three categories, namely black box, grey box and white box models. A selection of the models that are most significant and frequently used are explained below.
The third section elaborates on different modelling schemes for sewer networks. Such a model allows to evaluate the impact of green roofs on an urban scale.
Subsequently, more information is given on intelligent control strategies in the penultimate section. Earlier studies on Model Predictive Control are described, and the most important results are summarised, as this method is also applied in this research.
Linked to this, the consequences of forecast uncertainties on decision-making are further elaborated. This information will help to reach the final objective of this thesis.

2.1 Green roofs

2.1.1 Structure of green roofs

Three types of rooftops can be distinguished that aid in stormwater management according to the information of the Dutch organisations Stichting RIONED and STOWA [34]. A conventional green roof slows down and lowers the peak runoff [36, Getter et al., 2007] during a storm by using vegetation on a permeable substrate layer. Such roofs emerged in Germany in the 1980's [37]. A blue roof is nothing

more than a water buffer that captures rainfall. Afterwards the water can evaporate or the buffer can be emptied in a dry period. Lastly, a blue-green roof combines both strategies. Underneath the substrate layer, a buffer layer can capture the water when the substrate is saturated. As stated earlier in the introduction, this water can be kept in the buffer to help the plants during a dry period [33, 38].
In general, green roofs comprise four layers [39, Castiglia et al., 2016]: vegetation, substrate (also called soil), a filter layer and a layer with drainage material. In a blue-green roof, the buffer can be placed as a replacement of the drainage material, or underneath it.
Next, several characteristics of green roofs are further elaborated.

Substrate Although the specific values tend to differ among authors, the scientific literature makes a division in green roof configurations judging by the thickness of the substrate layer:

- **Intensive green roofs**: Thick substrate layer (150 mm [34] to 250 mm and up [37]), suitable for larger plants, shrubs and trees. This type of roof typically requires more maintenance [39, 37], and stability engineers should check the effect of this extra load on the roof [39]. For renovations, it often turns out to be economically infeasible, as these loads can exceed values of 100 and even 400 kg/m^2 [37].
- **Extensive green roofs**: Thin substrate layer (between 25 [40] and 100 mm [37] / 150 mm [34]), mostly used for smaller plants or grasses. This type poses extra loads between 30 and 100 kg/m^2 for layers until 100 mm [37].

Figure 2.1 is taken from a Dutch scientific and informative article [34]. The first two sections show possible intensive green roofs, the right section is an example of an extensive green roof. This research focuses on the latter.
Although survival of the plants is important for both cooling air and retaining water, research has shown that soil characteristics have a larger effect on the retention and detention capacity of extensive green roofs [41, Monterusso et al., 2004][40, Van Woert et al., 2005]. Both substrate composition and depth seem to play a bigger role than vegetation in the hydrological performance of a roof [29]. Usually, a deeper substrate layer leads to higher retention capacity [40, 42, 39]. But, with increasing depth, the relative gain in retention becomes less [34].
Furthermore, in substrate composition, the trade-off between permeability and weight has to be made. Less permeable soil is good for retention, but increases the load on the roof structure [29, 39].

Vegetation Very closely tied to this substrate thickness is the vegetation. As this research only discusses the extensive roofs, only extensive vegetation is described below.
Extensive green roofs are in its most basic form a copy of spontaneous vegetation on roofs [37] like mosses and grasses. A study from the KU Leuven has already

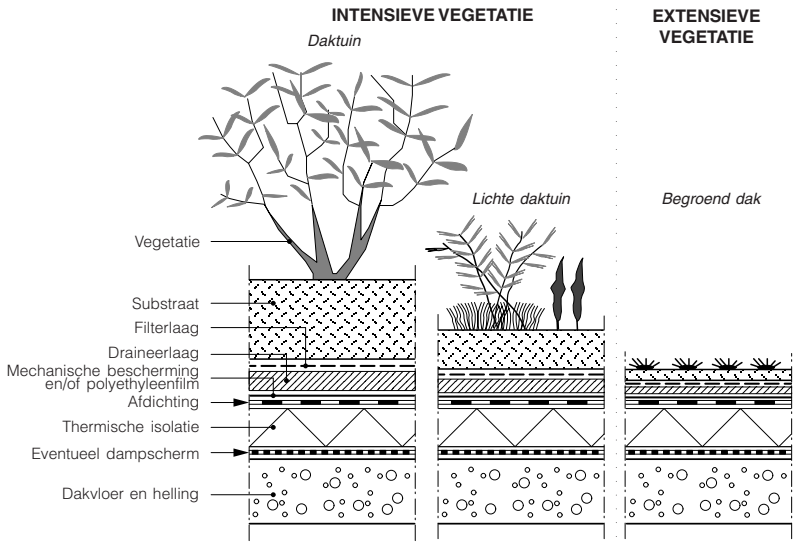

Figure 2.1: Three different roof types as a function of the substrate dpeth, as explained in [37].

pointed out the potential benefit from mixing several vegetation types [32]. For example, grasses and herbs can boast a large evapotranspiration rate. This means that the capacity of a substrate is quickly restored after a rainfall event. Moreover, this evapotranspiration is responsible for the cooling effect of the vegetated roofs [33, 34]. On the other hand, succulent plants like *Sedum* prove to be more resistant to frost and drought [32, 34].
According to research from the KU Leuven, some Mediterranean habitats show interesting similarities to extensive green roofs [43, Van Mechelen et al., 2015]. As the temperate climate in Belgium is expected to experience higher temperatures and fewer precipitation events [8], presence of such plants could also be a proactive way to design green roofs in more temperate climates [43, 32]. Especially annual plants from Mediterranean regions are seldom used but show potential [43].
Irrigation is also a valid option to cope with dry spells, but this process is considered unsustainable in regions where water is a scarce and valuable resource.
Selection of suitable plants, substrates and alternative irrigation, such as rainwater interception [38, 33] or intelligent control of irrigation are welcomed [43]. In this light, this thesis research aims to confirm the benefit of blue-green roofs and intelligent control for the survival of the roof throughout the summer.

Slope A last important difference among green roofs, besides vegetation and substrate, is the slope. Contrarily to intensive roofs, extensive roofs are more flexible. Installation on a steep slope until 45° is possible [44, 34, 37, Locatelli et al., 2014]. As a disadvantage to this flexibility, Van Woert [40] and Getter [36] noticed that the retention capacity decreases with increasing roof slope.

Buffer In blue-green roofs, the outlet of the buffer layer is another important aspect of the roof configuration. The first, very obvious strategy is to not provide the buffer with an outlet. This way, water either returns to the substrate or an overflow occurs to the sewer when the maximal volume is reached in the buffer.
Three other strategies are possible when providing an outlet situated below the maximal water level. The resulting runoff curves are shown in Figure 2.2. The first option is the effect of detention. This effect occurs because of the substrate layer, but can also be realised in the buffer with a weir. For instance, a V-notch weir already allows the creation of runoff below the maximal water level, but the runoff quantity increases with increasing water level.
Secondly, the outlet can be flow-limited. This outlet can be regarded as a floater that allows a constant (micro-)flow of water to leave the buffer. This way, sudden overflowing at the maximal level is prevented, and the water only enters the sewer in small quantities. Moreover, the buffer only empties slowly, allowing plants to take up water from it as well.
Lastly, in order to maximise water reuse by plants or by households (e.g. flushing of toilets), the water can be kept in the buffer as long as possible. When extreme weather is announced, the buffer can be emptied in a controlled way into the sewer system.

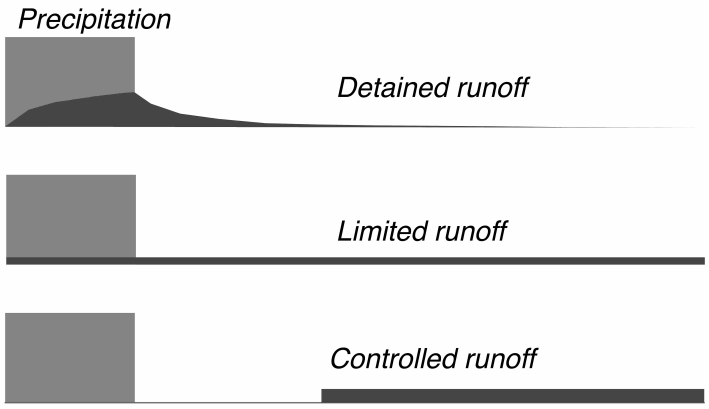

Figure 2.2: Overview of different runoff creation strategies (from: [34]).

2.1.2 Hydrologic performance of green roofs

The different measurement campaigns listed by Palla et al. [45, 2010] showed the importance of roof configuration (vegetation, substrate, slope) on the hydrologic performance, as mentioned above. Three other factors that are specified in the different studies, are the rainfall characteristics, the antecedent conditions and long term variations.

Rainfall characteristics For high rainfall depths (i.e. large amounts of water), extensive green roofs become less efficient in intercepting rainfall [29, 36]. For increasing intensity and duration of rainfall, this reduction in efficiency was reported for all soil depths modelled in [39] between 50 and 1600 mm. Interestingly, there was no significant difference found between the efficiency of very shallow (50, 100 and 200 mm) roofs during the simulation of extreme events [39]. All of these shallow roofs quickly become saturated and unable to retain the water during heavy rainfall. Again, the addition of a buffer and intelligent control of it, can lead to higher retention in such extreme cases.

Antecedent conditions Lastly, The antecedent moisture conditions in a green roof have a significant impact on the retention capacity [29, 37]. In cases with high moisture content before extreme rainfall, the retention capacity is lower and the runoff peak values are less efficiently diminished [39].

Long term variations For this thesis, long term hydrological performance is simulated and discussed. Therefore, temporal variations of retention and detention should at least be studied. A recent study from De-Ville et al. [46, De-Ville et al., 2018] investigates both long term and sub-annual (seasonal) variations for extensive roofs, either with *Sedum*, or Meadow Flower. As it turns out, long term variations are reported to be an order of magnitude smaller than seasonal variations.
The low variability on the long term is reassuring, both for the industry of vegetated roofs as well as for the research objective of this thesis. De-Ville states that this *Sedum*-based roofs have proven to be able to keep a good hydrological performance over time [46]. Neglecting an explicit formulation of ageing in the green roof model (*infra*) could be rectified based on this and on the fact that the research has another objective prioritised. Moreover, it can keep the model more reliable, since no long-term data is available to calibrate the model.
Concerning the short term (seasonal) variability, the calibration period is too short to correctly incorporate this in the model (*infra*). However, the calibration data spans the spring, summer and autumn months. As extreme rainfall events typically occur outside the winter months, this can still allow for a good hydrological model. Also, the study from De-Ville states that detention and retention variations are inverse and could therefore result in a somewhat consistent overall performance [46] on a yearly basis. Detention is weaker in summer because the flows are assumed to be more preferential in the dry substrate. Meanwhile, the higher potential evapotranspiration allows for better retention. In winter, retention is lower while detention becomes more effective [46]. This offers another argument to not consider this seasonality explicitly in the green roof model during calibration, validation and subsequent simulations. Instead, the complete and correct set of evaporation data in Flanders serves as an implicit seasonal variability in the model [47].

2.1.3 Other advantages of green roofs

As mentioned earlier in the previous chapter, green roofs provide several advantages compared to conventional black roofs, including but not limited to:

- **Acoustical comfort**. Although variations in depth and soil type did not have relative large effects, the installation in general showed interesting reductions in noise levels according to a study of Yang et al. in 2012. Specifically for traffic noise, a 4 dB(A) reduction was reported in an optimal situation [48, Yang et al., 2012]. A Dutch informative publication mentions a reduction up to 8 dB in the case of a dry substrate [34].

- **Thermal comfort**. As mentioned before in the introduction, green roofs keep the interior space cool in summer and warm in winter [25]. A thicker soil layer and a higher leaf area index (i.e. a coefficient that increases the evapotranspiration values when plants have large leaf surfaces) have shown to keep the air conditioning consumption in future climate scenarios at present levels. This way, the period over which the investment gets paid back is assessed at 10 years [49, Chan, 2013].
  However, a study in Hong Kong that confirmed these interior thermal benefits also pointed out that people are often hesitant to commit to the investment [50].

- **Urban Heat Island**. Another study shows that thermal benefits can also be reaped in the exterior environment [51]. Comparison between a concrete roof and a green roof show a diminished heat flux (-77%) and reduced air temperature (-13 K), measured one metre above the roof surface. Along with other studies proving the cooling effect [33, 27], the mitigation of the Urban Heat Island effect is evident.

- **Higher efficiency of PV-panels**. This cooling effect around green roofs can also be used to the advantage of PV-panels. On bare roofs, daytime temperatures in summer are often too high for an optimal conversion from solar energy to electricity. Several studies report the higher energy output for PV-panels over a vegetated roof [52, Alshayeb et al., 2016][53, Ogaili et al., 2016]. However, a study in Canada by Jahanfar et al. showed lower hydrological performances for the extensive green roof which is largely located under the panel. Elevation of the PV-panels to 1.2 metres above the vegetation did not significantly improve this. The vegetation growth however was better under elevated panels, thus conserving a lot of the other advantages that green roofs offer [54, Jahanfar et al., 2019]. Here a trade-off between elevation of panels and desired energy gain is needed, as a higher panel has less benefit from the underlying green roof [53].

- **Biodiversity**. The presence of vegetation is a way to help biodiversity in an urban ecosystem. However, this advantage has been proven hard to quantify. One study states that, due to the elevation and the low number of green

roofs, the positive effect on biodiversity often remains limited or unclear [55]. However, the relative abundance of plant and animal life on green roofs with respect to conventional roofs is clearly proven [56]. Therefore, it is safe to say that this type of roofs always provides a habitat for plants and animals in a city.

- **Purification of air and water**. A last interesting advantage to mention in this study of literature is the purification of air and water by the vegetated roof. During early research, the capture of carbon dioxide from urban environments is already mentioned [28, Rowe et al., 2011]. Research in the UK [57, Speak et al., 2012] studied the capture of particulate matter of 10 μm and less (PM10). Grasses showed to be capable at fixating larger quantities of PM10 than the *Sedum* roofs. The annual removal potential in a ideal case (maximal *Sedum* roof implementation in a city centre of 325 ha) resulted in a capture of 2.3±0.1 % of 9.18 tonnes of PM10 that were given as input to the scenario.
  Research in a Chinese city that experiences acid rainfall showed an increased pH (i.e. lower acidity) of the water after leaving the green roof test bed. The mean value turned from 5.61 to 6.84, an acceptable value for surface water (6.0-9.0). Furthermore, the study showed that a green roof can lower concentrations of TSS (total suspended solids) in the water. That being said, the water quality is also influenced by the soil substrate. Therefore, care should be taken when using fertilisers or untreated soil, as this might not be beneficial for the water quality [58, Zhang et al., 2015].

In conclusion, implementation of green roofs on a large scale ameliorates the liveability of a city in a lot of aspects.

2.2 Hydrological models

Generally, three large families of models can be defined:

- **White box or physical models**: white box models establish the relation between rainfall and runoff by solving the water balance [59, Carson et al., 2017] and describing the underlying physical processes, such as evapotranspiration and flow through the substrate. For this, parameters like hydraulic conductivity would need to be known or arbitrarily chosen.

- **Black box or empirical models**: this type of models is strongly data-based. Equations are built specifically to give a good approximation between model and data. The general risk is that calibrating the model on data from a green roof can only guarantee good approximation of that roof's behaviour. Its applicability for other roofs and rainfall conditions remains limited [59].

- **Grey box or conceptual models**: grey box models are a step down from the details in a white box model. When it comes to green roof modelling, the

water balance is still solved but the internal processes are not always explicitly described. The large, water retaining volumes like buffers or substrate layers, are aggregated to reservoirs. When multiple reservoirs are used, connecting flows are defined. For these flows, the parameters are not always physically based.

2.2.1 Black box models

Two event-based, empirical models are discussed here: the Curve Number method and the Characteristic Runoff Equation. It should be noted that both methods are not able to consider antecedent events, although this impacts runoff depth in reality [29].

CN

The curve number method is a model structure, developed by the Natural Resources Conservation Services (NRCS) [60], that has been applied worldwide. Only one coefficient has to be determined based on the available data, after which event runoff is easily calculated as follows:

$$R = \frac{(P - I_a)^2}{(P - I_a + S)}$$

$$S = \frac{25400}{CN} - 254$$

$$I_a = 0.2(S)$$

where the rainfall runoff R, the precipitation P, the maximum storage S and the initial abstraction I_a of the receiving surface are all given in mm water depth. The coefficient CN determines the storage and abstraction value, and can therefore be considered as a value that summarises all properties of the soil type, the surface and the antecedent conditions. The value for CN follows from minimising the MSE between R and measured runoff data. From the equations, one can deduce that a lower CN implies a lower value for the runoff.For extensive green roofs, values between 69 and 95 have been reported [59, 36]. Impervious surface like concrete slabs have even higher values for CN, with an upper limit of 100.

CRE

The characteristic runoff equation (CRE) works according to a similar philosophy, but the lumped rainfall-runoff relationship is described by more than one coefficient. For green roofs, a second order polynomial is generally applied:

$$R = C_1 \cdot P^2 + C_2 \cdot P + C_3$$

The missing coefficients C_i are either calibrated using individual events or annual data [59], by minimising the root mean square error.

Compared to CN, this method already has a more flexible form. However, it is only valid for a specific precipitation range. Because C_3 is normally non-zero and negative, R becomes zero for a certain value $P*$. Therefore, all events with $0 < P < P*$ are considered to have R equal to 0 instead of $R < 0$.

2.2.2 Grey box models

Several conceptual models have been developed by researchers. Most models start off with the same flows and reservoirs. Precipitation P is the only incoming flow, and evapotranspiration ET and runoff are the two outgoing flows of the system. At least one reservoir is used to represent the intercepting capacity of a green roof. Some use extra reservoirs, leading to the definition of internal flows.

Cirkel et al. (2018)

Conceptual modelling is not the main research topic of Cirkel et al. [33], so their model structure is made specifically for their research objective. In this study, the aim was to assess the evaporation benefits from a blue-green roof compared to a conventional green roof. A simple bucket model is used to simulate the actual evaporation. The model structure is shown in Figure 2.3, with precipitation P, evapotranspiration ET, drained runoff upon saturation D, permanent wilting point PWP, roof constant RC and soil moisture deficit SMD all expressed in mm. Where others would prefer to work with the moisture content of the soil (availability of water), the inverse variable is considered here (lack of water). If the moisture deficit SMD is between 0 and RC, the potential evapotranspiration ET_p has to be considered (abundant water present). When SMD becomes larger than RC, it decreases linearly until $ET = 0$ for $SMD = PWP$. When $SMD = 0$, complete saturation is reached and excess water leaves the bucket (D).
For potential evapotranspiration values, two approaches are mentioned. Either climate data is used from a nearby weather station, or a physical equation has to be used. The most common one is the Penman-Monteith equation [33].
For the green roof model in this research, data for ET_p can be used from the stations of the Flemish Environmental Agency [47] (*infra*).
Although this comprehensible model can be useful in some situations, the absence of internal processes like capillary irrigation makes it less interesting for this research.

Kasmin et al. (2010)

The et al.ped by Kasmin et al. [61] contains two components, as shown in Figure 2.4. Firstly, a substrate component can be filled with incoming precipitation until field capacity is reached. The excess rainfall is sent to the second component, the transient storage. From this storage, runoff is created through a routing model. Evaporation allows to restore the capacity of the substrate component.
The model has proven to be able to simulate both individual storm events and longer periods. Four strategies are tested to incorporate evapotranspiration in the model:

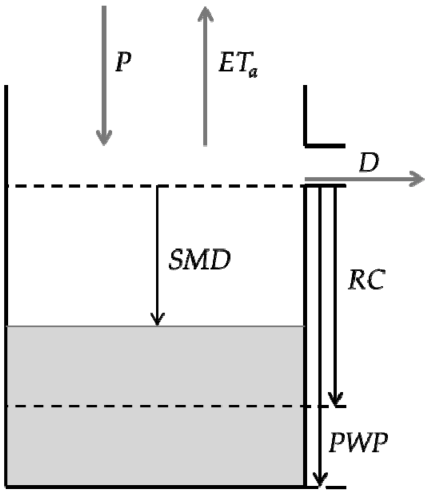

Figure 2.3: The simple bucket model does not give information on the water level in the buffer, and no permanent outlet from a buffer layer is present [33].

application of the Thornwaite formula, direct laboratory measurements, and two methods that are based on the available data, thus creating assessments specifically for the considered roof type and weather conditions [61].
However, as stated in the previous model description, equations for ET_p will not be considered for this research, as sufficient data is available in Flanders. Other than that, the modelling approach with a routed (delayed) outflow from a saturated substrate reservoir is proven useful to simulate conventional green roofs [61]. To correctly describe the behaviour of this substrate component, less parameters are needed in comparison to a physical model that tries to capture hydraulic conductivity, porosity and/or permeability of the soil. This is an important advantage of conceptual models, as the model appears to still be capable of adequately describing the roof response to rainfall.

Vesuviano et al. (2014)

A study in Sheffield, UK [62, Vesuviano et al., 2014] came up with a conceptual model to describe the different layers in a green roof separately. The model structure is shown in 2.5.
Although the model also considers a drainage layer (i.e. layer to evacuate excess water from substrate), the process of retention is not incorporated in the model. The substrate layer acts like a reservoir that only puts a temporal delay on the outflow. In other words, in absence of new precipitation, all water leaves the substrate. However, a normal green roof is observed to retain a certain part [34]. This remaining volume can only exit the substrate layer through evapotranspiration [33].
For the case of a blue-green roof, evapotranspiration is not the only flow that is explicitly missing here. In order to implement an intelligent control in the research,

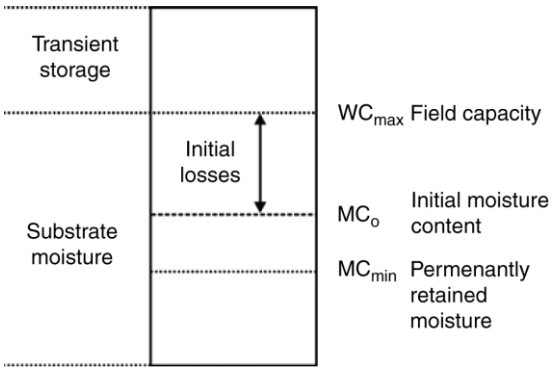

Figure 2.4: The runoff is created in the transient storage through a routing model [61].

the model needs to describe the effect of capillary irrigation on the water level in the buffer.
This shortcoming should not be surprising, as the research objective of that publication was to correctly expose the flows through the separate layers (substrate and drainage) during storm events in a rainfall simulator [62]. Interaction between both layers is not mentioned, and evaporation is negligible in such short simulations.
Therefore, applicability of this model to the current research is non-existent unless evapotranspiration and capillary irrigation are introduced.
The process of detention from the drainage layer was described based on earlier research from Vesuviano et al. [63]. The detention was established through a power-law relationship between storage and runoff, $Q = k \cdot S^n$. For roofs containing an outlet from the buffer reservoir, this formulation could be useful to implement (*infra*).

RainTools (Stichting RIONED)

This program is developed for the Dutch organisation Stichting RIONED, the group that comprises all parties charged with sewer management in the Netherlands [64, 34]. The model structure is shown in Figure 2.6.
Precipitation enters the system on the substrate layer, comprising both plants and soil. The substrate layer is also considered to have a wilting point and a field capacity point in this model. The difference between both values equals the static storage in the substrate (in mm). The storage capacity is restored through evapotranspiration and above field capacity, water starts running off or is directed to an underlying buffer layer. Processes inside the substrate layer are not considered. The detention caused by the travel time through the substrate is said to be negligible [34].
Water in the substrate layer can leave the substrate through evapotranspiration from both soil and vegetation. This is the first model considered in this study that mentions the evapotranspiration originating from both soil and plants. As mentioned earlier, grasses show a stronger ET-rate compared to *Sedum* plants [34, 33], so this

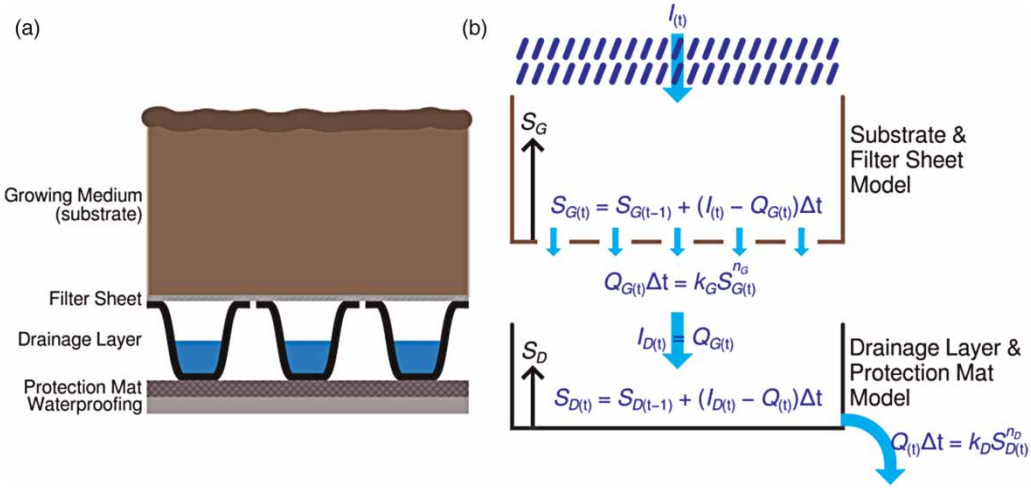

Figure 2.5: Vesuviano et al. only describe the process of detention, the delayed response between rainfall and runoff [62].

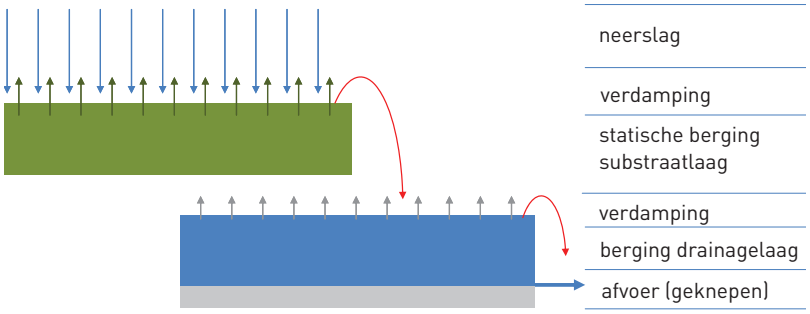

Figure 2.6: This model structure is also capable of describing blue-green roofs [34].

effect is important to consider. Since this research also studies the water stress for plants, and both grasses and *Sedum* are present on the test beds (*infra*), this is important to consider for the final model structure.
Furthermore, this is also the first model in this study that specifically describes the buffer layer. From the buffer layer, a small evaporation flow is defined. In this research, this flow should be modified to allow capillary irrigation towards the substrate layer. The outlet on the buffer is said to be flexible. The runoff flow can thus be limited, free, closed or even controlled [34]. If the model structure also considers that water can overflow towards the sewer when the buffer volume is exceeded, this model structure seems to describe the green roof in enough detail, while also leaving the option of intelligent control of the outlet.

Locatelli et al. (2014)

The last conceptual model that is discussed here is the model described by Locatelli et al. [44]. The model starts from the mass balance, and has some physical parameters. Other parameters are to be calibrated via data.
The model structure is shown in Figure 2.7. A first surface storage intercepts the rainfall. If this storage is full, new precipitation is directed to the subsurface storage. This represents the retention capacity of both substrate and drainage layer. It is said that the latter seldom has a retention function, but it is included in case it does [44]. From a certain moisture content ($a \cdot R_{max}$) the flow towards the detention storage increases linearly in magnitude until it becomes Q_{ss} when maximal moisture content R_{max} is reached. The detention storage is a temporary reservoir that puts a delay on the runoff that leaves the system. If this detention storage fills faster than it empties, the overland flow is included in the model when the storage is full. Both output flows are described through a power-law, as was the case in Vesuviano's model [62]. In this model, the field capacity is defined in another way than in earlier models. Water already migrates to the detention storage before the field capacity is reached, while other model define the field capacity as the point where water starts leaving the substrate [34, 61].
Evaporation and transpiration are included to restore capacity of all three storage reservoirs. For the calculation, Penman-Monteith is used, as was the case for Cirkel's research [33].
The model is shown to simulate both single event and long term responses well.

In conclusion, the multi-reservoir approach proves to work very well here [44]. However, this model does not explicitly talk about a buffer layer. Instead a drainage layer is mentioned, which could be adapted to fulfill the role of a buffer layer in the model structure.
However, this drainage layer is compounded with the substrate into one *substorage layer*, which impedes simulations with water level information in the buffer. This water level information is a key concept to intelligent control, so this model cannot be taken over directly for this study. In anything, the detention storage reservoir seems like a better candidate to represent the buffer layer in a blue-green roof model. In any case, the structure has a lot of useful elements that should be considered when choosing or building a green roof model for this research.

Overview

To conclude the subsection on grey box models, an overview is given in Table 2.1. The most important characteristics for this research are listed in the first column. Judging from this Table, the model from Locatelli and Rioned seem to be most promising, as they contain almost all desired features.

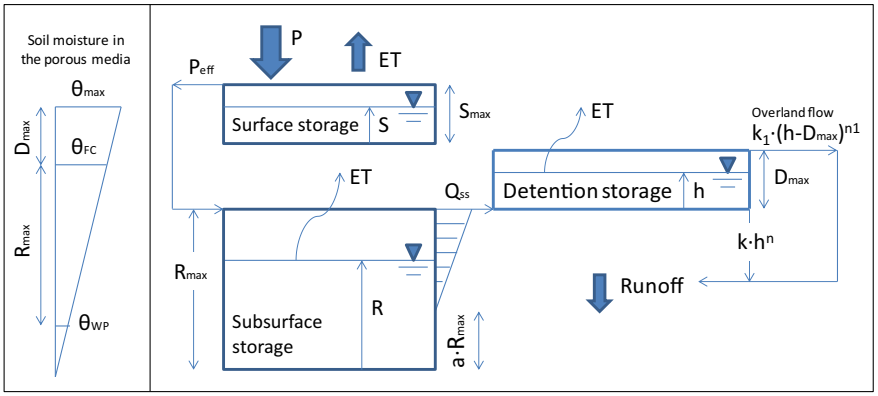

Figure 2.7: The multi-reservoir model as presented by Locatelli [44].

Table 2.1: Overview of the different grey box models, and their most important characteristics. Especially the models from Rioned and Locatelli are useful for this research.

	Cirkel et al. (2018)	Kasmin et al. (2010)	Vesuviano et al. (2014)	Stichting Rioned	Locatelli et al. (2014)
Capillary irrigation	No	No	No	Yes (only ET)	Yes (only ET)
Buffer layer	No	No	Yes (drainage layer)	Yes (drainage layer)	Yes (drainage layer)
Retention	Yes	Yes	No (limited benefit under severe storms)	Yes	Yes
Detention	No (direct outflow of excess water)	Yes	Yes (power law)	Yes (outflow formula)	Yes (outflow formula)
Evaporation	Yes	Yes	No	Yes	Yes

2.2.3 White box models

These numerical models are often developed in the form of software packages, and describe the flows through the green roof components. Here, two models are discussed, namely SWMM and HELP.

SWMM

The Storm Water Management Model is developed by the United States in 1971 and primarily aims at simulations of runoff in urban areas [65]. However, the Low Impact Development (LID) package specifically allows to simulate green roofs [59]. This software package represents a roof as a vertical stack of layers [66, Cipolla et al., 2016]. The flow of precipitation through this roof depends on the physical properties that need to be defined for each layer. This way, through the selection of surface cover (vegetation), soil type properties and drainage conditions, the created runoff is calculated.

According to Cipolla et al. [66], SWMM is also useful for long term simulations of green roofs. Performing both a calibration and validation using a year-long data set, the simulated values gave a fairly good comparison with the collected runoff data (high NSE). For urban designers and policy makers, this software proves to be useful in representing the hydrologic behaviour of green roofs.

HELP

The HELP software is originally used for behaviour of landfills, and models a column with several layers such as vegetation and soil [67]. The flows are because of this column approach only partly two-dimensional [59]. The world-wide use in engineering practice makes it interesting to use, although other white models have a more detailed approach.
Carson [59] used both HELP and SWMM. The main shortcoming of HELP is that it only describes one section (no third dimension). Since Cipolla et al. [66] already pointed out the good performance for long term simulations, this model seems to be preferred.

2.2.4 Conclusions on different model structures

The first family, black box or empirical models, the results from simulations other than the calibration and validation events are generally too uncertain to rely on. Moreover, the applicability of such models to other roofs and environments is non-existent. That being said, they can be quite useful to indicate the possible performance of green roofs. However, for this research, such models will not be used, as intelligent control is not possible without knowledge of the water level in the buffer.

The alternative of white box models also has some shortcomings. Too detailed models are more prone to overparameterization. Also, the available data is not

always sufficient to correctly calibrate the required parameters (such as soil characteristics) in software packages.

Conceptual models perform faster calculations than a white box model, while still keeping comprehensible parameters. Software packages like RainTools are a possible group of conceptual models that can be investigated more closely.
However, the already existing model for the Antwerp sewer network is developed in Matlab. Therefore, a custom-made conceptual model in Matlab can be made very compatible with this urban model while including all model elements that are relevant for this research. In Chapter 4 the green roof model structure is presented. Both model components from Locatelli's model [44] and RainTools [34, 64] have shown to be interesting and are incorporated in the final structure, as presented in section 4.1.

2.3 Sewer network modelling

This section discusses three possibilities for sewer calculations. The first two models represent each link in the network separately, whereas the third option aggregates the total network to reduce calculation time.

2.3.1 SWMM

The Stormwater Management Model (SWMM) does not only contain the possibility to model green roofs. In fact, its first objective is to describe the processes in urban sewer networks [65]. The easy up-scaling from the scale of one roof to a city makes it a frequently used hydrodynamic model for researchers [59, 66]. However, this detailed model will take a long time to perform long term simulations compared to a conceptual sewer model.

2.3.2 InfoWorks ICM

Comparable to the aforementioned model structure, InfoWorks ICM is also capable to simulate the response of a sewer network [68]. As each link is modelled, the bottlenecks that impede a fast evacuation of sewer water can be easily identified.
Again, since this model provides such a resolution, simulations with 100 years of rainfall data take a very long time to finish.

2.3.3 Conceptual Model Developer (CMD)

As mentioned in the previous section, earlier research on the city of Antwerp provides another model structure to calculate sewer volumes based on rainfall runoff values. The thesis of Bertels and Janssens [35] offers a conceptual model for the inner city. This model is conceived using the modelling tool developed by Wolfs et al. [69].
The Conceptual Model Developer (CMD) is a tool that can convert a detailed, hydrodynamic sewer network model into a storage cell system. This new model

structure can be calibrated to simulation data of the detailed network. This way, it becomes able to reproduce these detailed results as correctly as possible, with a sharply reduced computational effort. First, the global functioning of the model is explained to the reader, followed by the relationship between the sewer volumes and the volumes on the streets during flood events.

Storage cell model structure More specifically, the storage cell concept comprises a collection of *subcatchments* (SC). The SCs each represent a part of the total network, and can store a certain amount of volume. The water balance between the SCs is established via *fluxes*. An overview of this structure for Antwerp is shown in Figure 2.8a.
The original sewer network that serves as the basis for this new SC-flux structure, comes from more detailed software such as InfoWorks ICM. From a certain amount of rainfall events, the response in ICM is calculated. Then, the CMD creates a structure of SCs and fluxes to reproduce the data from the hydrodynamic model as correctly as possible.
The fluxes between the SCs can be simulated using three methodologies. The most basic relation to implement is a constant flow that can turn on or off. This represents a pump station in a sewer network.
Secondly, a piecewise linear static/dynamic relation can be used to model the flow between two SCs depending on their volumes.
Lastly, when the flux behaves non-linearly or there is no clear relation to deduce, Artificial Neural Networks can be used. Such ANNs have already shown good results in several water systems [69].

In the work of Bertels et al. [35], simulation results from InfoWorks ICM software are used for the configuration of the conceptual model of Antwerp's sewer network. The inner city of Antwerp is divided in five SCs, as shown in Figure 2.8b. Most notably, SC 3 and 4 are described best by the conceptual model. This also happens to be the most flood-prone part of the city. The model is calibrated to rainfall data at a time step of 10 minutes. However, the conceptual model allows to simulate volumes and flows for any given time step.

Flooding volumes Since the conceptual model only shows the volumes inside a subcatchment, more detailed information on flooding occurrences is lost in this approach. However, a flooding criterion for the conceptual results has been determined for Antwerp [35]. This criterion is too simple to link the sewer volumes directly to the flooded volumes, because of a hysteresis on the flooding phenomenon. This means that the maximal volume on the street does not coincide with the maximal volume in the sewers in a subcatchment. However, as shown in Figure 2.9 that is found in the research of Bertels et al. [35], a quadratic relation can be deduced between the maximal sewer volume and the maximal flooded volume of a single event. Similar relations are calculated for all SCs. To assess the performance of green roofs, the maximal flooded volume is a good indicator. Therefore, this criterion is

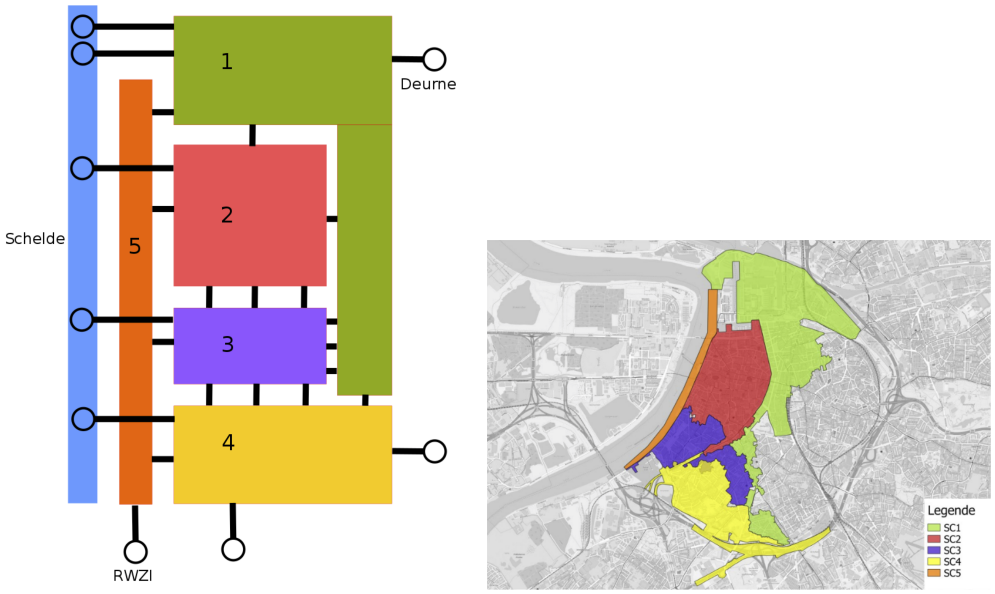

(a) Conceptual model structure showing the SCs and flows.

(b) Geographical distribution of the SCs over Antwerp.

Figure 2.8: Description of the conceptual model for Antwerp [35].

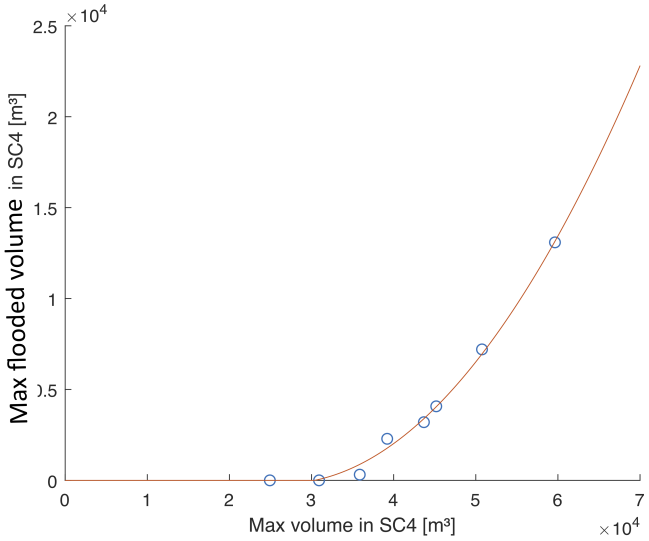

Figure 2.9: Assessing the flooding criterion for SC4. The blue dots represent separate rainfall events with floodings, and the orange line is a quadratic regression (From: Bertels et al. [35]).

also acceptable for this study. An important note is that the quadratic relation is based on sewer volumes and flooded volumes according to the Conceptual Model of Antwerp, and not according to the calibration data from InfoWorks. This safer approach prevents errors from the calibration step to accumulate in this calculation. Below, the quadratic relations for subcatchments 2, 3 and 4 are listed:

$$V_{fl,2} = \begin{cases} 3.071\text{e-}08 * V_{SC2}^2 - 1.514\text{e-}03 * V_{SC2} + 16.769 & \text{if } V_{SC2} > 20000 \\ 0 & \text{otherwise} \end{cases}$$

$$V_{fl,3} = \begin{cases} 5.921\text{e-}06 * V_{SC3}^2 - 0.154 * V_{SC3} + 955.196 & \text{if } V_{SC3} > 15000 \\ 0 & \text{otherwise} \end{cases}$$

$$V_{fl,4} = \begin{cases} 1.218\text{e-}05 * V_{SC4}^2 - 0.647 * V_{SC4} + 8410.118 & \text{if } V_{SC4} > 30000 \\ 0 & \text{otherwise} \end{cases}$$

where both the volumes in the street $V_{fl,i}$ and the volumes in the subcatchment's sewer network V_{SCi} are expressed in [m^3]. The conditional formulation reveals that only from a certain sewer volume V_{SCi} onwards, an actual flood occurs.

2.4 Intelligent control

When intense rainfall occurs and the substrate of a green roof is already saturated, the positive hydrological effect disappears. This is often the case in winter, when evaporation is barely present to restore the retention capacity [34]. However, a blue-green roof possesses one more layer that can intercept this rainfall, namely the buffer. Here, a trade-off presents itself between water availability for the vegetation and the retention capacity to mitigate flood risk.
This idea of optimising water availability and preventing floods by intelligent control of infrastructure is not entirely new. In 2008, the methodology of Model Predictive Control is already described by Barjas Blanco et al. [70, Barjas Blanco et al., 2008]. In that research, a Belgian river is described by a model that incorporates the hydraulic control structures (e.g. weirs and buffers). Next, the model modifies the settings of these structures in such a manner that the future damages over a certain time window are minimal. Historical weather data is used as *perfect weather forecast data* on which the decisions are based.
Simulations using this so-called intelligent control have shown the potential reduction in fluvial flooding [70][71, Falk et al., 2016] compared to river systems with Programmable Logic Controllers (PLC) on the hydraulic structures. In the case of a gate on a river, a PLC chooses one of a limited set of gate levels depending on the water levels before or after the gate [72, Vermuyten et al., 2018].
As the conceptual model of Antwerp's urban sewer network also comprises catchments and buffers just like a river system, MPC can be implemented here as well. Therefore, the following subsection treats the theory behind MPC in more detail.

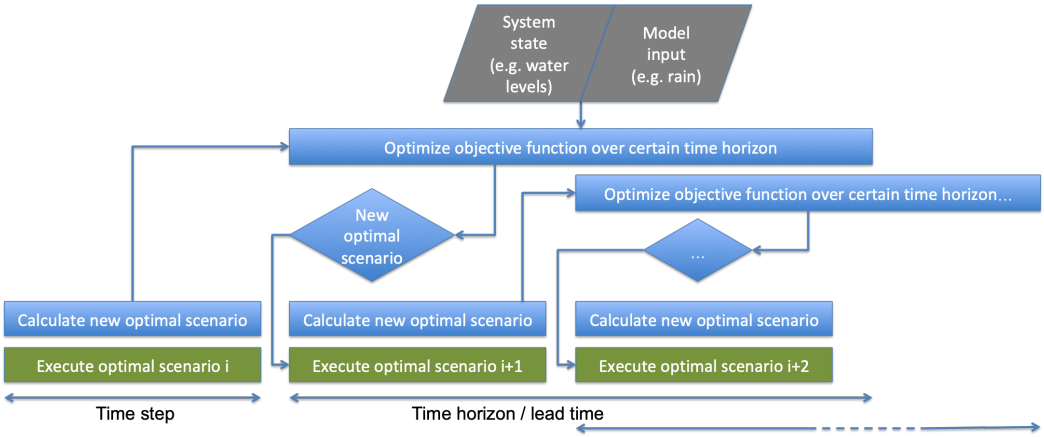

Figure 2.10: Flowchart of a general MPC. The green processes are the actual state of the system, blue elements represent the optimisation process and the grey components are input.

2.4.1 Model Predictive Control

MPC is a model-based decision making tool, which finds its origin in the chemical industry [73]. Figure 2.10 gives an overview of a general MPC. Each time step, the previously calculated scenario is executed while a new optimal scenario is determined. At the end of a time step, this newly found optimal scenario is followed, and the process starts again.
Some elements are always present in MPC, namely a system model, an objective function, a receding horizon and input variables. The following description of these elements is based on the explanation in [74, Blanco et al., 2010].
The system model has to describe the system state as correctly as possible. This can be with a very detailed physical model, or a computationally efficient conceptual model.
The objective function represents the state of all system variables that are deemed important by the user. Optimising this objective function within its constraints is equivalent to finding the optimal state of the system.
The receding horizon is the time period over which the model runs the scenarios. This lead time is typically longer than one time step. This implies that an optimal scenario is never fully executed, as a new scenario replaces it after one time step.
The input variables can be split up in two categories: the system state variables, which can be measured on site, and the model input variables. The second group contains time series that need to be applied over the entire receding horizon, and is mostly subject to uncertainties as it is situated in the future.

In a hydraulic system, some structures are installed which control the water levels and flows. For instance, rivers often have adjustable weirs. Applied to hydraulic systems, the goal of MPC is to select the best possible way to adjust all structures in the system in the optimal way within a certain predefined time period. In the case

of a fluvial system, an optimal scenario should, among other objectives, minimise the total damage of flooding [72]. The same objective applies to urban sewer networks.

2.4.2 Earlier research

Founded on this theoretical basis, several adaptations have been investigated in earlier publications. In the field of hydraulics and hydrology, most of the research concerns river systems.
For MPC, linear river models can provide a good approximation [71]. However, flooding of a river makes the system non-linear, which has its implications on the optimisation during MPC [72]. As an answer to this, non-linear MPC schemes have been developed [75, Barjas Blanco et al., 2010]. To bypass the computational efforts of solving the non-linear expressions, heuristic algorithms are introduced. For example, the work of Vermuyten describes such an algorithm which converges a lot faster compared to other heuristic approaches, albeit towards a near-optimal scenario [72].
However, the conceptual model of Antwerp is far less complex than a full river. On top of that, the blue-green roofs can probably be steered on a collective scale as opposed to individual steering of gates on a river, since the input variables (rainfall and evaporation) are applied more or less homogeneously on an urban scale. Because of this lower complexity, heuristic approaches are not really needed, as the global optimum should be attained in an acceptable time window by simply considering (almost) all possible scenarios at once.

2.5 Forecast uncertainties

In order to implement Model Predictive Control in real-time in hydrological applications, the model needs basic input such as future rainfall in the study area. As the future is uncertain, one cannot be sure about the resulting model response, and the decision that follows from the optimisation.
In this research, past rainfall events are used for simulations. The problem of uncertain input does not arise in that case. Measurements from the past can simply be considered as perfect forecast data. Still, it remains one of the objectives of this research to estimate the impact of such erroneous input to the efficiency of intelligent control. The following subsection covers ways to assess future rainfall intensities, since this is the most important input variable. Next, an adaptation of MPC is presented. This variation has a strategy to handle the uncertainties.

2.5.1 Nowcasting of rainfall

Nowcasting is the process of obtaining short-term predictions that follow from real-time data [76, Allaeys et al., 2018]. For urban applications, the real-time data is often radar images because of the details it contains both in time and space. The rainfall prediction is an extrapolation of the precipitation fields on the most recent radar image. Because of the uncertainties that arise from extrapolations, different

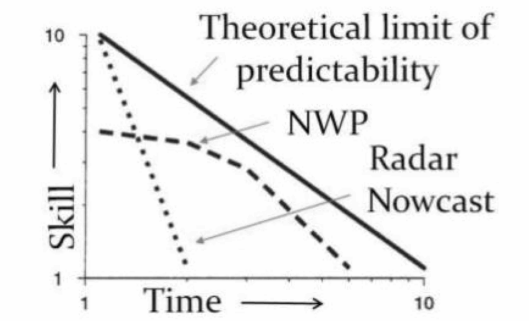

Figure 2.11: For shorter time periods, extrapolation of radar images is preferred over NWP [78].

possible images are calculated and bundled in one ensemble [77]. Each prediction is more commonly referred to as an ensemble member.
A frequently used way to generate the various extrapolations in one ensemble is the Lagrangian approach. Here, the chance of rainfall in a pixel (or cell) of the radar image depends on the surrounding cells [76]. The method explained in the next subsection starts from this approach.

2.5.2 STEPS and STEPS-BE

The deterministic Lagrangian approach succeeds in extrapolating the movement of the current precipitation field. The Short-Term Ensemble Prediction System uses this, but also addresses one more uncertainty. Stochastic perturbations are added as a way of describing the possible accretion or decline of the precipitation fields on the radar image [77]. Moreover, the extrapolated images in the ensemble are blended with results from a Numerical Weather Prediction model. This predicts the weather based on the physics of the atmosphere, which gives better results on larger scales and for longer lead times, as shown in Figure 2.11 [78].

For nowcasting on the urban scale, the results from NWP are less interesting. For lead times until 2 hours, the normal extrapolation of radar images outperforms NWP methods [78]. An adjusted system, called STEPS-BE, does not rely on NWP [77]. The ensembles that form the output of this prediction system are explained in the next chapter.

2.5.3 Multiple Model Predictive Control (MMPC)

This subsection explains the methodology of Multiple Model Predictive Control. Here, the optimisation problem starts from an ensemble of potential rainfall scenarios instead of a deterministic rainfall forecast. As explained in the work of Van Overloop [79, Van Overloop et al., 2008], the normal MPC strategy is followed with one modification. Every steering scenario is evaluated over the same model with the different rainfall inputs. If three rainfall series are derived from the ensemble of possibilities, then three parallel models are run for each steering scenario. In the

objective function, three terms replace each term from the normal MPC practice. All three are multiplied by the probability of occurrence of the corresponding rainfall scenario [79].
Application of MMPC on a flood-prone river in Belgium showed that the normal MPC with a heuristic optimisation outperformed the MMPC [80, Vermuyten et al., 2016]. The MPC used in the research proved to be robust enough to rainfall uncertainties because of the continuous updating of the optimal scenario. In this research, a similar investigation will be conducted. The only difference is the use of an urban sewer network instead of a river.

2.6 Conclusion

This chapter summarises the scientific literature that has been studied as the foundation of this research. First of all, the different advantages and characteristics of (blue-)green roofs are listed and discussed. Apart from water management, benefits can be reaped on a household and urban level. Green roofs show good acoustical and thermal properties. Wide-scale application also helps biodiversity, reduces the Urban Heat Island effect and purifies the air and precipitation.
Next, different green roof model structures are described. For this research, a conceptual reservoir model is preferred. Black box models do not show the required detail to implement intelligent control, whereas white box models sometimes lack in general applicability. Moreover, when considering the problem on an urban scale, the computational cost can pose problems. More specifically, the model discussed by Locatelli [44] and the one from Stichting Rioned in the Netherlands [64] serve as an inspiration for the new conceptual model that is built for this research.
To assess the performance of green roofs on an urban scale, a conceptual model for the city of Antwerp is used. This model is already calibrated and described in the work of Bertels et al. [35]. The model is created by a Conceptual Model Developer from the University of Leuven. This tool can be used to conceptualise any urban network [69].
A fourth section covers intelligent control strategies. In this research, an implementation of Model Predictive Control is tested on an urban scale. Contrarily to the work of Vermuyten [72], the search for the optimal scenario does not need to be conducted in an iterative way. Instead, the best scenario is selected from a large and random set of scenarios that covers most of the control possibilities.
Finally, the topic of forecast uncertainties is addressed. When controlling the green roofs in real-time, the search for an optimal control scenario is subject to errors on the input variables. The uncertainty that comes with the most important input variable, future rainfall, is addressed here. For calculations in the near future (i.e. 2 hours), nowcasting is more certain than numerical weather prediction. Nowcasting means that short term extrapolations of existing radar images are generated.

Chapter 3

Experimental setup and available data

This chapter provides the reader with some general background on the elements that support this thesis.
The backbone of this research is the test site in Antwerp, since this data leads to an adequate green roof model. Among other elements, the regional climate, the installed test trays and the data collection are described below.
For the sake of validation, measurements from two similar test sites in France are made available. Both sites contain green roofs from the same producer Vegetal i.D., but experience different weather conditions.
Next, to assess the impact on an urban scale, a conceptual model for the sewer network in Antwerp is used, as described in the work of Bertels et al. [35]. For this model, long term time series are acquired for rainfall and evapotranspiration.
Lastly, the implementation of intelligent control strategies depends on weather data. A fully measured rainfall event over Antwerp from 2016 is presented here. Also, rainfall ensembles are generated based on actual measurements. These ensembles can then be considered as uncertain forecasts of this past event.

3.1 Calibration data: setup in the city of Antwerp

3.1.1 General background

Belgium has a temperate maritime climate, with wet and cool winters and mild summers [32]. Climate data is made available by the Royal Meteorological Institute in Belgium [81]. The annual average rainfall amounts to 848.4 mm [81]. The precipitation days PD_x is the number of days in an average year where a precipitation of at least x mm/day is recorded. In Antwerp, PD_1 equals 132.7 and PD_{10} equals 23.7 days. Furthermore, an average year has 49.3 days where temperatures below 0°C are recorded, of which 5.7 days where the temperature never exceeds 0. The annual mean for summer storm hours is 26.5 hours, and for days 16.1. These last two values are determined based on data from 2004 until 2013.

The choice for the city of Antwerp as the location for this research should not be surprising. The city of Antwerp has the second biggest port on the European continent [82], and the city houses 524501 people [83]. Antwerp lies at the banks of the Scheldt, a tidal river.
The vulnerability of a not completely new sewer network and the proximity to the Scheldt increase the probability of a flooding in Antwerp. Considering the historical value of the city and the large population density of 2568 persons per square kilometre [83], damages can mount up to large sums. Combining the damages and the probabilities of occurrence, the risk of pluvial or fluvial flooding becomes significant. For this research, only the risk of pluvial flooding is discussed. This takes place when the sewer network cannot transport the volumes due to heavy rainfall. This pluvial flood risk in the city of Antwerp and elsewhere in the densely populated and urbanised region of Flanders has already been confirmed by some severe flood events in recent years [84, 85].
Moreover, the extreme rainfall events are expected to intensify during the summer periods in Belgium under several climate scenarios [8].
In short, the socio-economic importance of this densely populated city in Flanders, along with earlier research showing possible benefits of NBS on stormwater management [2, 31] and the prospect of a changing climate, serve as motivation to choose the city of Antwerp as the location for this blue-green roof test site.

More specifically, the test site is located on a roof in the heart of Antwerp, in the neighbourhood Sint-Andries (N=51.214008, E=4.398796). Figure 3.1 gives the geographical context of this roof. The population density in this part of the city equals 13969 persons per square kilometre [83], more than five times the overall density for the entire city. Researching new flooding mitigation measures are therefore particularly interesting for this part of town.
This pilot project for smart green roofs is financed by the BRIGAID-project of the European Union. This four-year programme fits in a larger programme of the European Union, namely Horizon 2020. The acronym BRIGAID stands for *BRIdging the GAp for Innovations in Disaster resilience*. As the name reveals, this project funds research into innovative solutions against natural disasters in Europe, including pluvial flooding and heat waves in urban areas [86]. The municipality of Antwerp is participating both as an end-user and as a test area for the new solutions.
Other partners of this project include Stadslab2050, Sumaqua, Beweging.net, the Catholic University of Leuven (KU Leuven) and the green roof producer Vegetal i.D.
.

3.1.2 Instrumentation and setup of green roof test site in Antwerp

This subsection explains every element of the test site. An overview of the entire roof is given in Figure 3.2. First the measuring station is briefly highlighted, followed by a description of the different green roofs. Lastly, some critical notes on the experimental setup are listed.

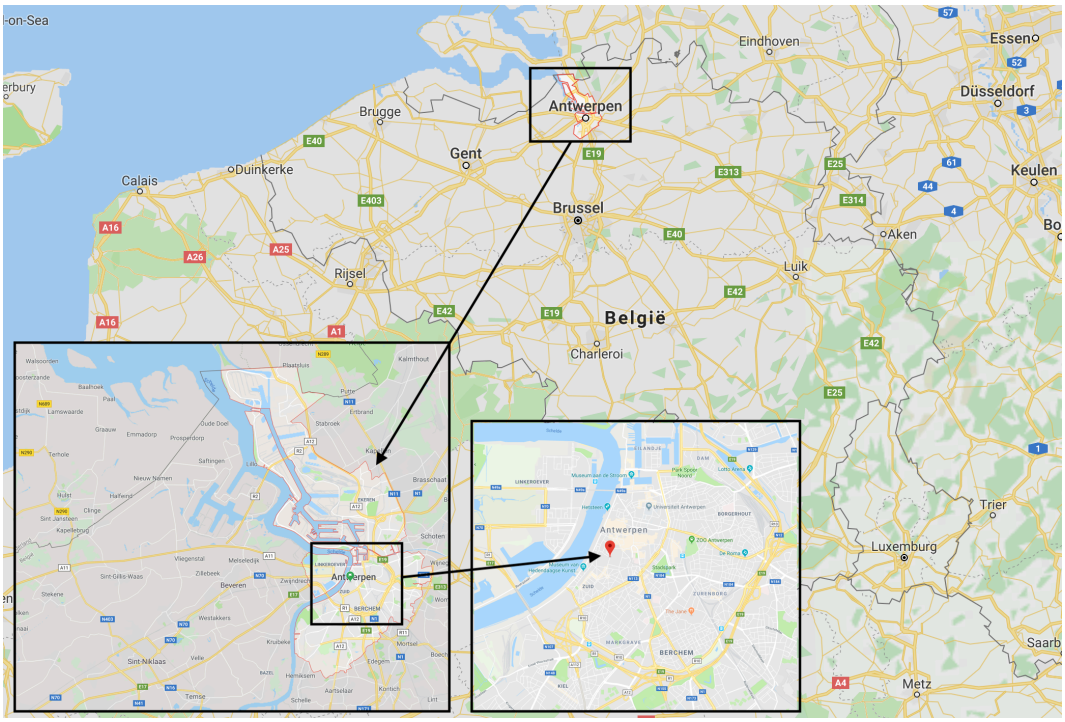

Figure 3.1: The location of the test site is right in the heart of the city centre of Antwerp, the biggest city in Flanders.

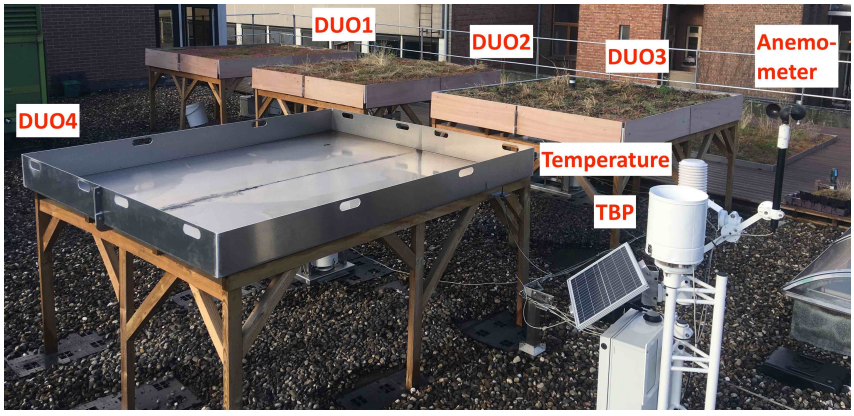

Figure 3.2: An overview of the experimental setup in Antwerp. The nomenclature of the green roofs is explained later in this subsection (picture by Ewout Vereecke).

On site, the temperature (°C), wind speed (m/s) and precipitation (mm) are measured each minute. Figure 3.2 shows the experimental setup containing a temperature sensor and a pluvio- and anemometer. The sensor sends out all data to a central server. The entire measuring station is powered via solar energy. The test site consists of four different roof configurations, as shown in Figure 3.2. All four test roofs are put in horizontal metal trays that span a surface of 2 by 2.4 metres. The

Figure 3.3: Each tray has a double pluviometer at its outflow (picture by Ewout Vereecke).

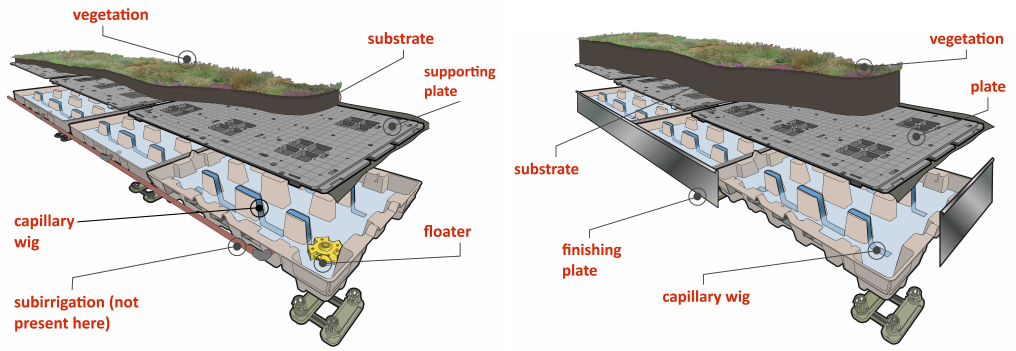

(a) (b)

Figure 3.4: (a) Layout of the green roof DUO2. (b) Layout of the green roof DUO3 (Source: [38]).

metal trays are put on a height of 1 metre with respect to the roof surface to provide space for the runoff measuring device.
Each tray disposes of a double tipping bucket pluviometer (TBP) to measure its runoff: one with an accuracy of 0.01 mm and the other 1 mm. The latter is used for heavy rainfall events where the small TBP cannot process the large volumes. Figure 3.3 demonstrates the layout of the installed pluviometers. For the roofs that comprise a buffer layer, the water level of the buffer is also measured each hour using

Table 3.1: Properties of the four test roofs.

	DUO1	DUO2	DUO3	DUO4
Vegetation	*Sedum*	*Sedum*, Grasses	*Sedum*, Grasses	none
Substrate layer (mm)	60	80	200	0
Buffer layer (mm)	0	80	80	0
Runoff creation	Overland, Outflow	Overland, Outlet, Overflow	Overland, Overflow	Outflow

an Ijinus sensor [87].

All (blue-)green roofs are manufactured by the same company Vegetal i.D. [38]. Therefore, most properties are identical. The most notable differences are listed below:

- **Conventional green roof**: more commonly referred to as DUO1. A green roof comprising a filter sheet and a substrate layer with *Sedum* vegetation.
- **Hydroventiv green roof**: more commonly referred to as DUO2. A green roof comprising a buffer layer underneath a substrate layer with *Sedum* vegetation and some more intensive grass types. If the water level in the buffer exceeds 90% of the maximal level, the water goes to the TBP via an overflow. A floater in the buffer channels a micro-flow to the pluviometer, thus preventing the buffer from overflowing regularly. The floaters are the so-called outlet of this test roof. Capillary wigs connect the buffer with the substrate and allow resorption of water to the plants. This reduces the drougth stress for the vegetation while reducing the water level in the buffer.
- **Oasis green roof**: more commonly referred to as DUO3. A green roof comprising a buffer layer underneath a substrate layer with *Sedum* vegetation and some more intensive grass types. If the water level in the buffer exceeds 90% of the maximal level, the water also overflows to a TBP. Capillary wigs connect the buffer with the substrate and allow resorption of water to the plants. This reduces the drougth stress for the vegetation while reducing the water level in the buffer. The two important differences with DUO2 are the thicker substrate layer and the absence of an outlet with a micro-flow.
- **Reference roof (black roof)**: more commonly referred to as DUO4. This metal tray does not contain any vegetation, but is also linked to a similar double TBP. This data shows the creation of runoff from rainfall in the absence of vegetation.

The geometrical characteristics are listed in Table 3.1, and the difference between DUO2 and DUO3 is clearly shown in Figure 3.4. On the extensive roofs, the main vegetation is *Sedum*, a flowering succulent with low water use [34]. As suggested by

Vanuytrecht [32], a vegetation combination is tried with grass species.
However, a dry month of May and a dry summer during the calibration period were not beneficial for the growth of those herbaceous plants, so their advantage is not really assessed in situ yet.

To conclude this section, four remarks concerning the reliability of the results should be made. Firstly, the elevation of the metal trays allows the underlying roof surface to reach very high temperatures during hot summer days. The possible effect on the green roofs is uncertain, but it can be assumed that this has an effect on the evaporation of water from the buffer layer and on the vegetation stress. Higher evaporation of water can lead to an underestimation of the runoff volume. On the other hand, the higher temperatures are unlikely to be beneficial for the vegetation's well-being.
Secondly, the high thermal conductivity of the metal trays should be mentioned. Under influence of the sun, this tray can heat up very easily and has therefore been clad with timber planks. The effect of these planks will undoubtedly be positive, yet it has not been properly investigated.
Thirdly, the measuring campaign took place in an exceptional dry spring and summer, with multiple official heat waves in Belgium [88, 89]. On top of that, no real extreme rainfall events are present in the calibration period. This should be taken into account when calibrating a model via this data.
Finally, the easy-to-assemble green roofs do not fit perfectly in the provided metal trays, leaving a bypass for the rainfall. Figure 3.5 shows that a part of the intercepted rainfall directly lands in the metal tray and goes to the TBP. This leads to an underestimation of the detention and retention capacity of some roofs. Especially the DUO2 roof seems to have this shortcoming.
Overall, it is hard to assess the overall impact of these four effects. However, it is important to keep them in mind during the analysis of the measurements and the subsequent calibration efforts.

3.1.3 Description of the collected calibration data

The measurements in Antwerp started on the fourth of April in 2018 and are still ongoing on the moment of submission of this thesis (June 2019). For the calibration, data up until the beginning of December 2018 is used. Since December 2018, the calibrated model has been used to run long term simulations. However, the data from two test sites in France served as a direct validation of the model (see *infra*). For the DUO3 roof, no comparable roof is present on the French sites, so the measurements in Antwerp between December 2018 and May 2019 serve as validation.
Concerning pan evaporation, values can be downloaded for measurement stations near Antwerp on the site of the Flemish Environmental Agency [47]. In total three stations are considered. In descending order of priority this is: Melsele, Herentals and Liedekerke. Herentals provides most of the entries. All three measurements station are indicated on Figure 3.6.

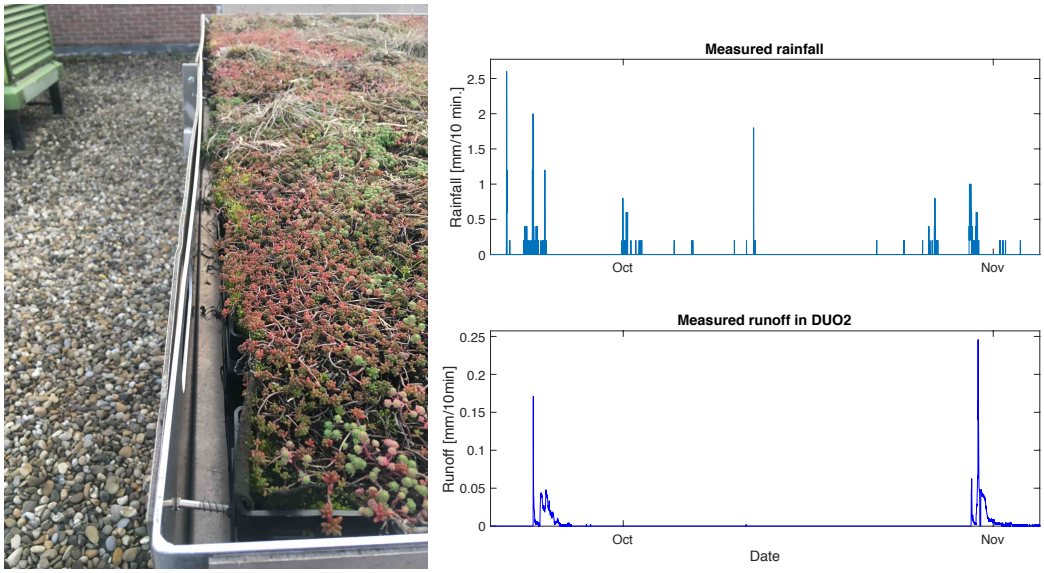

(a) (b)

Figure 3.5: (a) Gap between DUO2 and the metal tray (picture by Ewout Vereecke). (b) Early runoff peaks during some rainfall events.

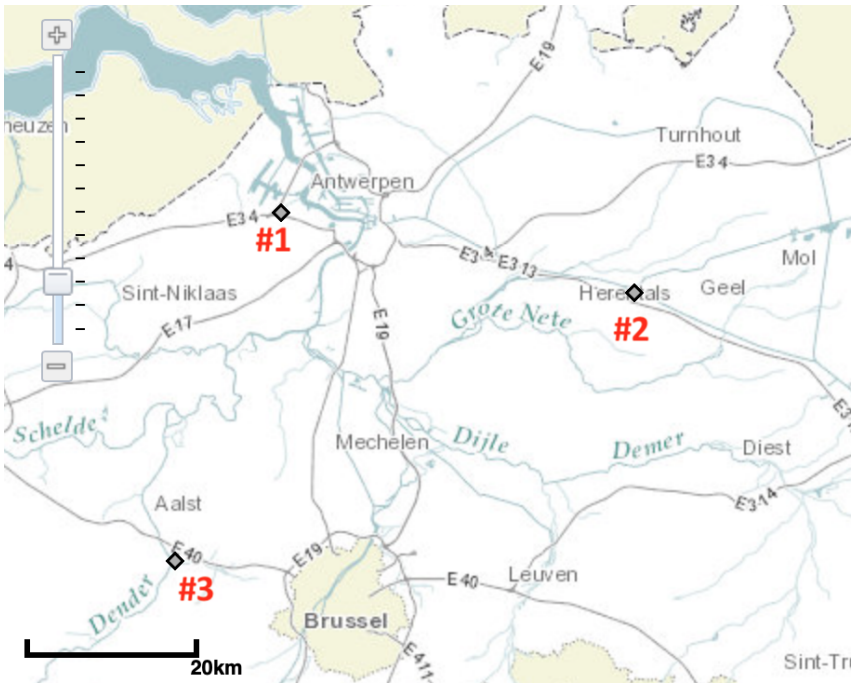

Figure 3.6: Evaporation measurements are done in Melsele (1), Herentals (2) and Liedekerke (3) [47].

3.2 Validation data: setup of test sites in France

3.2.1 Green roofs in Ivry (near Paris)

The test site in Ivry-sur-Seine is located just outside of the ring road (*périphérique*) of Paris. The exact coordinates (northing, easting) are N=48.810172, E=2.404150. The roof comprises 1 green (DUO1) and 2 blue-green roofs with an outlet (DUO2).

The average annual precipitation is 637.4 mm/year, with a PD_1=111.1 and PD_{10}=15.4 [90]. According to the climate records, the potential evapotranspiration ET_p equals 845.6 mm/year.
Detailed potential evaporation data is not freely available in France. Instead, an estimation is made based on monthly averages from the climatological record of Météo France [90]. The weather station is located at N=48.821667, E=2.336667, a mere six kilometres from the test site. The weather conditions are also assumed to be similar, since both the station and the test site are located right outside the ring road of Paris.
Rainfall and runoff have been collected since 2015, but buffer level data is only available from 2017 onwards.

3.2.2 Green roofs in Mions (near Lyon)

The test site in Mions is located within the metropolitan area of Lyon. The exact coordinates (northing, easting) are N=45.675772, E=4.934749. The roof comprises 1 green (DUO1) and 1 blue-green roof with an outlet (DUO2).

The average annual precipitation is 831.9 mm/year, with a PD_1=104.1 and PD_{10}=25.1 [91]. The annual average for ET_p amounts to 950.8 mm/year, but more detailed potential evaporation data for Mions is made available by a local partner.
Besides the evaporation data, rainfall and runoff have been measured since July 2015. Buffer level data is only available from 2017 onwards. Incomplete evapotranspiration data in the summer of 2015 results in a useful period ranging from November, 24 in 2015 to November, 30 in 2018.

3.3 Simulation data: synthetic time series of 100 years for Antwerp

For the execution of long term simulations, the conceptual model from Bertels and Janssens [35] is used, as described in Chapter 2.
The simulations span a period of 100 years. Required input time series for the model are precipitation, evapotranspiration and the water levels in the Scheldt river. The latter has an influence on the volumes in the sewer network, since the river acts as an outflow point for some pipes.
For both precipitation and evapotranspiration, synthetic time series have been developed. The time series gives precipitation values at an interval of 10 minutes, so the

unit of P equals [mm/10 min]. For the evapotranspiration however, hourly data is available. Hence, the unit for ET_p is [mm/h]. As the calibration for the conceptual model involved empirical relations for some subfluxes, the units of this model have to be respected. There, all flows may be distanced at a specific time step dt (expressed in [s]), but the unit always has to be [m^3/s].
In other words, the water balance is solved over an interval dt in the conceptual model. Water level values thus are the result of volume changes over 10 minutes $Q \cdot dt$ and flow values are distanced at 10 minutes, but expressed per second.

Unfortunately, such synthetic data does not exist for the water levels in the Scheldt river. There, Bertels and Janssens suggested the use of the Scheldt river time series from the year 2017, which is then put in a loop to end up with a time series of 100 year [35].

3.4 Weather forecast data

For intelligent control, the buffer settings mainly depend on the expected rainfall. Therefore, weather forecast data is needed.
To investigate the influence of imperfect forecasts on intelligent control, two options are considered here. Either a random error is added to the rainfall time series [80], or short-term weather forecasts are made based on measurements [76]. The latter is preferred in this research, since it is best suited to represent the reality in which the intelligent system would operate. Such predictions on the short-term, based on the extrapolation of existing radar images is often called nowcasting.

For the research on intelligent control, radar images from a recent extreme event over the city of Antwerp are collected. The first subsection describes the recorded radar images, and the second subsection elaborates on forecast data obtained after nowcasting.

3.4.1 Radar observations

On 30 May 2016, a severe rainfall event occurred over the inner city of Antwerp. From this event, both radar images and pluviometer records exist. Radar images are best suited for intelligent control in real-time, but tend to underestimate the rainfall [76]. On the other hand, pluviometers provide a more reliable rainfall record, but they are less useful for rainfall forecasting, which is needed in a real-time intelligent control. However, they can quantify the gap between the underestimated radar intensity and the actual intensity.

Description of the radar data

The composite radar image over the Belgian territory is obtained by 4 C-Band radars located at Wideumont, Jabbeke, Avesnois and Zaventem [76]. The images provided

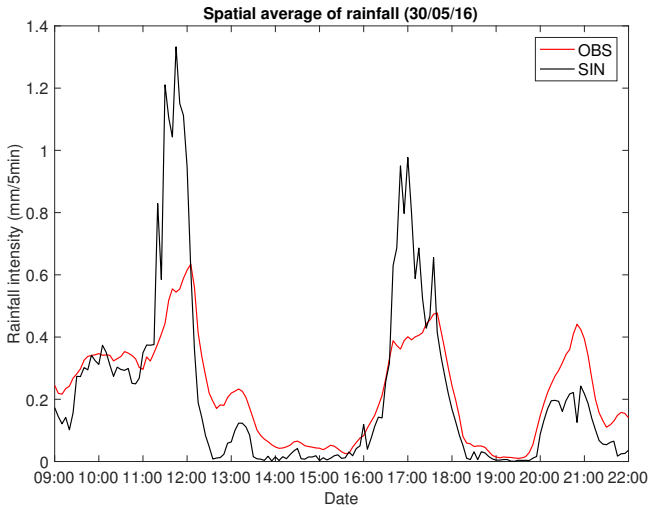

Figure 3.7: Original versus corrected measurements, according to the method from [92].

by the RMI form a grid of 512x512 cells, each with a resolution of 1058 metres. Roughly, this raster spans the north of France, Belgium, the Netherlands and the western part of Germany.

Correction of the radar data

Since the pluviometer records are collected over a dense network across the city, this gives a quite reliable image of the rain that really fell on 30 May 2016. Comparing these quantities with the radar measurements can reveal the systematic underestimation of the radar images. With this knowledge, the rainfall in the radar image can be artificially increased as a compensation. The radar images have already been corrected in previous research according to the method described in [92, Wang et al., 2015]. The result is presented in Figure 3.7 as a time series averaged over a grid of 36x36 cells. This grid is smaller than the 512x512 because the correction of [92] is relies on pluviometer data, and this is only provided in this smaller area.
In order to get a good comparison between the radar observations and radar extrapolations, the same correction needs to be applied to both. For the radar extrapolations, no corrections have been applied yet. Since this correction scheme from [92] is quite elaborate, it falls outside of the current research scope. Instead, a more straightforward method is followed. In a first attempt, a constant correction is applied over the entire 36x36 image. This constant is defined as the mean bias that exists between the total quantity of original rainfall and the total quantity of corrected rainfall according to [92]. In symbols this correction becomes:

$$BIAS = \frac{\sum_t \sum_{x,y=1}^{36} (I_{corr}(x,y,t))}{\sum_t \sum_{x,y=1}^{36} (I_{obs}(x,y,t))} \tag{3.1}$$

$$I_{obs/ens}(x,y,t) = BIAS \cdot I_{obs/ens}(x,y,t) \text{ for all x, y and t in the domain.} \quad (3.2)$$

with I the rainfall intensity in one cell of the radar image and at a certain moment. However, the results from this strategy were not satisfactory, as shown with the spatial averaged time series in Figure 3.8a. The $BIAS$ turned out to be close to 1, indicating that on average no big correction is needed. Indeed, analysis of the corrected radar image shows that the original radar image captures lower intensities quite well with some overestimations. Underestimations of the volume occur for the two local peaks with a high intensity. These local peaks lead to a small deviation of the total volume, which explains the low value for $BIAS$.
Secondly, an attempt is made to introduce a multi-bias correction. Under a certain threshold, the rainfall intensity of a radar pixel remains unchanged. But, when the threshold value is exceeded in a pixel, this intensity is corrected by magnifying it. In symbols:

$$I_{obs/ens}(x,y,t) = \begin{cases} BIAS1 \cdot I_{obs/ens}(x,y,t) & \text{if } I_{obs/ens}(x,y,t) < r_t \\ BIAS2 \cdot I_{obs/ens}(x,y,t) & \text{otherwise} \end{cases} \quad (3.3)$$

With $BIAS1 = 1$, r_t the threshold value and $BIAS2$ the correction on high intensities.
Since only the first peak around noon leads to an urban flooding, the multi-bias approach is established specifically for this part of the data set. Figure 3.8b shows two time series of corrected rainfall: the spatial average over all multi-biased pixels and the spatial average over the corrected pixels. The multi-bias parameters are approximated by matching these two time series. In the end, a value of 2.4 is found for $BIAS2$. The pixel threshold is fixed at 0.6 mm/5min.
This multi-bias rescaling method is henceforth applied on both the original radar images and the extrapolated radar images in the rest of this research. This ensures that no extra errors can be introduced due to different correction schemes.

Spatial variation of the radar data

For this specific event, the recorded rainfall intensities are quite homogeneous over the entire study area, as shown in Figure 3.9. However, this might not be the case for other events. Therefore, spatial heterogeneity on a neighbourhood scale will be assumed in the intelligent control in Chapter 5.
The first step is to determine which radar cells correspond to each subcatchments defined by Bertels et al. [35]. This information is extracted using GIS software. Relying on earlier work, a study area of 7 by 8 cells is selected from the 512x512 radar image [76]. If a cell is located over two subcatchments, it is assigned to the subcatchment with the largest surface area in that cell.
Now, each subcatchment possesses as much time series with rainfall intensities as it has cells in its territory. Each time series can be considered as a pluviometer record from a station located in the centerpoint of the cell. Taking the average at each time step gives one time series that serves as rainfall input for the subcatchment per square meter, defined as mm/5min. The mean time series for each subcatchment

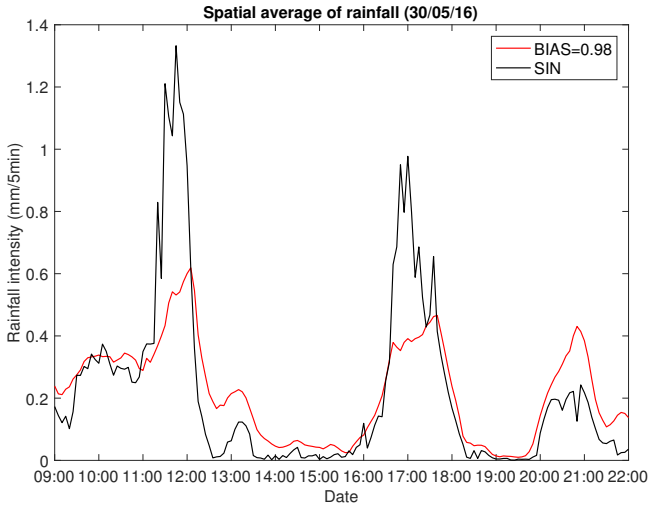

(a) Corrected according to [92] versus single bias correction.

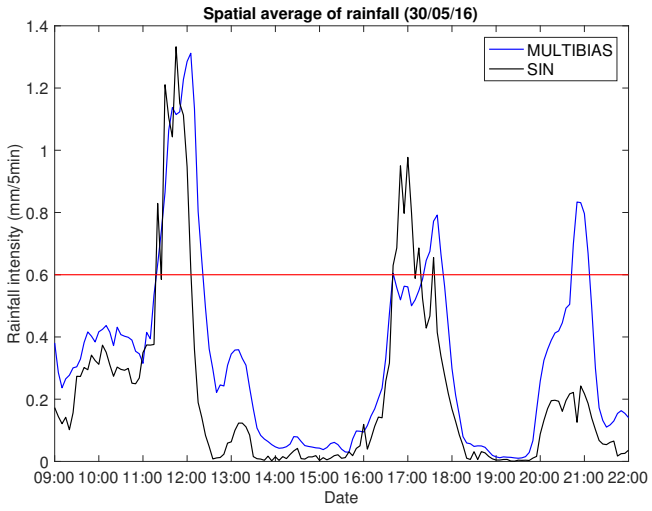

(b) Correction according to [92] versus a multi-bias correction.

Figure 3.8: Correction of rainfall time series, averaged over 36x36 pixels.

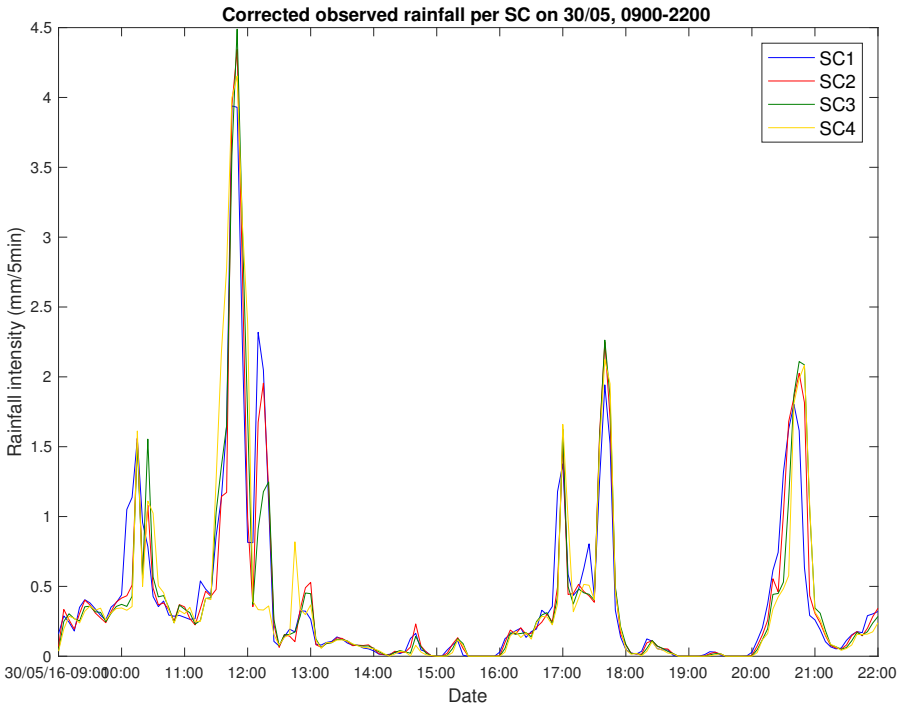

Figure 3.9: The precipitation time series for subcatchment 1-4, after the multi-bias correction.

is presented in Figure 3.9. As the set of radar images of this event presents a high temporal and spatial resolution, nowcasting can be used to calculate rainfall predictions. The following section explains the ensembles that are the result of this nowcasting.

3.4.2 Radar extrapolations using STEPS-BE

As explained in the study of literature, STEPS-BE is a nowcasting scheme that suits the needs of this research. For the extreme rainfall event of 30 May 2016, the Royal Meteorological Institute (RMI) in Belgium has created ensembles via STEPS-BE. With a lead time of 120 minutes, a new ensemble is generated every 5 minutes [76, 77]. Each ensemble contains 20 members with an equal possibility of occurrence. The members are radar images at a spatial resolution of 1.058 km, with 512 cells in both directions.
As a corrective measure, the same multi-bias is utilised on every pixel in zone of interest.

3.5 Conclusion

This chapter aims to inform the reader on all the elements that support this thesis research. Four major elements are explained: experimental data for calibration, experimental data for validation, synthetic data for long term simulations and weather forecast data.
Firstly, the location of the test site is defined. The city of Antwerp is situated in a temperate maritime climate with wet and cool winters and mild summers. As the largest city in the Flemish region with the second biggest port in Europe, the socio-economic impact of pluvial flooding is evident.
Secondly, the experimental setup in this city is described. The collected data from this site is used to calibrate a rainfall-runoff relationship for each green roof in the next chapter. The resolution of the data is deemed good, but critical notes are given. The calibration period is rather short, and the only recorded summer was extremely dry.
The validation of this model is done using data from France. Over there, similar green roof configurations have been installed on one location near Paris and one near Lyon.
The synthetic rainfall and evaporation data are distanced at 10 minutes for a period of 100 years. This allows for long simulations, with more certain conclusions on long-term performance in an urban setting.
The last section treats the input data used to test the implementation of intelligent control on the green roof buffers. The rainfall input data from before can be considered as perfect forecast data. To assess the impact of imperfect predictions, a STEPS-BE data set can be used. The extreme rainfall event of 30 May 2016 over Antwerp serves as a recent and representative example.

Chapter 4

Long term simulations for Antwerp using a new green roof model

This chapter reports in more detail how the green roof model was selected and built. For the rest of this thesis, this green roof model is then applied to quantify the performance of green roofs for past, future and design rainfall events.

Based on some very common models, an adapted green roof model was created. The adaptations to existing models are done in an attempt to describe some processes in more detail.
Calibration and validation of this final model leads to the selection of the best performing parameter values. The calibration is done using data from the test site in Antwerp, whereas two French test sites with nearly identical green roofs serve as validation data.
Next, the model is applied to a rainfall time series of 100 years. Using these long term results, the performances of the different roof types are quantified.
To conclude, long-term simulations are conducted on an urban scale. The percentage of surface covered with green roofs and the type of green roofs are the most important parameters that are observed.

4.1 Description of the model

This section explains the model in more detail, covering the global structure, the modelled processes and the selected parameters.

4.1.1 Model structure and processes

As shown in Figure 4.1, the general green roof model comprises three layers: a surface layer, a substrate layer and a buffer layer. By changing the volume retention capacity of each layer, everything from a black roof to a blue-green roof can be simulated.

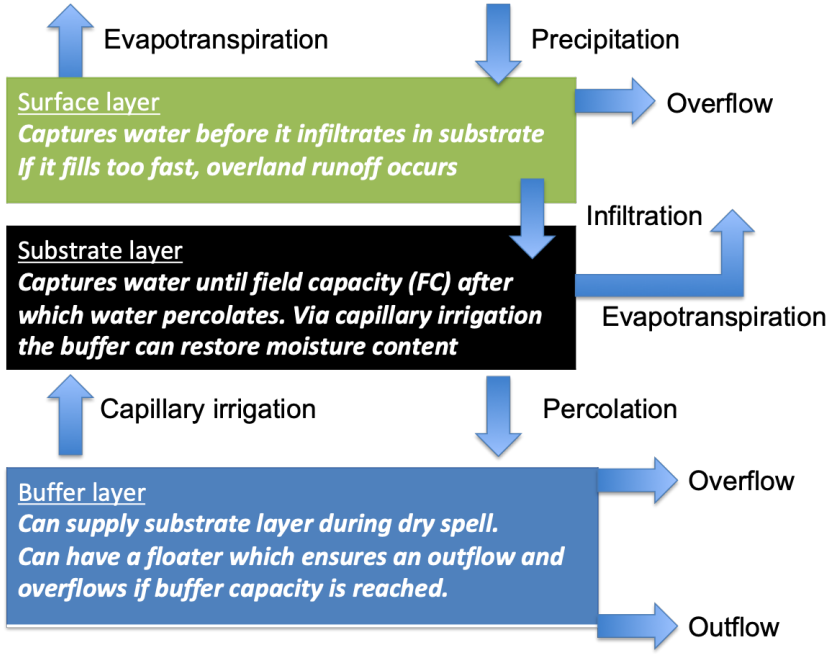

Figure 4.1: Overview of the model structure with all its in-, inter- and outflows per layer.

As explained in the previous chapter, precipitation forms the basic input. All three layers can retain a certain amount of this water, before runoff is generated. The retention capacity of the first two layers is restored via evapotranspiration. Below, all processes mentioned on Figure 4.1, are listed and explained.

Downward flows

This part gives all flows that follow the course of gravity. The entire model starts from one basic input time series: precipitation. This is measured on site as mm per minute.
This rainfall is intercepted by the surface layer, where it infiltrates towards the substrate layer. When the rainfall intensity is too large, the surface layer allows for some storage while water is infiltrating. If the maximal storage is reached, overland runoff is generated via a direct overflow. Direct overflow means that all excess water is directly transformed to rainfall runoff.
After infiltration, water is stored in the substrate layer. This soil can stockpile a certain volume of water until its saturation point. Beyond this saturation point, all excess water directly percolates through the substrate towards the buffer layer (if one is present). Starting from a certain degree of saturation, percolation already occurs, albeit to a lesser extent.
The percolated water ends up in the buffer layer. If a conventional green roof is modelled, this water is transformed to rainfall runoff. This conversion is clarified further on. In other cases, a certain amount of water is retained. In the case of a

DUO3 roof, runoff is only created when the water in the buffer reaches the maximal level. In the case of a DUO2 roof, runoff also occurs via a controlled outflow apart from the overflow option.

Upward flows

An upward flows is defined as the movement of water against the normal direction of gravity. This model contains two major upward flows.
First and foremost, evapotranspiration is the process where water leaves the green roof. This is done via evaporation and transpiration. The former occurs generally on every free water surface when the surrounding air is not saturated. Water transport in plants is responsible for the latter process. Water exits the plant via all parts that are in contact with air, of which leaves are the most important. Both the surface and the substrate layer give off water to the atmoshpere via evapotranspiration.

Secondly, capillary rise or irrigation occurs when a buffer layer is present. This flow is established via capillary forces that let water creep from the buffer towards the substrate. This only occurs when the saturation of the substrate drops below a certain parameter value, called the *Field Capacity* of the substrate.

4.1.2 Parameters

Surface layer

Two parameters need to be set for this layer: the infiltration rate and the maximal storage. For the maximal storage, values lower than 5 mm are assumed. As for the infiltration rate, two options present themselves: constant or variable. Some researchers aim to model substrate infiltration via variable infiltration rates [93, Wang et al., 2008][94, Zonta et al., 2012]. However, extreme rainfall data is so scarce in the considered data set, that there is probably no overland runoff measured. Determining variable rates would only make the model more complex without any certain improvement. Therefore, a constant infiltration rate is assumed.
The measured potential evaporation can be applied directly to the storage layer.

Substrate layer

Evapotranspiration This layer has two parameters to describe its evapotranspiration: the crop factor (referred to as Crop in this text) and the leaf area index (LAI). The measured potential evaporation needs to be multiplied by both factors to end up with the actual evapotranspiration. The crop factor is typically smaller than one, because Crop=1 represents the ideal situation of potential evapotranspiration of free water.
On the other hand, LAI can be larger than one. It is defined as the leaf surface per unit of ground surface, so LAI =leaf area (m^2) / ground area (m^2) [95, Watson et al., 1947]. Since all three green roofs have more or less identical vegetation (the grasses on DUO2 and 3 did not grow well during the dry summer), no distinction

has to be made via the Leaf Area Index. In this research, LAI is put equal to 1 in all cases because calibration of the actual evapotranspiration was already done using only the Crop factor. When comparing roofs with a very different vegetation bed, this parameter should be chosen different from 1.

Moisture content Several green roof models utilise concepts like *Wilting Point* (WP) and *Field Capacity* (FC) to define the moisture content of the soil [44, 61]. In this model, WP is defined as the degree of saturation where only permanent water stays present. This permanent water can only be extracted via an oven treatment. Therefore, the Wilting Point is considered as the starting point (zero) for moisture content in the soil. Figure 4.2 presents a table with the different regimes as a function of the Relative Substrate Moisture (RSM). RSM is defined as:

$$RSM = \frac{\text{temporary water in substrate}}{\text{temporary water capacity in substrate}} \tag{4.1}$$

The graph shows the water flows at each value of RSM. Two other parameters are used to distinguish these regimes inside the soil: $\Delta\theta$ and FC. The fraction of the substrate thickness that can be filled with temporary water is equal to $\Delta\theta \cdot H_s$, with the variable H_s equal to the actual height of the substrate layer in mm. Thus, the relative substrate moisture becomes:

$$RSM = \frac{VOL}{\Delta\theta \cdot H_s} \tag{4.2}$$

With VOL the temporary water in mm. When RSM exceeds the value 1, direct overflow towards the buffer layer occurs. This yields a flow $Q = (VOL - \Delta\theta H_s)/\Delta t$. The neutral point where water neither percolates to the buffer nor returns to the substrate via capillarity is called the Field Capacity in this model. The parameter FC, is defined as the RSM on this neutral point. Based on Equation 4.2, this means that $VOL = FC \cdot (\Delta\theta H_s)$ when the Field Capacity is reached.
When the moisture content exceeds the field capacity point, percolation takes place. This percolation increases with rising moisture content, as is the case in the model of Locatelli [44]. But, instead of a linear interpolation between zero percolation (at Field Capacity) and maximal percolation (at saturation), a constant exponent is added. Exponential behaviour towards an equilibrium relation is an often recurring process in nature. In symbols, the flow is calculated as:

$$Q = ((RSM - FC) \cdot \Delta\theta \cdot H_s \cdot Decay)/\Delta t \tag{4.3}$$

with

$$Decay = (RSM - FC)/(1 - FC))^{\text{substrate\_exponent}}. \tag{4.4}$$

Here, *substrate_exponent* is a parameter that follows from calibration. This *Decay* is responsible for the red curve in Figure 4.2.
On the other hand, if the water content drops below this field capacity point, water

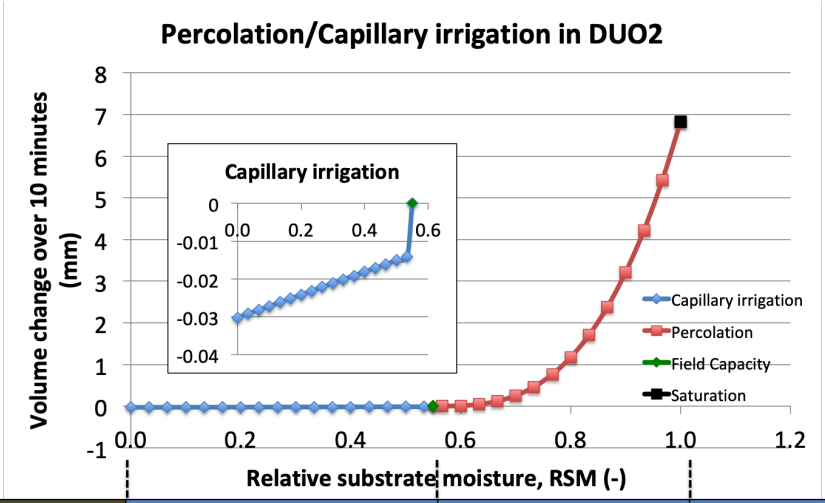

Regime	Oven dry -> Dry	Dry -> Semisaturated	Semi-saturated -> Saturated	Oversaturated
Volume (mm)	$(1-\Delta\theta)*H_s$	0 -> $FC*\Delta\theta*H_s$	$FC*\Delta\theta*H_s$ -> $\Delta\theta*H_s$	
Description	Not in situ	Capillary irrigation	Percolation	Full percolation
Flow Q	/	**MAX{** $(RSM-FC)*\Delta\theta*H_s/\Delta t$; $-Q_{max} * MIN(1 ; H_b/(0.1H_{bmax})) * (1-RSM)$ **}**	($(RSM-FC) * \Delta\theta * H_s$ *Decay) $/\Delta t$	$(VOL - \Delta\theta*H_s)/\Delta t$

Figure 4.2: Overview of percolation and capillary rise (zoom-in) as a function of the relative moisture content in a soil. The formulas are explained in the text.

migrates from the buffer towards the substrate (if there is a buffer). The irrigation only has one important parameter: the upper limit of capillary irrigation. At Wilting Point, the maximal value of capillary rise is attained. From there, the flow decreases with increasing moisture content in the substrate and with decreasing available volume in the buffer. In symbols:

$$\begin{aligned} Q &= \max[(RSM - FC) \cdot \Delta\theta \cdot H_s/\Delta t; \\ &\quad -Q_{max} \cdot \min[1; H_b/(0.1H_{b,max}) \cdot (1 - RSM)]] \end{aligned} \tag{4.5}$$

The maximal flow Q_{max} is determined before the automatic calibration based on the DUO3 measurements of May 2018. There, a long dry period without any new rainfall shows a continuously decreasing water level in the buffer layer. From there, a value $Q_{max} = 4.35$ mm/day $= 5.035 \cdot 10^{-8}$ m^3/s is found.

An overview of the processes of capillary rise and percolation is given in Figure 4.2. The horizontal axis shows the relative moisture content ranging from 0 (Wilting Point) to 1 (Saturation). Below the graph, a table shows the different regimes that are set between Wilting Point, Field Capacity and Saturation. Note that the capillary flow, shown in the zoom-in, is three orders of magnitude smaller than the percolation flow. For the graph, the final parameter values for DUO2 are used for the sake of

illustration. These optimal parameters are determined further on.
A second way to illustrate the interaction between the substrate and the buffer is through a time series of both. This is shown in Figure A.2 in Annex A. There, one can distinguish the different processes, such as capillary irrigation and percolation.

Buffer layer

Outflow A green roof without a buffer has no thickness for this layer. For blue-green roofs, some options are included in the model. A separate parameter is created to let the user choose the desired option.
For DUO3, the buffer option is *direct overflow*. The only remaining parameter is the maximal buffer level. Based on calibration data, a value of $0.9 \cdot H_{b,max}$ is picked, with $H_{b,max}$ the actual height of the layer in mm.
For DUO2, both outflow and direct overflow are possible. This outflow can be defined via a linear reservoir model or another custom discharge equation. Eventually, a non-linear reservoir method is assumed, based on the work of Locatelli [44]:

$$Q = \begin{cases} a \cdot (H_b(t) - H_0)^b & \text{if } H_b > H_0 \\ 0 & \text{otherwise} \end{cases} \tag{4.6}$$

with a en b two unknown parameters. The threshold buffer level H_0 at which outflow starts, is taken equal to 14 mm based on the calibration data. This formula of Locatelli's research is originally for a conventional green roof, so this formula is also assumed for a DUO1 roof as runoff equation for water that percolates through the substrate. For DUO1, this runoff creation starts immediately at $H_0 = 0$.

Hypsometry Finally, the buffer layer also needs a parameter that contains the hypsometric relation. This is the link between the height and the volume of an object. In theory, a rainfall depth of 1 mm is equivalent to 1 litre on 1 normal square metre. The layout of the buffer layer makes the relation between the water level and the water volume less straightforward. In the case of DUO2 and 3, the layer of 80 mm can hold up to 52 litres per square metre [38]. Thus, the linear hypsometric relation becomes $V_{max} = C \cdot H_{b,max} \rightarrow C = 80/52 = 0.65$ L/mm if a linear relation is assumed. Because the overflow threshold is taken at $0.9 \cdot 80 = 72$ mm, the maximal buffer content becomes $0.65 \cdot 72 = 46.8$ mm.

4.2 Calibration of the model

A first attempt to find the adequate parameter values for each roof configuration was done via an existing function in Matlab, *fmincon*. Afterwards, some parameters are further specified based on existing literature and via further manual calibration. The final calibration results for each green roof type are discussed separately.

4.2.1 Automatic calibration using *fmincon* in Matlab

This subsection starts with a short explanation of this automatic calibration. Afterwards, some shortcomings of this approach are listed.

Methodology

The Matlab function *fmincon* minimizes (min) a function (f) given a series of constraints (con). For this concrete application of automatic calibration, the objective function is a summation of the errors of the model with respect to the measured data. This function is then minimized by choosing the best parameter values within physical constraints. For instance, the water retention capacity of a layer (per square metre) is always greater than zero and lower than the height of that layer.
More specifically, the objective function is based on the research from Locatelli [44] and is of the form:

$$f = \frac{w_1}{m}\sum_{t=1}^{m}\frac{(RR_{obs}(t)-RR_{sim}(t))^2}{\sigma_1^2} + \frac{w_2}{m}\sum_{t=1}^{m}\frac{(CRR_{obs}(t)-CRR_{sim}(t))^2}{\sigma_2^2} \tag{4.7}$$

$$\left(+\frac{w_3}{m}\sum_{t=1}^{m}\frac{(WL_{obs}(t)-WL_{sim}(t))^2}{\sigma_3^2}\right)$$

where w_i is the arbitrary weight of each error calculation. A weighted error can be determined for any variable that is simulated and measured. Frequent options are the cumulative rainfall runoff volumes (CRR) and the runoff volumes (RR), as is done in Locatelli's work [44]. For this research, the water levels in the buffer layer (WL) can also be used (for DUO2 and 3). This way, the function f becomes a sum of two or three error summations. For each objective with m observations, the offset between the observed and simulated value at time t is squared and scaled according to the variance σ_i^2 of the observed values from objective i.

Limitations

Application of this method led to some intermediate results that were not satisfactory yet. An important reason for the mediocre results is without a doubt the large amount of parameters that are kept for optimalisation. Moreover, Locatelli utilised a more complex algorithm than this Matlab function to end up with good parameters [44]. A few challenges that are linked with this methodology are further explained here.
First of all, the optimization sometimes had a tendency to propose a 'zero-solution'. Here, the parameters are set in such a way that the model does not produce any runoff. This is partly a shortcoming of the applied method, and partly a bad choice of weighting coefficients w_i. On the one hand, the applied method can converge to a local minimum for f. On the other hand, the optimization will prioritize the larger w_i in the equation. If the user chooses not to prioritize the runoff time series, it becomes easier to make it completely zero instead of matching the 10 runoff spikes of one minute in a time series of 8 months. A possible solution can be to determine

a better starting point for the iterations, and a better choice of w_i.

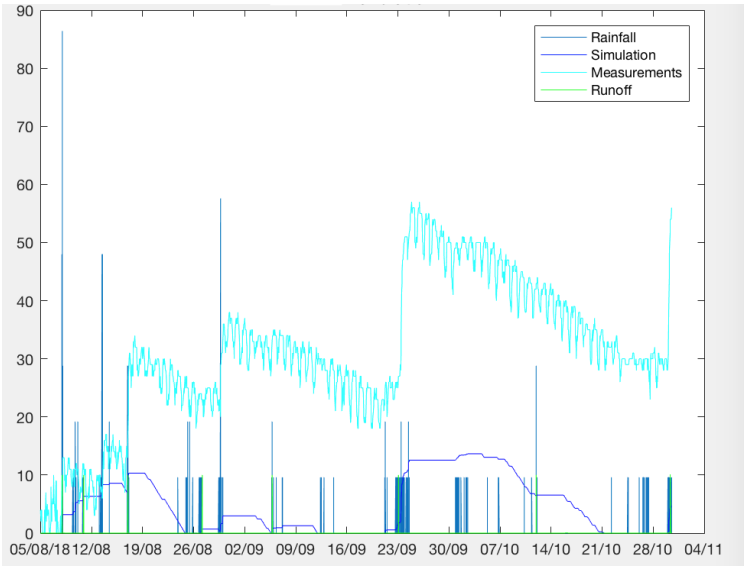

(a)

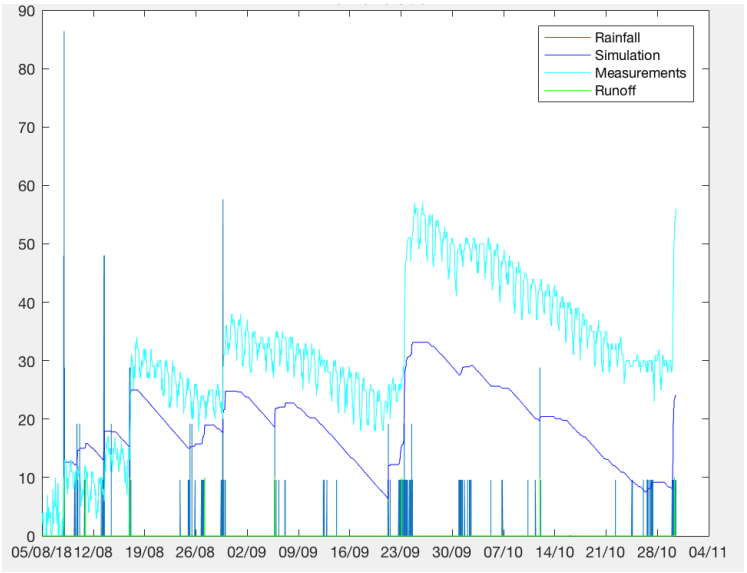

(b)

Figure 4.3: Calibration of DUO3. Both plots show simulated and measured water levels in mm, along with rescaled rainfall and runoff measurements. These last two series are added to expose the interaction between the buffer and the weather. (a) Before calibration, the simulated water levels are bad (b) After calibration, the results are better but the retention capacity is not realistic.

Secondly, the convergence could lead to physically acceptable values that are not logical. Figure 4.3 shows an automatic calibration for DUO3 where the substrate storage goes from 25 mm to only 5 mm or 5 litres per square metre. This value does not correspond in any way to results from literature. Moreover, DUO1 and 2 end up with higher values for retention, even though the substrate thickness is less than half the thickness in DUO3. All this leads to the conclusion that this value is not applicable.
Lastly, Figure 4.4 shows the accuracy that has been obtained via a typical automatic calibration. The last two graphs in this Figure clearly demonstrate that a further fine-tuning of the model parameters after application of the *fmincon* function can have a big positive effect.

4.2.2 Final choice of parameter values

In addition to automatic calibration, another approach was tested. As stated before, the large pool of unknown parameters does not allow for an immediate and good result. Therefore, the new strategy involved predefining more parameters based on literature and physical reasoning. Figure 4.5 presents an overview of all the sources for the final values.
Most scientific publications publish their parameter values along with their model structure. These values can sometimes, after critical analysis, be used directly or as an indication of parameter values for the new model structure. These values are then further fine-tuned via manual calibration.

Surface storage In the absence of heavy intensity rainfall events since the beginning of the measurements, it is hard to assess the surface storage capacity and the infiltration rate of the green roofs. For these two variables, literature provides a good order of magnitude, from which manual calibration is attempted.
Generally a surface storage only describes the formation of pools on the surface when the water infiltrates too slowly. Normal values for surface storage on impervious surfaces are between 1-3 mm [35].
For the infiltration capacity, the assumption is now made that rainfall intensities up to a shower with period of occurrence of 20 years can almost certainly infiltrate without a problem. Note that this assumption would need to be confirmed by means of an experiment.
Under this assumption, the graph from [12, Willems, 2011] shows that a T20 rainfall event has an intensity around 110 mm/h. This is assumed as upper boundary for further manual calibration.

Substrate storage To come up with good values for the actual evapotranspiration, a good Crop factor needs to be determined. The Joint Research Centre of the European Commission stores a database containing several crop parameters. More specifically, appendices C and D from the publication of the European Soil Data

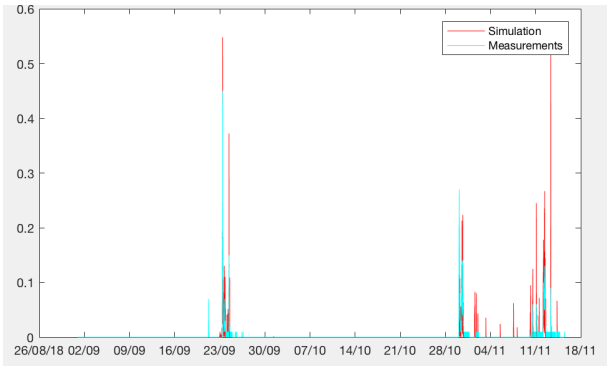

(a) Before calibration, measurements and simulations do not match properly.

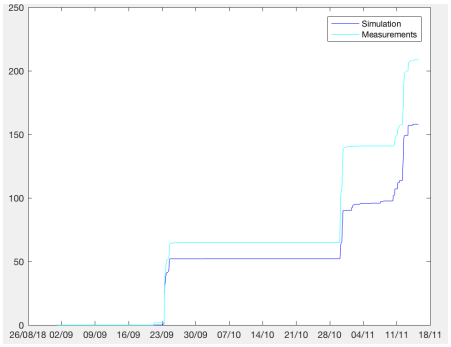

(b) The model greatly underestimates the runoff.

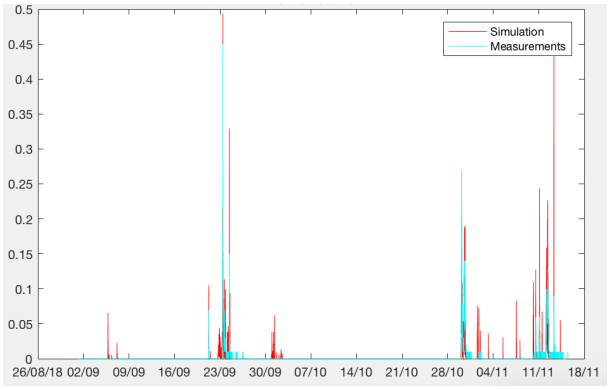

(c) After *fmincon*, the runoff time series still overestimates a lot of the peaks.

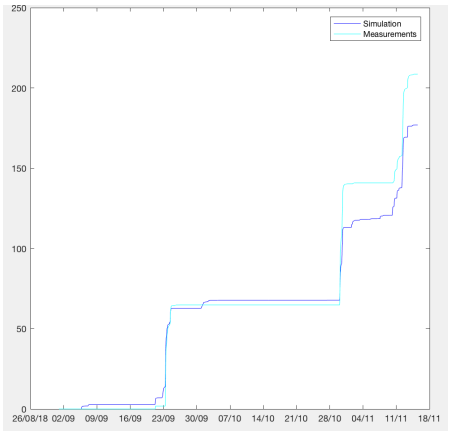

(d) The cumulative runoff is approximated better.

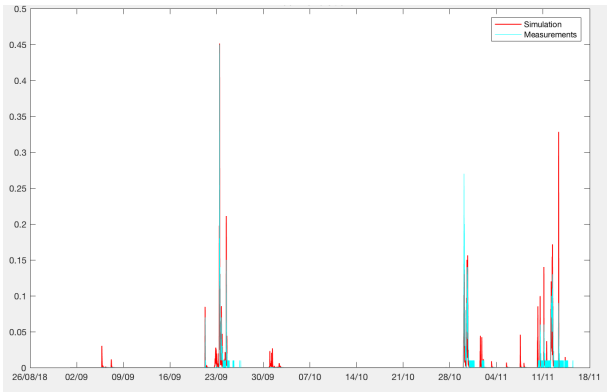

(e) The runoff time series is better approximated by changing the detention parameters.

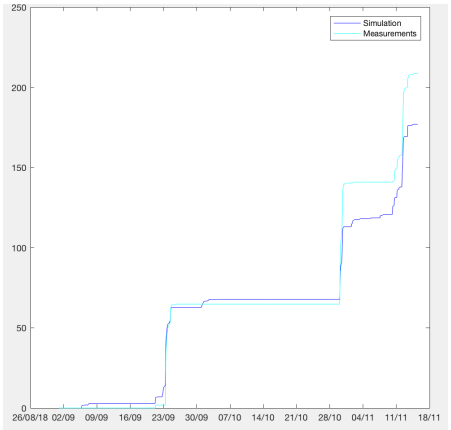

(f) The cumulative runoff remains the same.

Figure 4.4: DUO1: (a-b) Before calibration, (c-d) After automatic calibration, (e-f) After fine-tuning. Light blue represent measured values, red and dark blue show simulated values.

Centre from 2001 contain crop parameters for common vegetation types [96]. There, Table D.1 shows the PFAC, the pan evaporation factor. Values range from 0.72 (hops and vines) to 1 (grass). Even though *Sedum* is not present in the table, this shows that the reduction on the pan (potential) evaporation should remain limited. According to the product folder from Vegetal i.D. [38], the retainable water volume of their blue-green roofs ranges from 80 L/m^2 to 95 L/m^2. Taken 52 litres into account for the buffer, the substrate layer is responsible for some 28-43 litres. For DUO3 with a thicker substrate layer, this value could be even higher.
To obtain the parameter value $\Delta\theta$, this volume needs to be divided by the substrate volume (as the unit is mm/mm or m^3/m^3).

Buffer storage As the outflow equation for DUO2 is based on Locatelli's work [44], his values for a and b serve as a starting point and a good order of magnitude. For Locatelli, the values for a and b were 0.215 mm^{-1}·min^{-1} and 1.67 respectively. In what follows, the final selection of parameters values is given for all three green

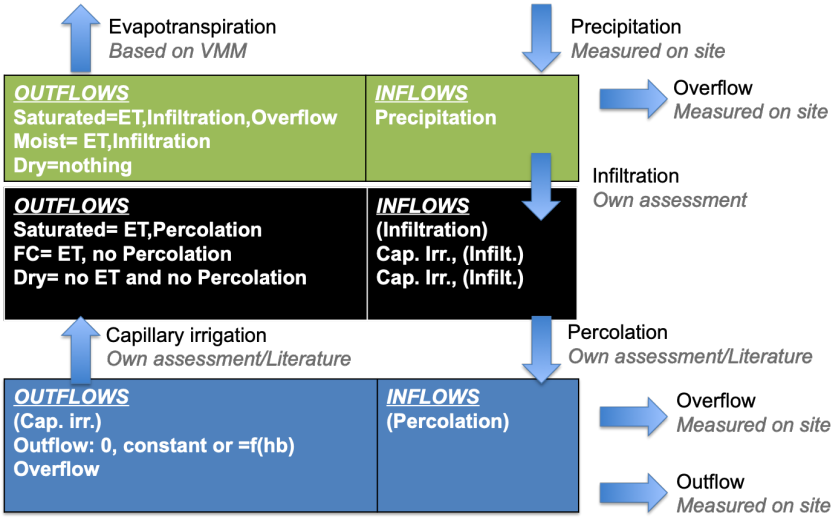

Figure 4.5: Overview of all in-, inter- and outflows and their origins in the final calibration result.

roof types. The match with the calibration data is verified qualitatively via different plots in this text. Apart from that, the simulation results for water levels in DUO2 and 3 are evaluated using the Nash-Sutcliffe Efficiency (NSE) number.

4.2.3 Conventional green roof (DUO1)

For the conventional green roof, the final parameter values are shown in Table 4.1. Parameters that do not matter for a conventional green roof are intentionally left out to keep the table clear, but are best put to zero.

Two interesting plots to analyse are the rainfall runoff and the cumulative rainfall runoff during the calibration period. Figure 4.6 contains both. The runoff chart

Table 4.1: Overview of the selected parameter values for DUO1.

SURFACE	
Infiltration (mm/h)	78
Storage (mm)	2
Overtopping	no detention
SUBSTRATE	
H_s (mm)	60
$\Delta\theta$ (mm/mm)	0.5
Field capacity, FC (-)	0.5
Leaf Area Index, LAI (-)	1
Crop factor (-)	0.97
substrate_exponent (-)	3
BUFFER	
$H_{b,max}$ (mm)	0
Option	discharge equation
Hypsometry (m^3/m)	1
Coefficient a ($1/m^3/10$ min)	0.3
Coefficient b (-)	1.4

shows that, apart from one peak in summer, the simulation never underestimates the runoff from the roof, which is a conservative approach. The one peak that is missed occurs right after a period of more than a month with hardly any rainfall. These extremely dry conditions might have lead to changes in the green roof mechanism, which explains this mismatch. One example could be slow infiltration on a soil crust, leading to overland runoff. Another possibility is that the bad state of the vegetation leads to inferior detention and retention capabilities.
Overall, in a period with more precipitation like the autumn months, the green roof is more successful in simulating the runoff.
Looking at the overall cumulative runoff, one notices again a conservative approach. The simulated runoff is some 10% overestimated from the measurements after 8 months. A double validation with green roofs in France will have to determine if the model is robust enough to correctly simulate other rainfall events.

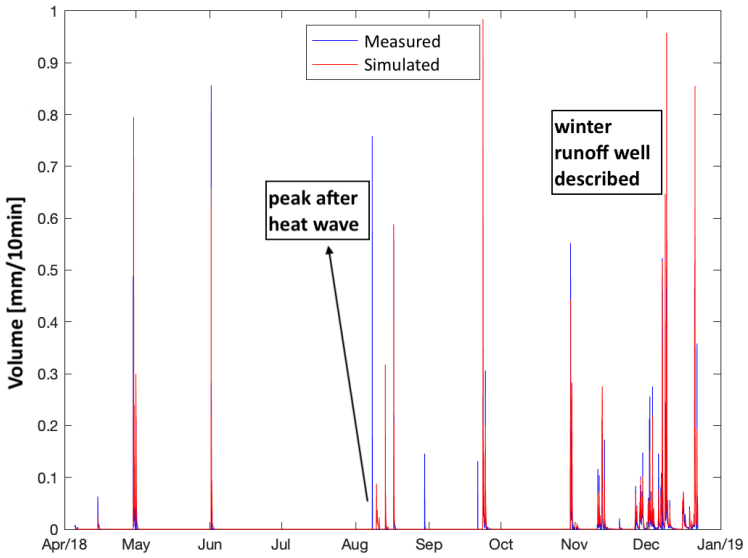

(a) Rainfall runoff

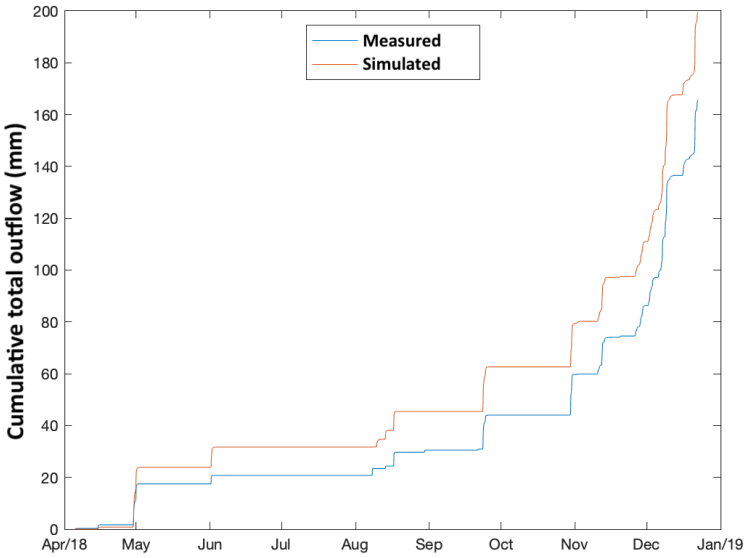

(b) Cumulative volumes

Figure 4.6: Measured versus simulated data for DUO1 in Antwerp after the final calibration.

Table 4.2: Overview of the selected parameter values for DUO2.

SURFACE	
Infiltration (mm/h)	40.97
Storage (mm)	2
Overtopping	no detention
SUBSTRATE	
H_s (mm)	80
$\Delta\theta$ (mm/mm)	0.375
Field capacity, FC (-)	0.55
Leaf Area Index, LAI (-)	1
Crop factor (-)	0.97
substrate_exponent (-)	4
Capillary max Q_{max} ($m^3/m^2/s$)	5.03E-08
BUFFER	
$H_{b,max}$ (mm)	72
Option	discharge equation
Hypsometry (m^3/m)	0.65
Coefficient a ($1/m^3$/10 min)	0.3
Coefficient b (-)	1.4

4.2.4 Blue-green roof with controlled outlet (DUO2)

The settings for a blue-green roof with controlled outlet are mentioned in Table 4.2. Important things to note compared to DUO1 are the maximal infiltration, the value for $\Delta\theta$ and the buffer settings. The different infiltration rate follows from manual calibration to describe the runoff peaks better. Even though $\Delta\theta$ is different, it retains in fact the same volume as DUO1, 30 mm. Dividing it by the substrate thickness H_s to make this volume dimensionless results in $30/60 = 0.5$ for DUO1 and $30/80 = 0.375$ for DUO2.
Concerning the buffer settings, explanation can be found in the earlier section of this chapter.

Figure 4.7 shows the individual and cumulative rainfall runoff for DUO2. A first important conclusion is that the total recorded runoff of 111.2 mm in the calibration is very low. On top of that, the majority of it is concentrated in the autumn months. All measurements until mid September add up to a mere 10.49 mm, some 10% of all runoff. This makes a robust selection of parameter values very difficult.
As indicated on the figure, some small runoff events start with a small, isolated peak. This is here attributed to the bypass of rainwater, as explained by Figure 3.5 in the previous Chapter. Apart from those peaks, some other summer runoff is also absent in the simulation results (peak in June and in August). However, these measured peaks are small and they often occur at unexpected moments such as at low measured water levels. On top of that, the simulated cumulative runoff shows a good overall performance and the water levels shown in Figure 4.8 show a good

description of the internal processes. The NSE value for the water levels equals 0.8793, which shows a strong correspondence between recorded and simulated data.

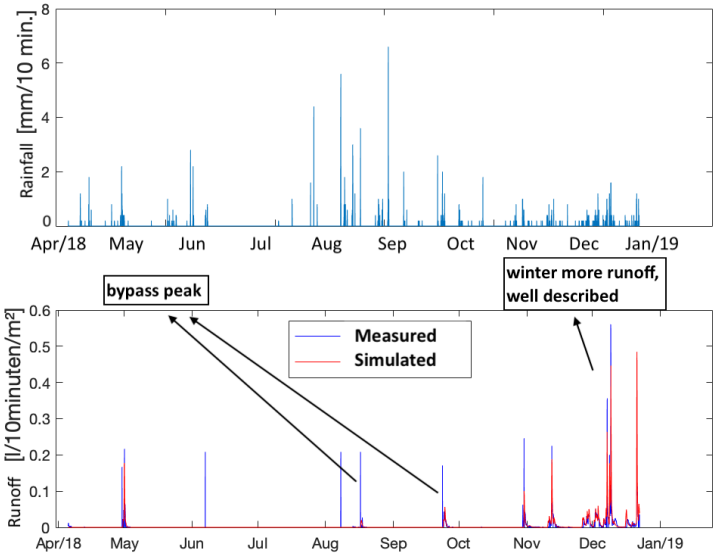

(a) Rainfall runoff

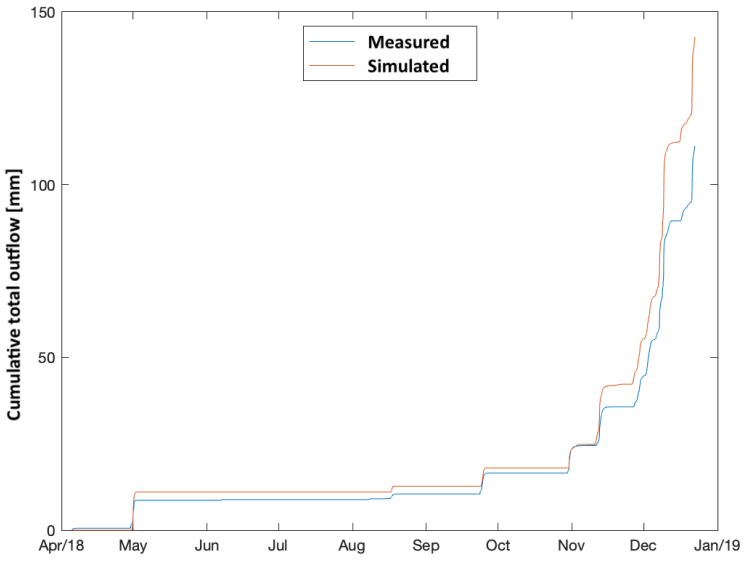

(b) Cumulative volumes

Figure 4.7: Measured versus simulated data for DUO2 in Antwerp after the final calibration. The explanation for the bypass peaks is already shown in Figure 3.5.

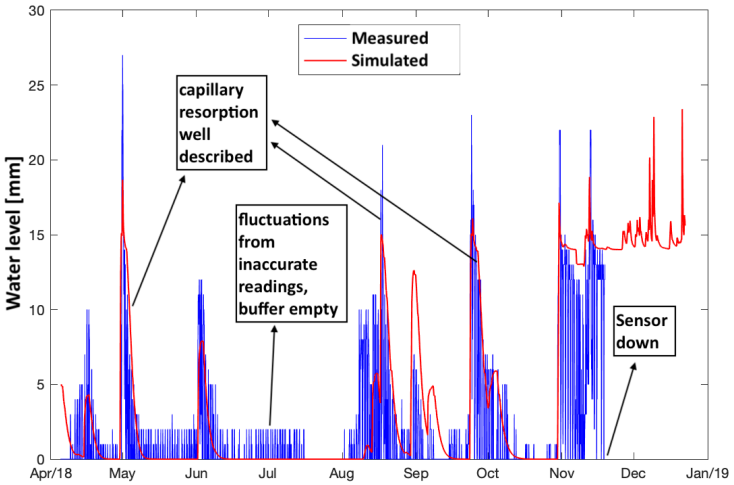

Figure 4.8: Measured and simulated water level data for DUO2 in Antwerp.

4.2.5 Blue-green roof without outlet (DUO3)

The final parameters for the DUO3 type are listed in Table 4.3.

Table 4.3: Overview of the selected parameter values for DUO3.

SURFACE	
Infiltration (mm/h)	40.97
Storage (mm)	2.74
Overtopping	no detention
SUBSTRATE	
H_s (mm)	200
$\Delta\theta$ (mm/mm)	0.225
Field capacity, FC (-)	0.35
Leaf Area Index, LAI (-)	1
Crop factor (-)	0.72
$substrate\_exponent$ (-)	3
Capillary max Q_{max} ($m^3/m^2/s$)	5.03E-08
BUFFER	
$H_{b,max}$ (mm)	72
Option	direct overflow
Hypsometry (m^3/m)	0.65

Note that the Crop parameter is chosen quite low, which resulted in good water levels in the buffer layer. From a biological perspective, this seems odd, as the vegetation type is identical to DUO2 which has a high crop factor. The only difference between DUO2 and 3 is the substrate thickness. For members of the genus

Sedum, translated to English as stonecrop, this extra soil is not really necessary. For instance, the species *S. acre* has been observed to grow on rocks and thin layers of soil in the wild [97, Gabrych et al., 2016]. Moreover, the fact that extensive green roofs are easy to implement on roofs without large structural modifications, explains why most research on succulents like *Sedum* is done for a substrate thickness under 10 cm [38, 29, 50][98, Van Woert et al., 2015].
If a green roof has to support larger vegetation like grasses, research typically recommends deeper substrate layers around 20 cm instead of 10 cm [97][99, Dunnett et al., 2008].
This leads to believe that the extra substrate depth in DUO3 is mainly interesting for herbaceous plants with deeper roots. As these grasses did not develop well during the dry spring and summer, the lower parts of the substrate are probably less exposed to evapotranspiration from the *Sedum* species with low root depths. A lower crop factor is an effective way to model this lower uptake and evapotranspiration of water by plants. Consequently, this higher soil saturation allows for faster percolation and higher, more correct water levels in the buffer.
Other values which might draw the attention of the reader are the lower Field Capacity and the content $\Delta\theta$ compared to DUO1 and DUO2. However, one needs to consider these together with the substrate thickness H_s, which is a lot higher. Overall, DUO3 has a larger retention capacity $\Delta\theta \cdot H_s$ than DUO1 and DUO2. Admittedly, the increased capacity is not proportional to the extra substrate thickness. Since DUO3's substrate type is identical to DUO1 and DUO2, this seems odd. However, several arguments can confirm this decision. Firstly, the special circumstances in the calibration period are mentioned above for the crop factor. The condition of the blue-green roof might have had an influence on the retention capacity as well. Secondly, the research of Feitosa also showed that among the substrate depths of 5, 10 and 20 cm, there was no significant difference in the efficiency [39]. Lastly, the validation results discussed in the next section give reason to believe that these calibration values might be correct for the calibration period, but the normal condition of the roof might need slightly higher parameter values.
From Figure 4.9, it is clear that the measured runoff in the calibration period is very low. Therefore, calibration based on cumulative volumes or peak volumes is very challenging. Instead, the water level in the buffer layer serves as reference data. The comparison between the measured and the simulated data, shown in Figure 4.10, results in a very good match (NSE=0.9854). Indicated on the figure are the declining water levels during capillary rise.

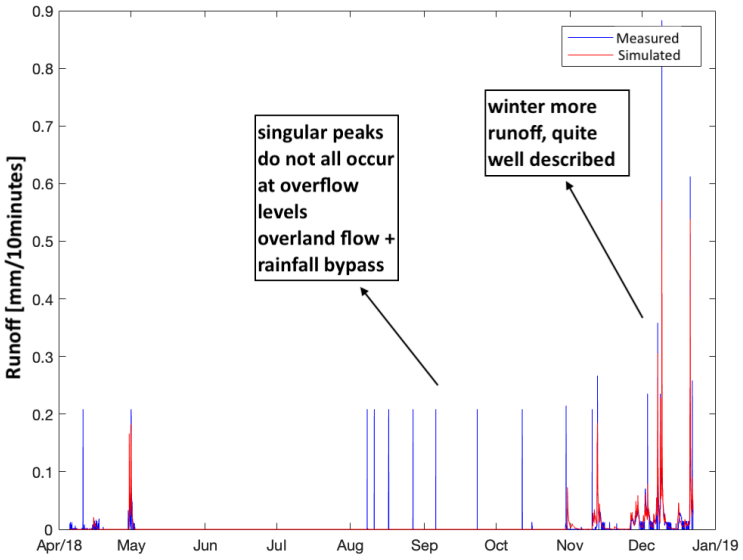

Figure 4.9: Measured and simulated runoff data for DUO3 in Antwerp.

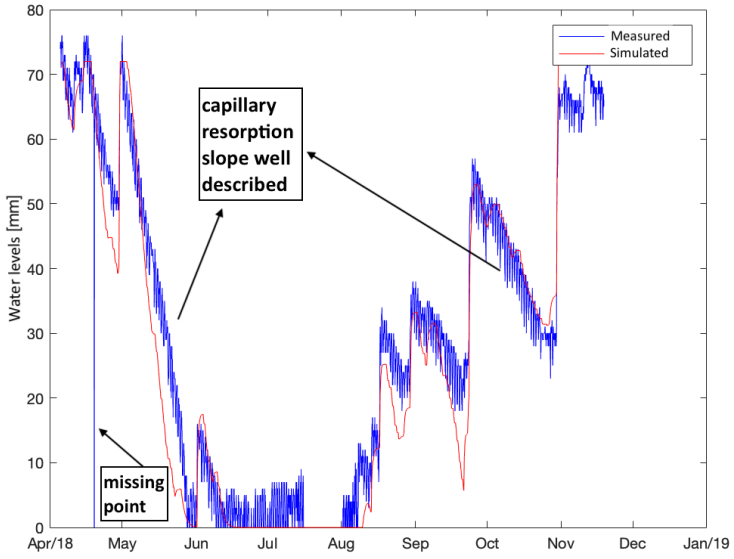

Figure 4.10: Measured and simulated water level data for DUO3 in Antwerp.

4.3 Validation of the model

This section presents the results of the validation process. Both test sites in France, Ivry and Mions, contain green roofs of type DUO1 and DUO2. Here, the model performance is evaluated for each roof type separately.

4.3.1 Conventional green roof (DUO1)

Ivry test site

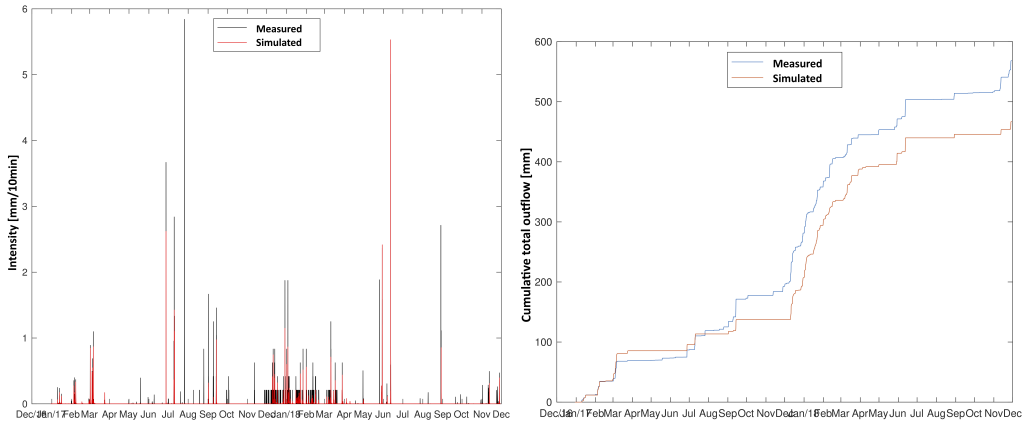

(a) Rainfall runoff (b) Cumulative volumes

Figure 4.11: Measured versus simulated data for DUO1 in Ivry. The validation period starts at January 2017 and goes on until December 2018.

The measurements in the vicinity of Paris run from January 2017 until December 2018. The time series of rainfall and runoff are presented in Figure 4.11.
The simulated runoff follows the measurements quite well. The only two deviations are a large peak in July 2017 which is not simulated and a peak in June 2018 which is exaggerated in simulations. A few minor peaks are also measured, but do not appear on simulations.
The cumulative plot shows that the model systematically underestimates the volume that runs off from the green roof by some 20%. When looking at the runoff graph, it is also clear that the simulation never catches the full peaks.
However, this result does not mean that the model calibration was performed in a bad way. The climate in Antwerp and Paris shows some similarities, but annual rainfall averages differ. On top of that, the roof configuration was assumed identical, which is not completely certain. Plants might thrive better in one climate than another. Moreover, the evapotranspiration time series is constructed artificially from monthly averages by dividing this average value equally over each time step of 10 minutes. This is a rough estimation, since evaporation rates typically fluctuate a lot more.

Despite all the critical remarks, it is still possible that the calibration process had its shortcomings. The main issue is the limited length of the time series, which does not allow for very precise parameter values.
Considering all this, the calibrated model seems acceptable to continue with. The second validation in Mions will serve as a *second opinion*.

Mions test site

In Mions, the rainfall time series is longer and ranges from the end of 2015 until 2018. On top of that, hourly evapotranspiration rates are known. This validation is therefore more valuable. As stated in section 3, the provided evaporation data contains zeros from July 2015 until November 2015. Therefore, this part of the simulation cannot be considered. Directly after this period without evaporation, the simulation generates two large runoff peaks at the beginning of 2016, which is not measured on the green roof. Because this occurs at the start of the simulation period, this is probably due to the oversaturated green roof in the absence of evaporation in 2015, leading to a faster generation of runoff. Therefore, the validation period is reduced from February 2016 until December 2018.
Figure 4.12 shows the collected data, along with the simulation results. The rainfall runoff time series indicate a decent replication of the measurements. When disregarding the two faulty peaks around January 2016, only one large runoff peak is missed by the model. Other than that, the model either describes the measurements well, or overestimates the measurements.
Contrarily to the validation in Ivry, the model gives a overestimation of the total runoff volume. Also, the course of the cumulative plot also indicates that the overestimation is not systematic. The test site recorded more rainfall in the first part, after which the simulation generates more rainfall.
This validation leads to the conclusion that the calibration is performed correctly. It is more reliable than the one in Ivry because of the evaporation data, and the overall overestimation of the runoff volumes makes the model performance conservative.

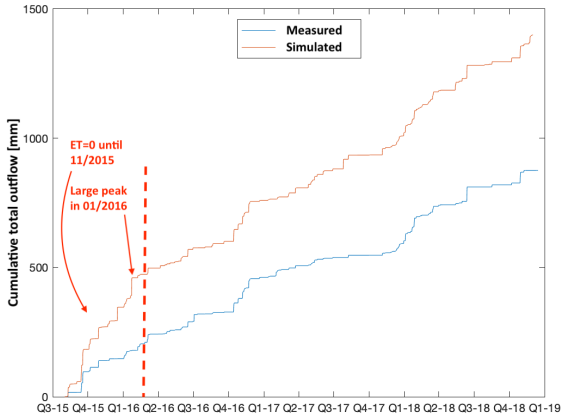

(a) Cumulative volumes from July 2015 onwards.

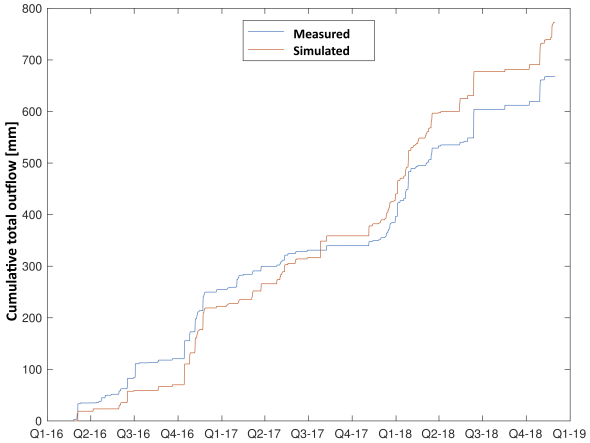

(b) Cumulative volumes after January 2016

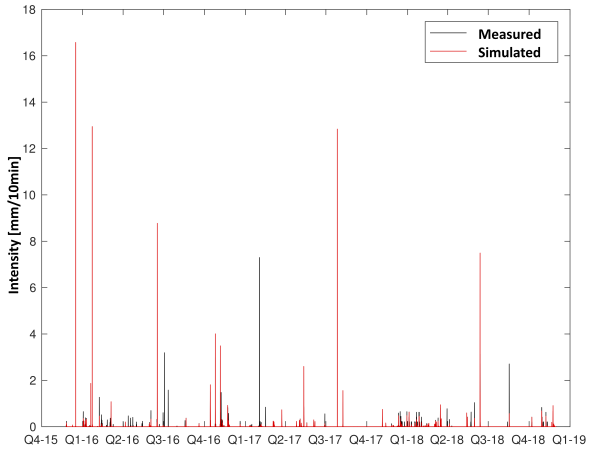

(c) Rainfall runoff

Figure 4.12: Measured versus simulated data for DUO1 in Mions. The data before January 2016 is not useful, since no evaporation data is known here.

4.3.2 Blue-green roof with controlled outlet (DUO2)

Ivry test site

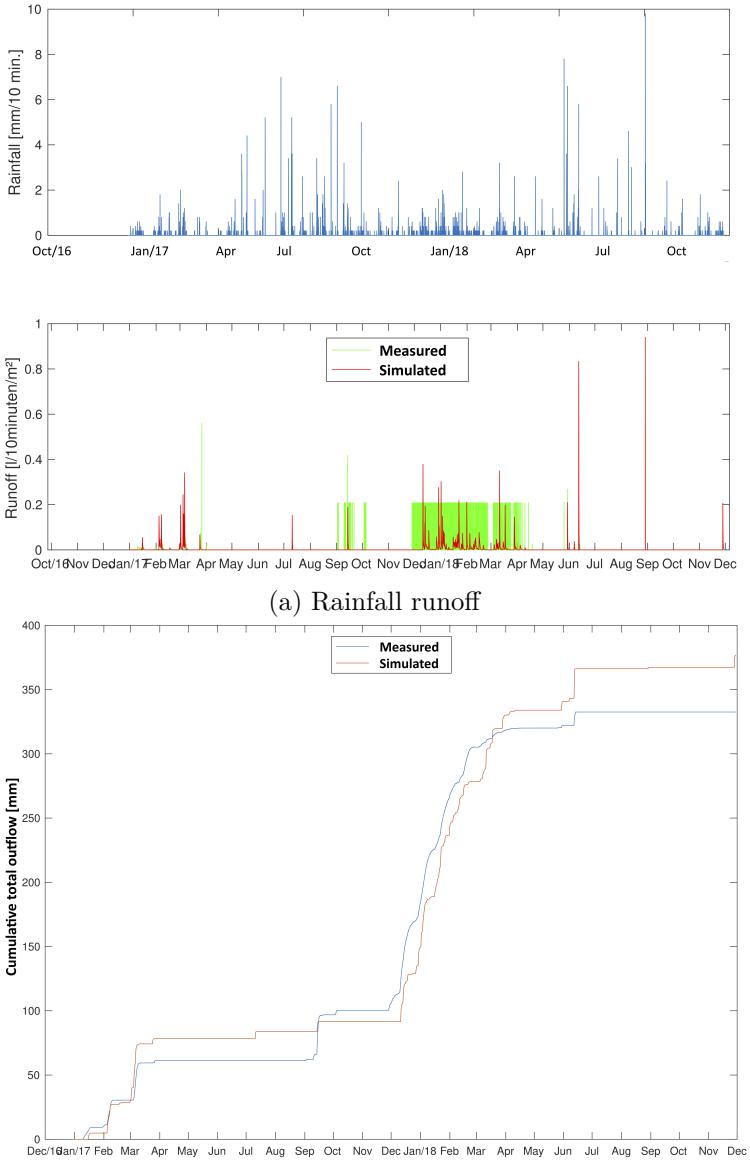

(a) Rainfall runoff

(b) Cumulative volumes

Figure 4.13: Measured versus simulated data for DUO2 in Ivry.

For the blue-green roof with a controlled outlet, the same validation procedure is repeated. Figure 4.13 compares the measured and simulated runoff values.
The resolution of the recorded runoff seems limited to 0.2 mm per 10 minutes, which makes the validation of the peaks in the winter and spring period hard. However, the cumulative runoff plots follow each other very well during the winter and spring

months. This indicates that the volumes are correctly simulated in this period.
Outside of the winter months, only few runoff is recorded. In the last months the model generates a few isolated runoff peaks which are not present in the measurements. The peaks in June 2018 are almost completely responsible for the overestimation of cumulative volumes.
Overall, no real grave errors are noticed, and the model performs in a conservative manner. Moreover, it should again be noted that the roughly estimated evaporation rates might have an influence on the results.

Mions test site

Next, the Mions test site is investigated again. Here, two blue-green roofs are provided to validate the model. Figure 4.14 contains the data for the blue-green roofs, along with the simulation results. Again, the graphs are clipped because of the bad evaporation data in 2015. On top of that, one of the green roofs has an incomprehensible runoff peak around June 2016 which occurred in absence of rainfall. This is most likely due to actions on the test site. Perhaps the buffer was clogged and completely emptied on this moment. This long and large peak skews the cumulative plots. However, after this jump in cumulative volume, the three graphs continue in an almost parallel way. The clipped version of the cumulative plots shows that the model again performs conservative, ending 9% and 30% above the measured total volume. The 9% offset is due to two rainfall events (indicated on the figure) and an overestimation of the winter runoff volumes.
The water levels in the buffers are also measured on site, but this data does not run over a continuous period. On top of that, the water levels in both buffers are not identical. This data is not further considered, taking in mind the good results of the runoff simulation.
In conclusion, the calibration of the blue-green roof model with outlet can be considered acceptable based on the two independent validations.

4.3.3 Blue-green roof without outlet (DUO3)

Lastly, the third green roof type requires a validation. Since no other test site is known, measurements from Antwerp are used. The validation period runs from 20 November 2018 until 13 May 2019 and follows directly after the calibration period. The rainfall in this period is presented in Figure 4.15a. The simulated and measured water levels in the buffer are shown in Figure 4.15b.
Compared to the calibration period (see Figure 4.10), the model performs worse in simulating the water levels. In the winter months, from November until mid February, the water levels are acceptable. There, they remain at overflow level more or less continuously. However, when the spring starts, the real substrate appears to start the uptake of water from the buffer a lot sooner. On the other hand, after the long dry period in April, the real roof takes longer to replenish the buffer.
Since this validation data only came available very late in this research, a recalibration was no longer possible. All DUO3 simulations which follow in this research, are

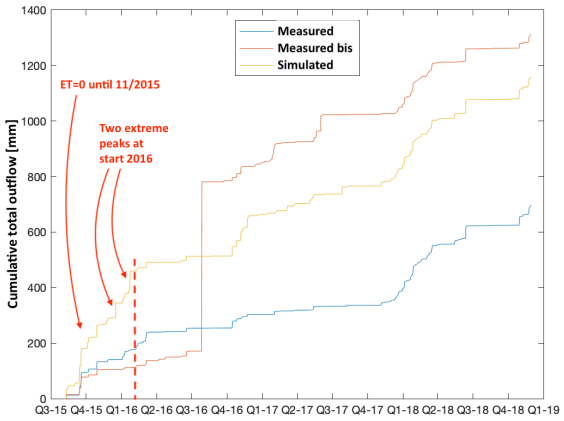

(a) Cumulative volumes

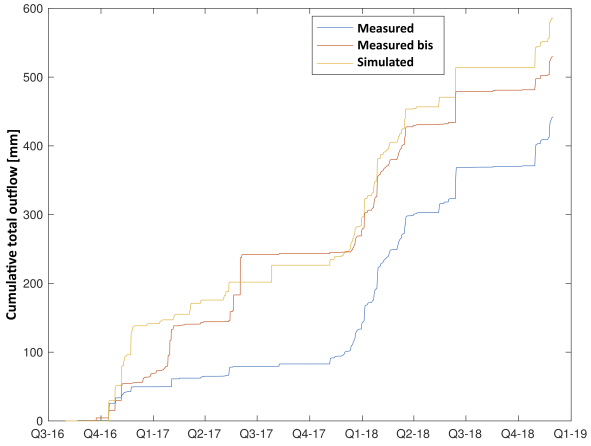

(b) Cumulative volumes after June 2016

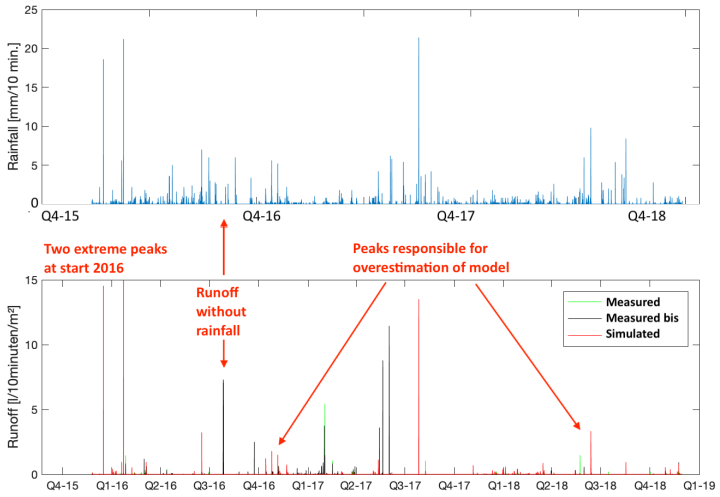

(c) Rainfall runoff

Figure 4.14: Measured versus simulated data for DUO2 in Mions.

conducted with these suboptimal parameter values. So, comparison of simulation results is still possible, but the results will not reveal the real potential of a DUO3 green roof.

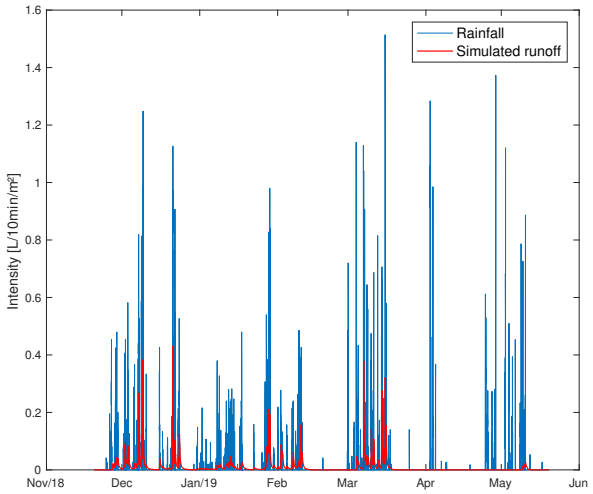

(a) Rainfall and simulated runoff

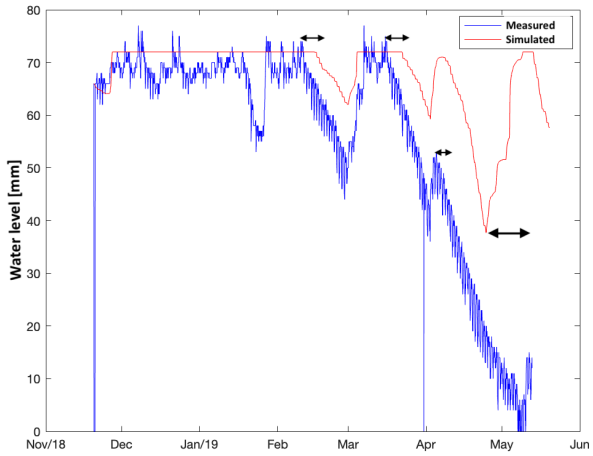

(b) Measured and simulated water levels

Figure 4.15: Validation for DUO3 in Antwerp. The black arrows indicate that the substrate's retention capacity is calibrated too small, leading to sooner uptake of water from the buffer, and later percolation towards the buffer.

Critical remarks

Parameters The fact that the simulated buffer starts emptying sooner and refilling later than the real buffer indicates that the retention capacity of the substrate layer was underestimated in the calibration. Three parameters can be responsible for this. Either the volume of the substrate is too low, the field capacity point in the substrate is put too low, or the evapotranspiration rate which restores the capacity of the substrate is too low. Indeed, if more volume can be stored in the substrate, less water ends up in the buffer. Also, if the substrate already starts interacting with the buffer at a higher soil moisture (higher field capacity), the uptake of water to the soil will occur faster and the percolation towards the buffer will start later after a dry spell. Thirdly, if the plants release more water to the atmosphere, the substrate falls empty faster, resulting in a faster uptake of water from the full buffer.
In the calibration of DUO3, the low values for all three parameters were already noticed, but gave a good match with that dataset. At least one of these parameters would need to be reconsidered once a longer calibration period is collected.

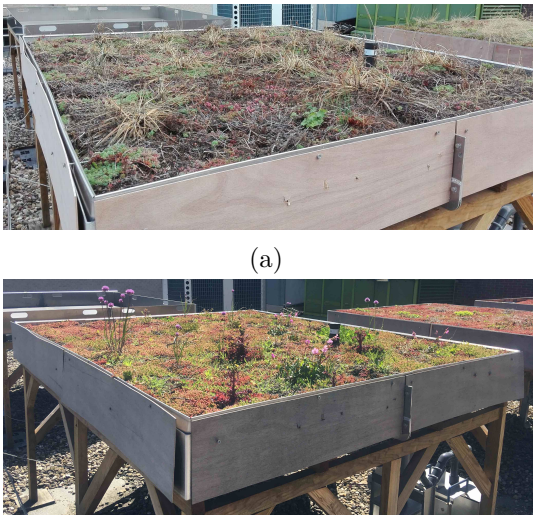

(a)

(b)

Figure 4.16: The different DUO3 vegetation in (a) August 2018 and (b) May 2019 (pictures by Ewout Vereecke).

Test site Apart from the model parameters, other factors contribute to the differences between the simulation data and the measured data. Firstly, the condition of the green roof in 2018 is not comparable to its condition in 2019. Because of an exceptionally dry summer in 2018, the grasses on the DUO3 roof did not grow well. In May 2019, this situation is quite different. Grasses and weeds are present in between the *Sedum* plants. Both situations are depicted in Figure 4.16. This can partly explain the better retention of water in the substrate layer and the higher evapotranspiration. This would mean that the calibration in itself was done cor-

rectly, but the condition of the roof during the calibration period was not a good representation of the roof in general.
Secondly, the rain gauge on the test site in Antwerp was down for quite a long time between January and May. Because of this, a dataset from the weather station in Melsele is used during validation (for location, see Figure 3.6). This rain gauge is located a lot further, and only measures each 15 minutes instead of each minute. This also contributes to the aberrant simulation results.
If recalibration occurs in future research, the dry summer in 2018 and the different rainfall data in 2019 should be taken into account.

4.4 Long term simulations for one roof

This section summarizes the results of long term simulations on an individual green roof. The roof is subjected to a synthetic rainfall and evaporation time series of 100 years, as explained in Chapter 3. Both hydrological performance and drought stress resistance are evaluated. The former is done by quantifying the retained volume, the latter by checking the periods of drought for the vegetation.

4.4.1 Hydrological performance

In order to compare the retention capacity of each roof type, the most useful tool is to quantify the different in- and outflows of the model. Figure 4.17 shows the water balance for each roof type. The bar at the left hand side is the total input. This is the sum of the precipitation during the simulation and the initial volume present. The other bar symbolizes the total outflow and remaining volume at the end of the simulation. Here, one is able to see the conversion from rainfall (left) to runoff (right).

Table 4.4 shows the cumulative volumes over 100 years for each green roof type. To check the data, the average annual rainfall can be calculated. Dividing the rainfall of 80.54 m^3 by 100 and multiplying by 1000 gives an annual rainfall of 805.4 mm. This value is close to the average of 848.4 mm [81]. The table indicates that DUO2 creates the lowest amount of rainfall runoff, evacuating only 50.7% of all precipitation. In comparison to DUO1, the buffer and thicker substrate in DUO2 explain the higher retention. In comparison to DUO3, the benefits from the micro-outflow in DUO2 outweigh the effect of a thicker substrate in DUO3. Because the capillary irrigation is such a slow process, the static buffer remains quite full throughout the year. This lowers the retention capacity of DUO3, which explains the slightly lower performance on the long term.
From this, the hypothesis can already be formulated that DUO2 is the most effective in flood reduction on an urban scale. It should however be noted that the performance of each type is quite similar when looking at the long term. In comparison to the water balances obtained in the calibration period (see A.1), this result is not very intuitive. There, the DUO2 and DUO3 roof perform a lot better. However, several circumstances need to be considered.
First of all, the calibration period does not contain the winter months January

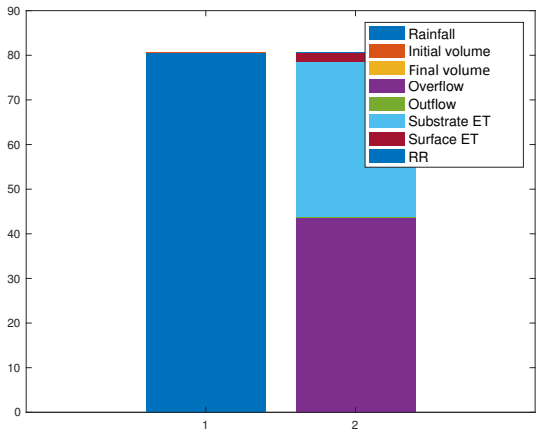

(a) DUO1

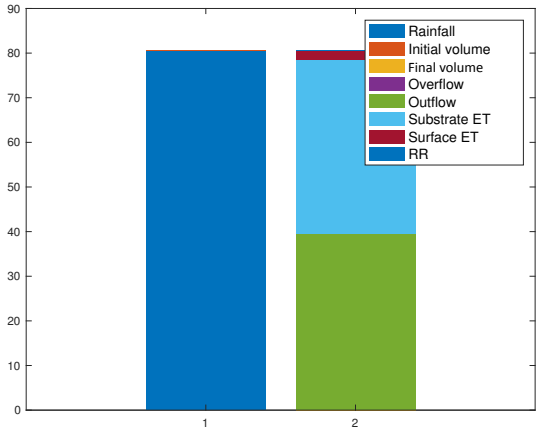

(b) DUO2

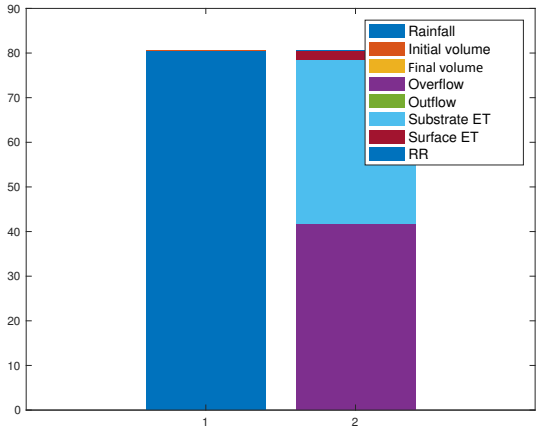

(c) DUO3

Figure 4.17: Water balance for three roof types over 100 years, expressed in m^3. Index 1 is input, 2 is output. DUO1 is a conventional green roof, DUO2 is a blue-green roof with discharging buffer, DUO3 is a blue-green roof with static buffer.

Table 4.4: Overview of the hydrological performance of each green roof type.

	DUO1	DUO2	DUO3	
Rainfall P	80.54	80.54	80.54	m^3
Runoff RR	43.74	39.52	41.68	m^3
Evaporation ET	36.78	40.86	38.68	m^3
Efficiency ($=ET/P$)	45.7	50.7	48.0	%

and February. These are characterised by low evaporation rates and frequent, low intensity rainfall. The buffer in DUO3 remains full due to the low evaporation so, all this rains becomes runoff. In DUO2, all rain percolates and leaves the buffer via the continuous outflow. If this period would have been in the calibration, the balances would have shifted towards a lower performance.
Secondly, the calibration period is one with a very low amount of rainfall. This is ideal for roofs with a large retention capacity, since this allows a full recovery of its potential via evaporation. For instance, the entire static buffer from DUO3 ran dry in the month of May. However, for a green roof such as DUO1, the smaller substrate can restore its capacity a lot faster than a thicker DUO3 with a full buffer. This means that the long dry periods during calibration favour the blue-green roofs. In periods with more rainfall, the antecedent conditions of the three roof types would differ less. This explains why the performances in the long term simulations differ less.
Thirdly, this water balance does not show *when* the runoff is created. This behaviour will be investigated directly on an urban scale in the next section.
In conclusion, the long term simulations for a single green roof tell a different story than simulations of the calibration period. Apart from the main causes listed above, the parameter values might also play a role in this result. If a larger calibration period is available, this should be investigated in more detail.

4.4.2 Reduction of water stress

In order to asses the water stress for the vegetation, two indicators can be considered. Firstly, the buffer is used to irrigate the plants during dry spells via capillary effects. Thus, an empty buffer indicates drought for the plants. Secondly, the water content of the substrate layer (expressed as mm/m^2) shows the actual moisture that is directly accessible by the plants. On top of that, the substrate water content is a stricter indicator. If the substrate layer is dried out, this implies that the buffer cannot provide water any longer. Lastly, defining water stress based on the substrate also allows comparison with conventional green roofs (DUO1).
On the other hand, the internal processes in the substrate layer are less certain. Because the water levels in the buffer were calibrated directly to data, this less strict but more certain indicator is also considered in the discussion of the results.
For both the buffer and the substrate layer, a summation is made of all the time steps of 10 minutes where the water level goes below 1 mm.

This sum can be expressed as a duration in days and divided by 100 to obtain the water stress for an average year. For example, 403200 time steps (of 10 minutes each) showed a value below the threshold for DUO3 over 100 years. This is the equivalent of

$$\frac{403200 \text{ time steps} \cdot 10 \text{ min}}{60 \text{ min/h} \cdot 24 \text{ h/day} \cdot 100} = 28 \text{ days of drought in an average year.} \quad (4.8)$$

Figure 4.18a gives the number of *dry buffer days* for each month in such an average year.
The exact same method is followed to obtain the number of *dry substrate days* in an average year. This time, all three configurations can be compared, as shown in Figure 4.18b.

One clearly sees the added benefit of a buffer. Without such a feature, the plants face dry conditions in a summer month for some 10 to 11 *days* on a total of 30 or 31 days. This amounts to one third of the time.
For DUO2 and DUO3, both substrate and buffer results strengthen the hypothesis that a buffer supports the vegetation. The absence of an outlet guarantees higher water levels in the DUO3 roof. In an average year, the substrate is dried out only 8 days. One should also keep in mind that this graph does not show real days or consecutive intervals with dry conditions. At worst, assuming that *dry days* would be actual and consecutive days, the plants on a DUO3 barely suffer from drought. An average August is the most extreme month with only 2 dry days. A succulent like *Sedum* has no trouble surviving that period.

In conclusion, it is clear that DUO3 is the best configuration to cope with water stress. Although DUO2 is more efficient in the retention of rainfall, the difference with DUO3 was relatively small. Considering the fact that DUO2 suffers more from dry periods due to the continuous outflow, DUO3 seems the best configuration for an individual green roof.

However, evaluating the individual hydrological performance based on the water balance is not sufficient. From this analysis, it is not certain which configuration achieves the best reduction in runoff peak volumes. This is treated in more detail in the next section.

4.5 Long term simulations for the city of Antwerp

4.5.1 Method

This section discusses the results from long term simulations on an urban scale. The main objective is to assess the effect of a large scale implementation of green roofs. In a way, this is a continuation of the work of Bertels et al. [35]. There, a normal rainfall runoff model and a green roof model were used to calculate the runoff on an impervious and a vegetated surface. This then served as input to a conceptual sewer

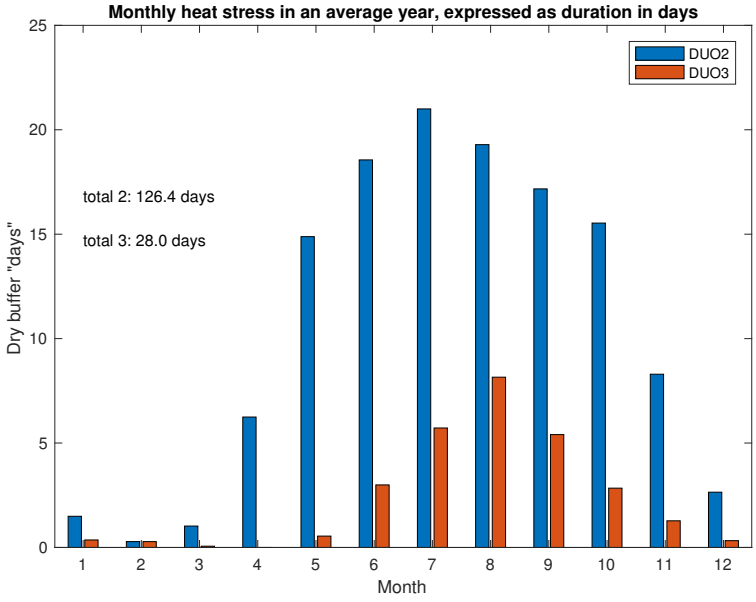

(a) Buffer

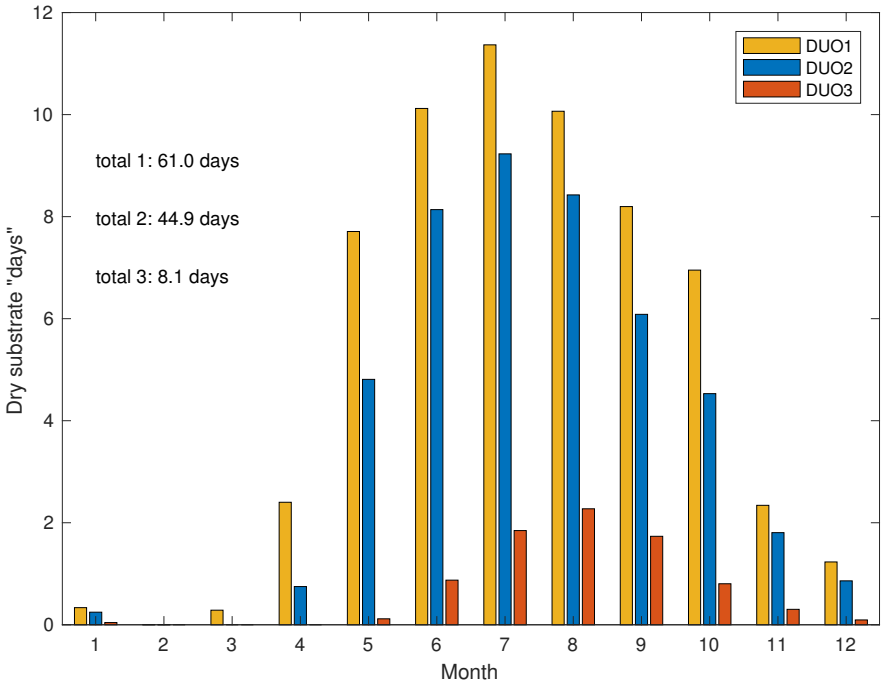

(b) Substrate

Figure 4.18: Duration of water scarcity in an average year, expressed as days per month.

Table 4.5: Potential surface area suited for green roofs in Antwerp, calculated via GIS software [35].

Subcatchments	Population	Total area (m^2)	Potential green roof area (m^2)	Percentage of total
SC1	30408	3681805.075	378595.861	10.28 %
SC2	21112	2204238.776	190998.747	8.67 %
SC3	15301	1133105.344	84408.577	7.45 %
SC4	14178	1372946.199	123708.984	9.01 %
SC5	1	0	0	0 %

model, from which flooded volumes can be derived. Now, the new green roof model is used instead. Because of this, a second objective is formulated. Using the green roof model, the effect of different green roof configurations can be evaluated.
As described earlier, the conceptual model divides the majority of the inner city centre of Antwerp into 5 subcatchments. For each of them, Bertels et al. [35] determined the surface area which is suitable to install green roofs on. Table 4.5 gives an overview of the absolute and relative areas. In the long term simulations performed here, different scenarios are considered. In the scenario *basis*, all subcatchments stay in their current state. In the scenario *g100*, the maximal area suitable for green roof installation is converted in all subcatchments. Summed over all SCs, this amounts to 777712.17m^2 of 8392095.39m^2, or 9.27%. The other scenarios, *g12.5, g25, g50, g75*, consider a city where respectively 12.5, 25, 50 and 75% of the suitable area is converted into green roofs.

For each type of green roof (DUO1, 2 and 3), all scenarios from *basis* until *g100* are simulated. As the green roof model calculates the response in mm (L per square meter), the simulated runoff needs to be multiplied by the green roof area in the scenario for each SC. The remaining area is considered impervious. In this case, the rainfall is routed over the same runoff model applied by Bertels et al. [35], and the resulting runoff time series is multiplied by the remaining impervious area in the subcatchment (i.e. total area - green roof area). The sum of the 'green roof runoff' and the 'impervious runoff' gives one discharge time series per subcatchment.
A last component is the daily water usage per capita in the subcatchment. In these simulations, this is put equal to 150 litres per person per day. This discharge is spread evenly over the 24 hours for the sake of simplicity.
Annex B contains graphs illustrating the flood volumes over 100 years in Subcatchment 3 and 4, for the three different roof configurations (DUO1-3).
A *Peak-over-Threshold* analysis yields 30 flood events over 100 years. The flood volumes of all these events are sorted and plotted with their average period of recurrence in Figure 4.19. The empirical period of recurrence T of each event is determined as

$$T = \frac{n}{i} \tag{4.9}$$

with i the ordinal number of the event, and n the period over which the PoT is

Table 4.6: Long term results for different roof types and different degrees of installation (*g25*, *g50*, *g100*). The percentages are expressed with respect to the flood volume in the scenario without any vegetated roofs (*basis*).

	DUO1	DUO2	DUO3	
mean flood reduction under *g25*	-8.0	-15.1	-15.5	%
mean flood reduction under *g50*	-14.0	-27.0	-25.5	%
mean flood reduction under *g100*	-25.0	-47.4	-46.1	%

Table 4.7: An estimation of the relation between flood volume and flooded area, based on results in an Infoworks 1D-2D model for 2 extreme rainfall events in Antwerp [35].

	30 May 2016	27-28 July 2013	
Flood volume V_{flood}	6272.7	6422.4	m^3
Maximal flooded area A_{flood}	7.87	5.30	ha
Factor ($=V/A$)	797.5	1212.8	m^3/ha
Average factor	1005.2		m^3/ha
Average factor	9.95		m^2/m^3

conducted, expressed in years. So, the largest event has $T = 100/1 = 100$ years, the second has 50 and so on until $T = 100/30 = 3.33$ years. Alongside the plot, a text box is added showing how much each green roof type can mitigate the T20 flood. Apart from this qualitative comparison of different green roof types via graphs, Table 4.6 gives a summary of the average flood reduction that is achieved in these long term simulations.

A more comprehensive approach to look at floods is by calculating the flooded area in square metres. Table 4.7 shows a rough estimation of the relationship between flood volume and flooded area in the city of Antwerp. This is calculated as a constant factor $C = V_{flood}/A_{flood}$ for two historical events in Antwerp. The values for V_{flood} and A_{flood} are found in InfoWorks with a 1D sewer model coupled to a 2D flood model [35]. The average value for C becomes 1005.2 m^3/ha. This allows for fast conversion from volume to area. If one considers that 1 ha = 10000 m^2, one finds that 1 m^3 in the results can be considered as $9.95 \approx 10$ m^2 of flooded area. This implies an average water depth of approximately 0.1 m.

4.5.2 Discussion

From these long term simulations, some conclusions can be drawn. These numbers should however be analysed in a critical way. The results rely on a green roof model, a runoff model and a conceptual model which can all introduce errors. Moreover, they only consider one specific type of green roof every time. Lastly, the percentages until *g100* are illustrating hypothetical situations for the city of Antwerp.

DUO1 For DUO1, the most important conclusion is that the green roofs have a positive effect, reducing the flood volumes each time. On average, the reduction

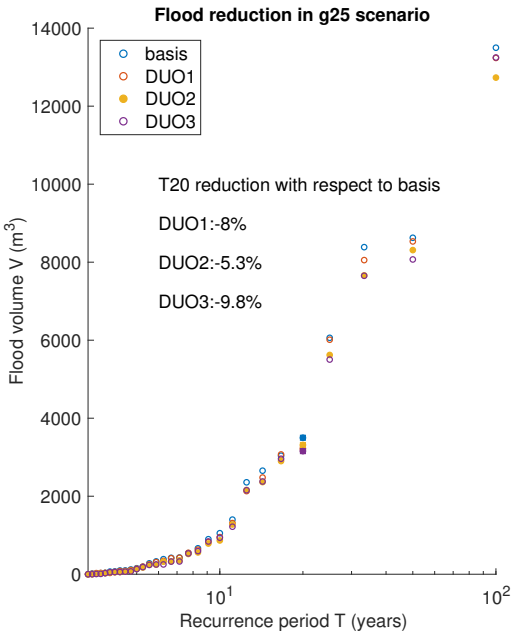

(a) 25% of potential green roof area used.

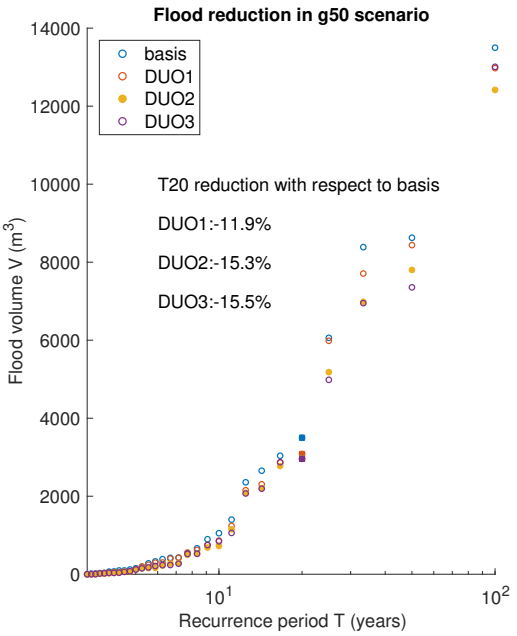

(b) 50% of potential green roof area used.

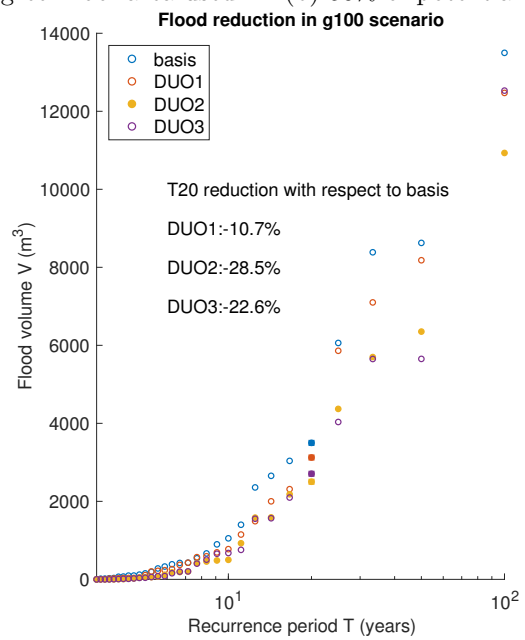

(c) 100% of potential green roof area used.

Figure 4.19: Graphs showing the flood volumes (m^3) for events T100 until T3, assuming different green roof types and degrees of green roof installation in Antwerp. The T20 event is indicated in solid markers, and these reductions are expressed in percentages.

amounts to 8-25% of the original volume, depending on the percentage of green roofs installed in the city. However, some would consider it a Pyrrhic victory, since this reduction only comes after a considerable investment. Even in the best scenario *g100*, the most extreme flood in 100 years only drops from 13498 m^3 to 13237 m^3, a reduction of 7.6%. On the other hand, the *g100* is a scenario where only some 9.27% of the total city surface gets vegetation. This makes an average flood volume reduction of 25% and a maximal flood volume reduction of 72.9% over the period of 100 years actually quite impressive.
However, a normal impervious surface outperforms a vegetated surface for one flood event. This result is of course illogical. For large intensity rainfall events, the poorly calibrated infiltration rate might be responsible for high values of overland runoff, explaining this result. Another possible contributing factor is the behaviour of the impervious rainfall runoff model. This is calibrated in [35] to another set of data. In any case, this inaccurate result confirms once more the added value of long term simulations. This means that the results need to be looked at more critically, but it can be assumed that the long term trends remain valid. Moreover, the conventional green roof is no longer considered in the following chapters. This means that this calibration error will not introduce systematic errors in the further conclusions.
Finally, one notices that in some flood events, the flood does not reduce proportionally to the surface covered with green roofs.

DUO2 This roof type reduces the effect of every simulated flood event. The positive impact is also more significant here compared to DUO1, because the thicker substrate and the buffer provide more retention capacity. However, Castiglia et al. [39] found in their research that under very intense and long rain events, the runoff reduction diminishes and the difference between 5 or 20 cm substrate depth becomes insignificant. This suggests that the buffer outweighs the effect of 20 millimetre extra substrate between DUO1 and DUO2 (from 60 to 80 mm).
Looking at Figure 4.19 and at Table 4.6, one sees that this roof configuration achieves the best average reductions in *g50* and *g100*. For *g25*, roof type DUO3 is slightly better when looking at the average reduction. However, DUO2's maximal and minimal reduction for *g25* are greater, and the largest flood is reduced by 5.7%, from 13498 to 12732 m^3. DUO3 only attains a reduction until 13247 m^3, a mere 1.9%. In the best case scenario, *g100*, the largest event is even reduced to 10391 m^3 with DUO2 roofs, which is a lot better than the volume of 12530 m^3 for DUO3. This is equivalent to a reduction of 19.0% versus 7.2%.

DUO3 Lastly, the green roof with a 200 millimetre substrate layer and a 80 millimetre buffer layer is investigated in more detail. Similarly to the previous configuration, it is expected that the buffer is responsible for the good performance rather than the extra 120 millimetres of substrate.
Overall, the graphs of flood volume V and recurrence period T indicate that DUO2 clearly outperforms DUO3 for events up until T20. Above T20, their flood reductions are quite similar, but for T100, DUO2 is clearly the best. Considering the lower

retention capacity of a DUO2, this better performance is directly linked to the continuous and small outflow in this system. DUO3 can achieve greater reductions than a DUO2, but is often limited by its antecedent conditions of the static buffer. The mean flood reduction shown in Table 4.6 confirms this result.
The next chapter investigates if the antecedent conditions can be manipulated via a control system in such a manner that the maximal flood reduction is attained for every event.

4.6 Conclusion

This chapter presents a new green roof model, based on earlier research [44, 64]. This model structure introduces variables that are required for simulations with intelligent control. Initially, an automatic calibration was conducted. Via an iterative process, adequate parameter values are selected, each within its respective boundaries. However, the amount of parameters hindered a good set of values. For some parameters, the final value is obtained by consulting literature, followed by a manual fine-tuning.
For two of the three roof configurations, a double validation was done using two datasets from independent test sites in France. Overall, the new model proves to be quite robust.
Simulating the green roof response to a time series of 100 years gives an indication of the best performing configuration for the long term. The conclusion of this analysis is shown in Table 4.8. The added value of a water buffer underneath the substrate is clearly demonstrated. The blue-green roofs retain more water, and less vegetation stress is reported. Some differences arise between a buffer with a continuous outflow (DUO2) and a static buffer (DUO3). The continuous outflow helps restoring the retention capacity of the roof, improving its hydrological performance from 48.0 to 50.7% despite the smaller substrate layer. This means that 50.7% of all incoming rainfall is converted to evaporation with DUO2, while DUO3 only evaporates 48.0%. On the other hand, the plants experience more situations of drought with DUO2, where the buffer and sometimes the substrate fall empty. In an average year, the total duration of drought for the substrate is 44.9 days for a buffer with outflow versus 8.1 days for a static buffer.
Using a conceptual sewer model for the city of Antwerp, the long term green roof response can be placed in an urban context. From these simulations, it appears that a configuration with a continuously emptying buffer is most reliable in the reduction of flood volumes. A static buffer, such as in DUO3 is hardly empty, so the retention capacity is not always at its highest, making this system less trustworthy in flood reduction. Even though it has a larger substrate layer, the T20 flood event is only reduced by 22.6%, whereas for DUO2 this is 28.5%. For one flood event, conventional green roofs without a buffer (DUO1) even lead to an increase of flood volumes. This would mean that a green roof surface retains less rainfall than an impervious surface during this event. The contribution of the poorly calibrated overland runoff should

Table 4.8: The most important conclusions with respect to the long term performance of different green roof types.

	DUO1	DUO2	DUO3
Evaporated rainfall (%)	45.7	50.7	48.0
Dry substrate days per year	61.0	44.9	8.1
T20 reduction (m^3) at *g100*	-375 (-10.7%)	-996 (-28.5%)	-792 (-22.6%)

however be studied more closely in these cases. This type of green roofs is no longer considered in the rest of this research.
In the next chapter, an intelligently controlled buffer is proposed as a compromise between a continuously emptying buffer and a static buffer. Such system has the potential to reach good drought reductions like a DUO3 roof, and good flood reductions like a DUO2 roof.

Chapter 5

Intelligent control with perfect weather forecasts

In this chapter, the benefits of intelligent control are evaluated on an urban scale. First, two possible control strategies are explained in more detail. The first control methodology, called Semi-Intelligent Control (SIC) adds a very straightforward logical operator to the buffer. The second method is the Model Predictive Control, as described in Chapter 2.
The next section presents the results of long term simulations for SIC, as well as single event simulations for SIC and MPC. In such a way, the intelligent control strategies are weighed against each other and against conventional blue-green roofs like DUO2 and DUO3.
After the added benefit of a more rigorous strategy like MPC is demonstrated, a sensitivity analysis is conducted on the parameters that govern the MPC system. Here, the model predictive control is also tested for a blue roof. The green roof model from Chapter 4 can be used to represent virtually any type of urban buffer, with or without intelligent control. For a blue roof, the model simply disregards the effect of a substrate layer in the green roof model, and adds evaporation from the buffer layer.
The chapter concludes with some general recommendations for practical implementation of an intelligent system.
For good understanding, the following time perspectives are assumed in the intelligent control strategies:

- Short term forecasts: predictions up until two hours in advance.
- Long term forecasts: predictions up until 24 hours in advance.

5.1 Comparison of intelligent control methods

As described in the literature review, Model Predictive Control is a frequently used strategy. Apart from this, a more straightforward approach is also tested. This Semi-Intelligent Control (SIC) is not based on literature but is easier to implement.

Table 5.1: Most notable differences between the two control strategies SIC and MPC.

	SIC	MPC
Scenario-based	no	yes
Objective 1	intercept rain	minimize flooding volumes
Objective 2	/	minimize drought stress
Computational speed	few seconds per time step	tens of seconds per timestep

Both are explained here.

An overview of the important differences between MPC and SIC is shown in Table 5.1. Most notably, SIC is not scenario-based. This implies that this system will always react the same to predicted rainfall. If a shower approaches, the SIC prescribes outflow from the buffer in order to intercept the coming rainfall. The impact of this behaviour is not calculated beforehand. The safest way to do this, is to let SIC react to long term forecasts. This way, there is a higher chance that most of this water is already out of the sewer.
The MPC strategy calculates in advance the consequence of its discharge on the total urban system. However, since the calculations of the entire urban network are only meaningful with reliable forecasts, this control mechanism works with short term forecasts.
The different behaviour of SIC and MPC is illustrated in Figure 5.1. In the following subsections, both methods are treated in more detail.

5.1.1 Semi-Intelligent Control strategy (SIC)

Two different variations of SIC are tested on the scale of one roof. The easiest controlled outflow that can be added to a roof is a constant flow. If the predicted rainfall cannot be completely intercepted by the buffer, the system starts to empty at a constant flow rate. If the evacuation of water from the buffer starts too late, overflow can still occur in this system. So it is best to keep a long lead time or a high outflow rate in such a control system. In Figure 5.1 for example, the SIC manages to empty the entire buffer before the rain falls.
The second variation works with a variable outflow. Similarly to the first SIC, a comparison is made between the forecast rainfall volume $V_{forecast}$ and the free volume in the buffer V_{free}. If the free capacity is not sufficient, a continuously decreasing outflow rate is generated. The variables in both SIC systems are the time horizon and the parameter that governs the outflow. The outflow is defined as follows:

$$Q = \begin{cases} 0 & \text{mm/10min, if } V_{forecast} < V_{free} \\ C & \text{mm/10min, for constant SIC} \\ \frac{1}{x} \cdot (V_{forecast} - V_{free})/\Delta t & \text{mm/10min, for a variable SIC} \end{cases} \tag{5.1}$$

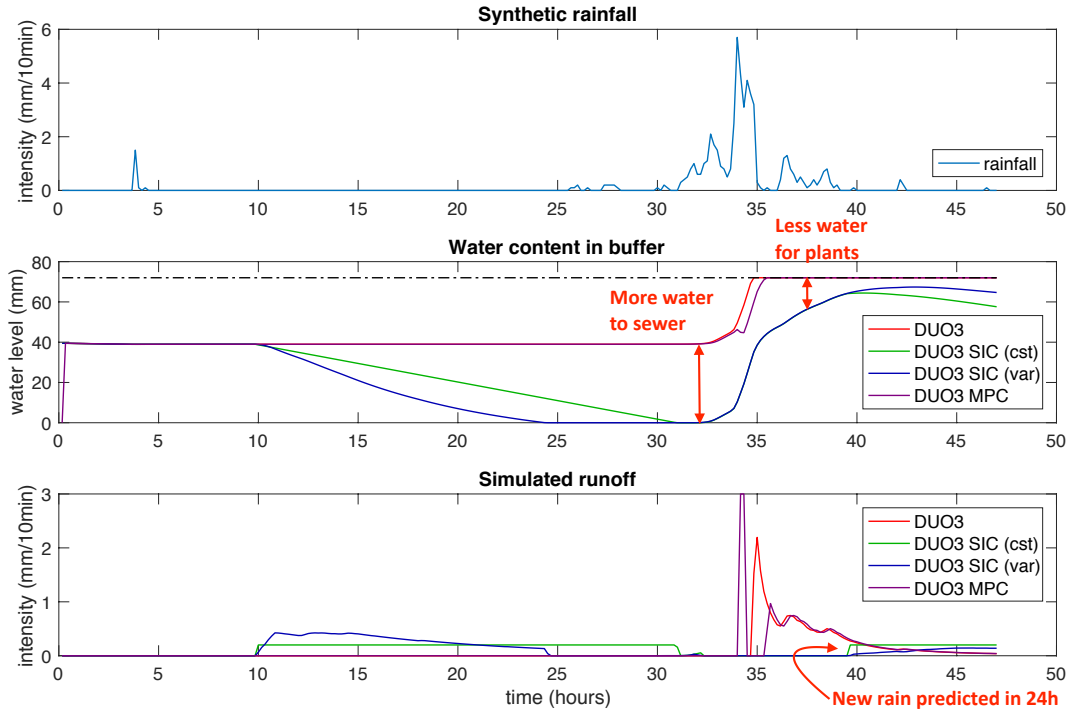

Figure 5.1: Illustration of different outflow rates for intelligent control strategies. The Semi-Intelligent Control starts emptying small volumes beforehand, while the Model Predictive Control only notices the flood one hour beforehand. If the conceptual sewer model indicates that a controlled outflow reduces the flood volume, MPC will release water before the flood.

where C is the constant outflow rate, $1/x$ is a user-defined fraction called the *release factor* and Δt is the time between two forecast calculations. This fraction $1/x$ is constant, so the outflow rate systematically decreases. Based on tests with one rainfall event, a time horizon of 24 hours is chosen. The constant outflow is fixed at 0.2mm/10min for the constant SIC. This allows the buffer to discharge 28.8 litres in the 24 hours, which is two thirds of the total capacity. The value for C is quite low because the strategy does not look at the impact on the sewer network, so it was deemed better to be cautious. For the variable SIC, $1/x = 1/48$ was a good value. Via this value, a simulation of 10 years showed that only 17.6% of all runoff is released via overflow, the rest occurs via the intelligent outflow. Figure 5.1 allows for a comparison between the constant and the variable outflow rate.

5.1.2 Model Predictive Control (MPC)

In Chapter 2, the basic philosophy of MPC is already explained. Specifically for the control of blue-green roofs in an urban setting, the flow chart in Figure 5.2 is followed.

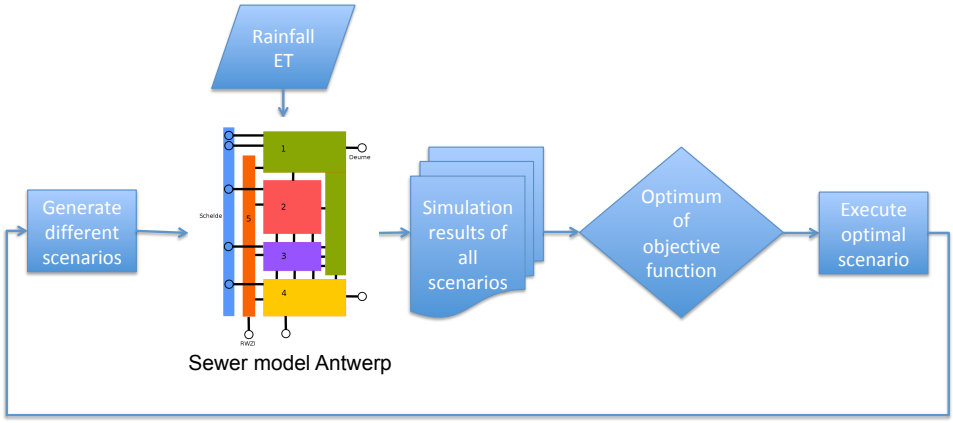

Figure 5.2: A flowchart describing the selection of the optimal steering scenario.

Every time step, the buffer determines the best way to operate over a certain time horizon, called the lead time. To find this optimal steering action, a random set of possible scenarios is created. The impact of all these scenarios is calculated via the conceptual sewer model as far as the lead time allows. Afterwards, the performance of each scenario is assessed via two objectives, and the best one is executed until the next time step. Then, the whole process starts over.

For the intelligent control of green roofs, this research defines two objectives to determine the optimal outflow strategy. For the second objective, two options are presented:

- Priority 1: minimal flooding volumes - *flood* criterion
- Priority 2a: minimal water stress - *days ahead* criterion
- Priority 2b: maximal water storage - *drought* criterion

The next paragraphs elaborate on each of the three criterions.

Priority 1: minimal flooding volumes - *flood* criterion In order to quantify the flood that each scenario evokes, a flood criterion is calibrated and validated for the conceptual model of Antwerp [35]. This is already explained in Chapter 2. It is specifically configured to approximate the maximal volume on the streets for extreme rainfall events. This is applied to each scenario, and the first selection of the optimal scenario(s) will all lead to an identical, minimal amount of water on the streets.

Priority 2a: minimal vegetation stress - *days ahead* criterion When there is no or little rainfall foreseen as far as the lead time goes, several scenarios will turn up with a zero cubic metres of flooding. Also, it is possible that multiple scenarios predict an equal peak flood volume different than zero. In both cases, a second priority has to be defined to pick the optimal scenario from this smaller set of possibilities. If the socioeconomic damage for the city is minimized, the health

of the green roofs come into focus. Depending on the water availability for the plants, some scenarios might be preferred. The scenario selection is represented in a flowchart in Figure 5.3. This demonstrates that the *days ahead*-criterion will not always prefer storage of water. If the water balance of available water and expected water is positive, the system will partly empty the buffer to create a safer situation when an actual flood event occurs.
In the flowchart, several parameter values need to be further specified. The calculation of the water balance at time t_i is as follows:

$$\text{water balance}(t_i) = V_{buffer}(t_i) + \Sigma_{t=t_0}^{t_f}(P(t) - x_{veg} \cdot ET_p(t)) \tag{5.2}$$

A very important user-defined parameter in this calculation is the number of days to look at, $t_f - t_0$. Over this period, the MPC categorizes the weather as wet or dry. Next, the water need for the vegetation needs to be quantified. This is done via the parameter x_{veg}. Based on a list from the university of California [100], *Sedum* generally thrives in a water availability of at least 10 percent of the potential evapotranspiration rate. For plants that cannot be classified as succulents, the value of x_{veg} will be higher.
If the flows in the sewer network depend on the water levels in a river, as is the case for Antwerp, two extra checks appear in the flowchart. These are placed there to make sure that the precautionary emptying of the buffer happens in a smart way.
When the blue-green roofs release water at high tide, it might not lead to a flood within the lead time, but it is still a more risky action than emptying at low tide. Indeed, if more intense and unforeseen rainfall follows after the lead time, the evacuated water from the buffer which is still in the sewer system might increase the total flood volume. Therefore, a sewer that depends on a tidal river should behave more cautiously, which explains the extra checks.
It is highly unusual to add such explicit controllers into an MPC system, since the entire philosophy is that the calculation of the impact model dictates which control scenarios are best. Indeed, this would be possible here as well, but then a longer lead time would be needed. This way, the impact model would be able to see whether large evacuations are possible. However, keeping in mind the uncertainty that comes with long term weather forecasts, such an MPC system will not be interesting in real-time.
To summarize, following parameter values are assumed for this *days ahead* criterion:

- Water usage as fraction of evaporation: $x_{veg} = 0.1$
- Length of long term forecast: $t_f - t_0 = 1$ day
- River level threshold: ≤ 3 metres TAW

The threshold for the river is fixed at 3 metres, but this is highly dependent of the sewer network. In Antwerp, the Scheldt fluctuates approximately between 0 and 6 metres TAW [47], as shown in Figure 5.4. The water stays below 3 m TAW for 60% of the time. Considering that evacuation only happens at falling tide (water level at next step lower than at current step), some 30% remains. This is still plenty of time

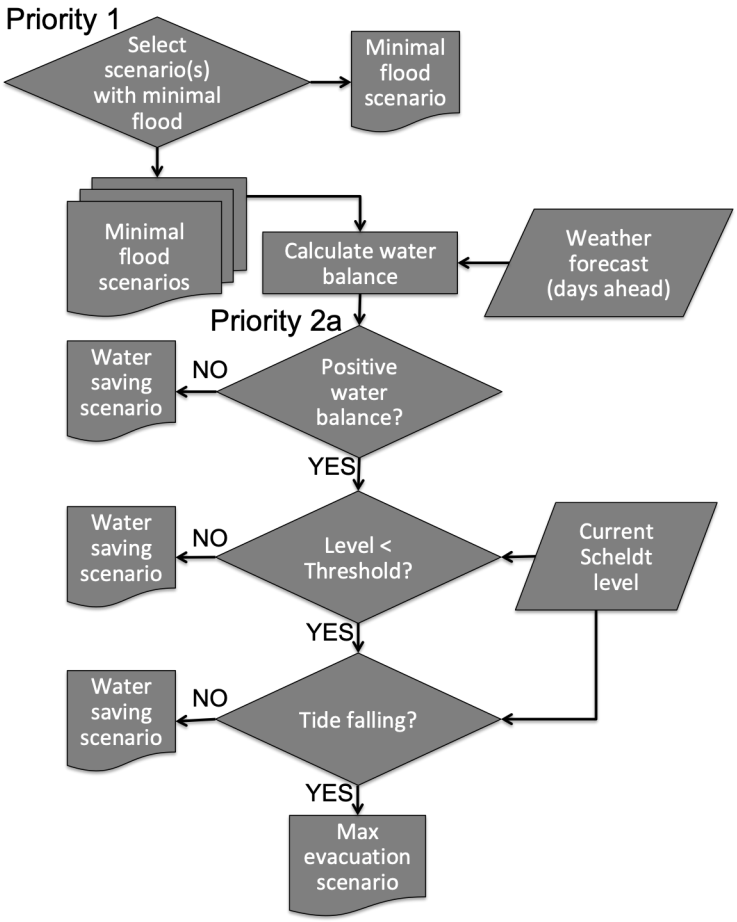

Figure 5.3: A flowchart describing the selection of the optimal steering scenario.

to empty a buffer of 52 litres with a maximal outflow rate of 15 litres per 10 minutes. Figure 5.5 serves as a schematic overview of the ideal cooperation between the *flood* criterion and the *days ahead* criterion. For the first priority, a lead time of one hour is assumed. For the second, the system looks 24 hours ahead. At T=0, the first priority cannot choose an optimal scenario, as they all lead to a situation without flooding. The second criterion however notices some rainfall over the following 24 hours. If the water balance turns out to be positive and the river conditions are favourable, precautionary measures are taken to free up part of the buffer capacity. The system then selects a scenario with maximal evacuation until the next time step, where the process is repeated. At T=23, when the storm comes into focus of the first criterion, the optimal scenario will be the one minimizing the flood from this event.

Priority 2b: maximal water storage - *drought* criterion This alternative second criterion is more simplistic, but guarantees the least spillage of water. After the first priority selects all scenarios which minimise the flood, this criterion determines the scenario which discharges the smallest possible amount of volume from the buffer.

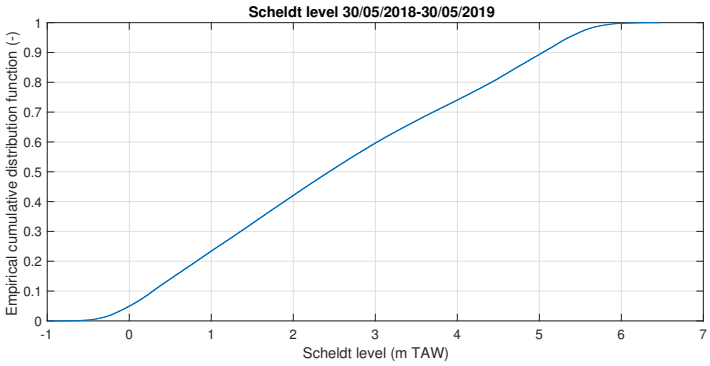

Figure 5.4: Scheldt levels in Antwerp (source: [47]).

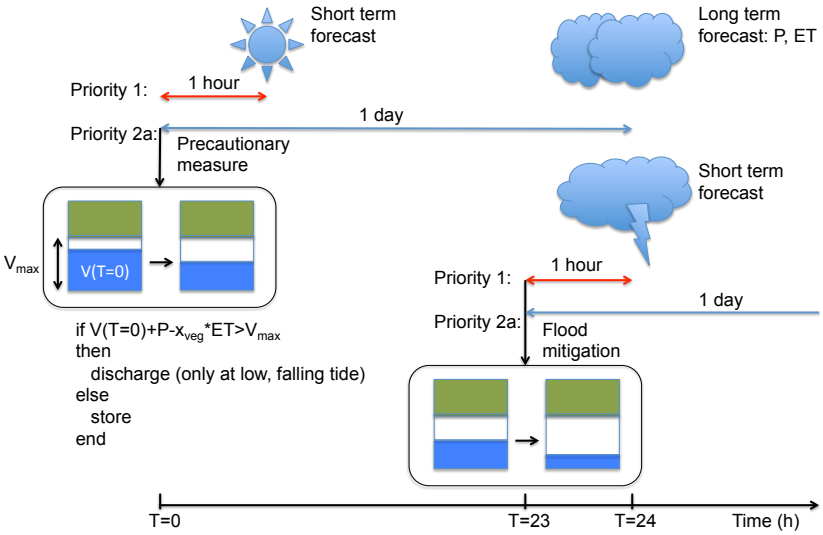

Figure 5.5: Schematic example of the function of both objectives in the MPC. At T=0, the second objective determines the best scenario based on the water balance over the next day. At T=23, the first objective determines the best steering scenario for the buffer.

If no flood is predicted in any scenario, the buffer will simply behave as a static buffer.

Other elements of MPC Lastly, two extra features are added to improve the performance when considering a low number of steering scenarios. The first feature allows the model to store the X optimal scenarios. These can then be reused in the next time step of the Model Predictive Control. This is especially interesting when long lead times and multiple outflow rates are assumed. In this case, not all mathematical options are generated as a scenario, so keeping the X best scenarios from the previous time step might be useful.
The second addition provides a so-called *release-store* scenario for each possible outflow rate. Such a scenario starts releasing water in the first step of the lead time, but stores all the water in the following steps. When a low number of scenarios and high number of different ouflow rates is given to the system, most scenarios tend to release too much. This feature still guarantees a constant set of scenarios with a low outflow.
Although the MPC steers all blue-green roofs in Antwerp in a collective way during the simulations, the code can deal with spatial heterogeneity. The model inputs (rainfall, evaporation) and the system state variables (buffer levels) are considered for each subcatchment separately if such data is provided. For the extreme event of 30 May 2016, the radar data described in Chapter 3 are used. The model assigns the correct rainfall to each SC. Next, it takes the correct buffer levels, which also differ among SCs, and calculates the green roof response for each randomly generated scenario. With this info, the urban impact is defined, and the best scenario is chosen and followed until the next time step of the code.

5.2 Results for SIC and MPC

First, the long term results for SIC are presented. A comparison with the findings from the previous chapter is also included. Next, the two intelligent control strategies are weighed against each other using two single event simulations.

5.2.1 Long term simulations with SIC

Water stress Similarly to the findings in Chapter 4, one can again investigate both the water stress and the flood mitigation on the long term. For the SIC with a constant outflow of 0.2mm/10min starting 24 hours in advance, the water stress results are shown in Figure C.1 and Table 5.2. The duration of water stress in an average year is quantified in *dry days*, as demonstrated in Equation 4.8. The most important change using intelligent control is that DUO2 experiences less water stress (- 19.6 days without water for substrate). On the other hand, DUO3 gets slightly more water stress (+ 0.7 days without water for substrate). This is expected, because intelligent control makes the compromise between a static buffer which never releases (DUO3) and a buffer with continuous outflow (DUO2). The number of dry days is

Table 5.2: Overview of days without water in an average year. The results for non-intelligent roofs are copied from Chapter 4.

	DUO2	Intelligent DUO2 (SIC)	DUO3	Intelligent DUO3 (SIC)
dry substrate days	44.9	25.5	8.1	8.8
dry buffer days	126.4	65.7	28.0	30.4

Table 5.3: The average flood mitigation efficiency of non-intelligent and intelligent roofs over 100 years. The percentages are expressed with respect to the flood volumes in the *basis* scenario without any green roofs.

	DUO2	DUO2 with SIC (variable outflow	DUO3	DUO3 with SIC (variable outflow)	
mean flood reduction under *g25*	-15.1	-17.2	-15.5	-17.9	%
mean flood reduction under *g50*	-27.0	-30.4	-25.5	-30.1	%
mean flood reduction under *g100*	-47.4	-53.0	-46.1	-54.7	%

however still different due to the other soil layers in DUO2 and DUO3.

Flood mitigation With a time step of 10 minutes, long term simulations are conducted for the city of Antwerp. Both for DUO2 and DUO3, Semi-Intelligent Control with constant and variable outflow are tested. For SIC with variable outflow, the resulting flood volumes are shown in Annex C. The flood mitigation for a constant outflow was also simulated and proved to be quite comparable, but slightly less efficient than the variable outflow. This is expected, since the variable outflow discharges smaller volumes closer to the actual rainfall, resulting in a less full sewer network. The plots with flood volume V versus T in Annex C show that intelligent DUO2 roofs reduce the T20 event by an extra 17 percentage points compared to conventional DUO2 roofs in the *g100* scenario. For DUO3, an extra 14.4 percentage points is recorded. In absolute numbers however, the T20 event becomes smallest with DUO3 roofs, from 3498m^3 to 2204m^3. With DUO2 roofs, the T20 is reduced 2259m^3. This trend is noticeable for other flood events as well. When applying intelligent control, DUO3 generally outperforms DUO2. This result is logical, since DUO3 still possesses a thicker soil layer with a larger retention capacity. This result is also confirmed by the general flood reduction efficiencies, shown in Table 5.3.

5.2.2 Single event simulations with SIC and MPC

To compare the performance of both SIC and MPC, two rainfall events that caused flooding are selected from the time series of 100 years. Table 5.4 shows the maximal

Table 5.4: Overview of flood volumes in two events with or without intelligent control. The scenario is *g100* in all cases, and the time series of the floods are included in Annex D.

g100	no IC	SIC (constant)	SIC (variable)	MPC	
V_{flood} event 1	4034	4028	4033	3831	m3
V_{flood} event 2	2707	2236	2203	2121	m3

flood volumes that are recorded for simulations with 100% of the potential roof area used for blue-green roofs of type DUO3. The time step is taken at 10 minutes. The two events are listed horizontally, the different control strategies are given vertically. The graphs that show the flood volumes are included in Annex C. In the first event, MPC removes an extra 200m^3 water from the streets, where SIC fails to make a significant reduction. For the second event, the MPC removes almost 600m^3 whereas SIC only takes away (2707)-(2203)=504m^3 in the case with a variable outflow. In relative terms, the extra reduction with SIC amounts to $504/(2707) \cdot 100 = 18.6\%$, while the MPC can establish an extra reduction of 20.8% compared to non-intelligent blue-green roofs.

5.2.3 Trade-off between SIC and MPC

The two events are an excellent way to illustrate the difference between SIC and MPC. In the second event, SIC can almost achieve the same reductions as MPC. This means that both systems are an improvement compared to a blue-green roof with a static buffer. However, as the first event clearly shows, the good performance of the SIC is not guaranteed. Here, the system barely takes away water from the streets. The MPC however is able to reduce the flood by some 200m^3 by only looking one hour in advance.
In conclusion, the MPC is a more reliable strategy, as it always checks the consequences of its actions before it actually performs them. The next section describes further research into the MPC strategy via a real and recent rainfall event.

5.3 MPC during the rainfall event of 30 May 2016

5.3.1 Results

As explained in Chapter 3, the MPC is tested out for a recent and extreme rainfall event over the city of Antwerp, on 30 May 2016. Several simulations have been conducted, changing parameters such as green roof percentage in the city, lead time, number of scenarios, possible outflow rates and drought criterion. Here, the time step is put at 5 minutes. In all simulations, the 10 best scenarios are reused in the next time step. All simulations start from the roof type DUO3. In some cases, the substrate layer has no thickness to mimic a blue roof, but the other roof parameters remain unchanged.
To get realistic initial conditions in the blue or blue-green roof, the entire model starts

Table 5.5: Total rainfall and runoff in the months of May until August in 2016, as found online [47].

	Precipitation (mm)	Evaporation (mm)
May	131.53	77.79
June	127.42	66.6
July	33.36	89.59
August	44.35	83.91
September (1-16)	5.73	36.87

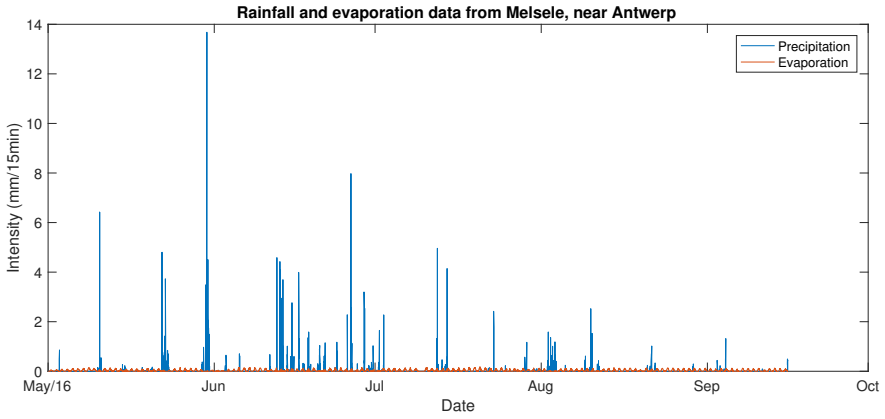

Figure 5.6: Rainfall from 1 May 2016 until 16 September 2016. Before the extreme rainfall event of 30 May takes place, the weather is dry for almost a full week. Afterwards, June is quite wet, but July and August are very dry again.

running from 1 May 2016 onwards. Figure 5.6 shows the rainfall and evaporation during the month of May and the subsequent months in 2016. For long term simulations, data up until September is foreseen [47]. The rainfall and evaporation per month is included in Table 5.5.
Figures in Annex D show the rainfall and outflow intensities of some simulations, along with the flood volumes on the streets, the water levels in the river and the behaviour of the green roof. At 1 May 2016, the initial buffer volume is set at 45.5 litres (maximum is 46.8 litres), and the substrate is at Field Capacity. After a few weeks in the simulation, MPC starts around 27-30 May 2016. The first time stamp of each simulation indicates the exact moment at which intelligent control is applied to the static buffers. Typically, the initial conditions for the buffer are around 38-40 litres around that time. The substrate moisture is generally close to the Field capacity.
The values shown in Figure 5.6 also serve as the long term forecast for the *days ahead*-criterion.

Table 5.6: Overview of simulations results for several blue-green (g) and blue (b) roof scenarios. The MPC works with 100 scenarios, a lead time of 60 minutes and outflow rates until 15mm/10min. These results are visualised in Figure 5.7.

	Flood without MPC (m^3)	Reduction wrt *basis* (m^3)	Flood with MPC (m^3)	Reduction wrt *basis* (m^3)	Extra volume removed by MPC (%)
basis	4239.7	/	4239.7	/	/
g12.5	4098.7	-141.0	4028.2	-211.5	50.0
g25	3949.6	-290.1	3811.7	-428.0	47.6
g50	3652.7	-587.0	**3389.3**	-850.4	44.9
g75	3407.5	-832.2	**3023.9**	-1215.8	46.1
g100	3180.3	-1059.4	2668.2	-1571.5	48.3
b50	3755.4	-484.3	**3372.5**	-867.2	79.0
b100	3385.9	-853.8	2666.7	-1573.0	84.2

5.3.2 Discussion

Based on the results presented in the previous subsection, a sensitivity analysis is performed on the most important user-defined settings of the MPC.

Green roof percentage

The most evident parameter to investigate is the percentage of green roofs that is installed in the city. The simulation is run with and without MPC for all different green roof scenarios, and the results are summarised in Table 5.6 and Figure 5.7. The MPC is set here at a lead time of 60 minutes and creates a set of 100 scenarios every 5 minutes, from which the optimal action is determined. The allowed discharge rates have a value up until 15mm/10min. The results show that it is economically more feasible to convert the system to MPC instead of planting another 25% of the potential green roof area with normal blue-green roofs from g50 onwards. For lower percentages (g12.5 and g25), it is still better to double the amount of green roofs although the difference is sometimes very small. For all degrees of green roof installation considered, the conversion to an intelligent system makes the roof 45-50% more efficient. In other words, the MPC keeps another 45-50% of the already removed flood volume from the streets.
When speaking from the perspective of the *basis* scenario without any green roofs, the maximal application of intelligent blue-green roofs can reduce the flood from 4239.7 to 2668.2m^3, a reduction of no less than 37%. Via the simple conversion explained in Chapter 4, the area spared by flooding is:

$$(4239.7 - 2668.2\text{m}^3) \cdot 9.95\text{m}^2/\text{m}^3 \cdot 1/10000\text{ha}/\text{m}^2 = 1.56\text{ha}. \tag{5.3}$$

Note that this *g100* scenario only requires a conversion of 9.27% of the inner city surface area, namely the flat or nearly-flat rooftops.

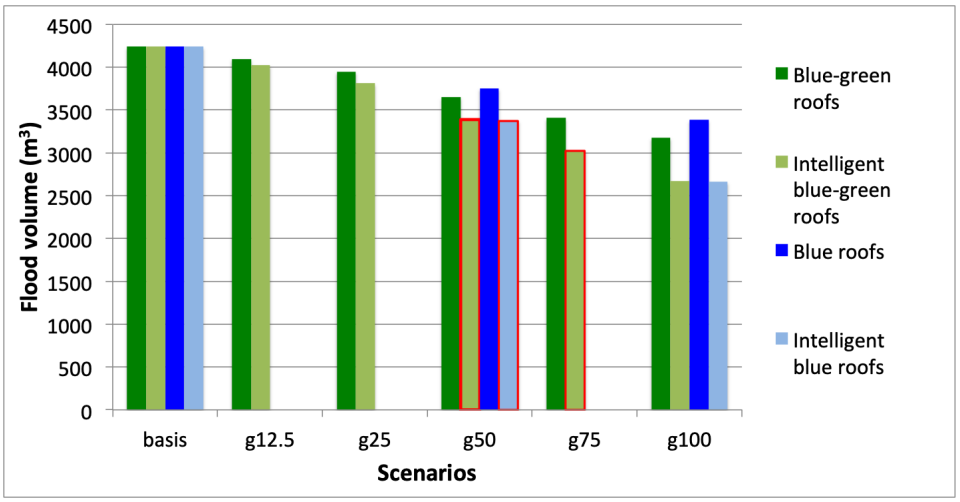

Figure 5.7: Dark and light green show the flood volume for blue-green roofs without and with MPC, dark and light blue for blue roofs. The red lining indicates that intelligent control reduces the flood more than another 25 percentage points of non-intelligent roofs would.

For the other variables in the sensitivity analysis, the simulations are mostly run with the *g100* scenario. This way, the trends become more visible.

Vegetation

The impact of the substrate layer and the vegetation can be analysed by removing this layer in the model. To prevent instabilities in the model, the layer should be assigned an extremely small thickness. In this case, the model immediately recognizes the intent of the user, and adds evaporation to the buffer layer. The results can also be found in the previous Table 5.6 and Figure 5.7.
Although the water is no longer needed to sustain vegetation, the MPC still prefers storage of water. Keeping the buffer as dry as possible so that it can intercept rainfall at any time would be a case of bad water management. When the buffer is full, the water can be utilised in the surrounding households. On top of that, it has a cooling effect on the vicinity. So, the *drought*-criterion is still active, now with $x_{veg} = 0$ in the water balance calculation, because vegetation is absent.
The graph shows that any percentage of blue roof installation reduces the total flood, albeit in a less effective way than blue-green roofs. This is expected, since the substrate intercepts an extra amount of rainfall, and slows down the process of runoff creation. However, when applying Model Predictive Control, blue-green and blue roofs attain an identical minimal flood volume. Note that this is only the case as long as the total rainfall in the event stays below the maximal capacity of the blue roof. This implies that the added benefit of intelligent control is even larger for blue roofs than for blue-green roofs. The sixth column in Table 5.6 shows an extra volume reduction up to 84% of the original reduction can be achieved. Compared

Table 5.7: Effect of lead time on the performance of MPC.

Lead time (min)	Controlled outflow volume (mm)	Flood volume (m^3)
120	13.5	2668.2
60	***0***	***2666.7***
60	13.5	2668.2
50	12	2668.2
45	12	2668.2
40	12	2668.2
35	12	2668.2
30	12	2668.2
25	12	2668.2
20	12	2668.2
15	12	2708.0

to the efficiency increase of 45% for blue-green roofs, this result is very impressive. Lastly, it becomes more beneficial to install intelligent blue roofs on half of the flat roofs rather than placing non-intelligent buffers on all flat roofs.

Lead time

To assess the effect of a longer or shorter lead time, several simulations are performed. The resulting flood volumes are included in Table 5.7. All other parameters remain the same. Every time step, 100 scenarios are calculated and five different outflow options are given to the system. The green roof scenario *g100* is assumed in all cases. The only exception is the third simulation, indicated in bold and in italic. Compared to the other, the initial buffer conditions were different. Because the buffer had been empty for a longer time here, the substrate is drier. This explains why the flood volume is slightly lower in this simulation.
The simulations indicate that the minimal flood remains the same for all lead times larger than 20 minutes. However, the reader should keep in mind the other circumstances of these simulations. The flood event described here also develops in 20 minutes. At 11:55, the volume starts from zero and attains the peak at 12:15. The peak rainfall occurs at 11:50, and any evacuation before this time does not appear to contribute to the peak volume on the streets. So, if the flood creation (from zero to peak) takes a longer time, late evacuations are expected to become impossible.
Most of the other simulations discussed here are performed with a lead time of 60 minutes. This lead time is already chosen with the prospect of forecast uncertainties in the next chapter. According to the thesis research of Allaeys [76], the STEPS-BE data was only able to see part of the peak rainfall with nowcasts up until 45-60 minutes. So any lead time that is larger than one hour is not useful when tackling the last objective of this research in Chapter 6.

Table 5.8: Flood volumes and water stress for different MPC scenarios. All simulations ran from 1 May 2016 until 1 September 2016. A more complete overview of the simulations is included in Annex D.

	Flood volume (m^3)	Dry buffer days
No MPC	3180.2	2.63
MPC using only *flood* criterion	2668.2	2.63
MPC using *days ahead* criterion	2680.0	4.42

Number of scenarios

The required number of scenarios to achieve the real optimum is also investigated in some of the simulations. A summary of the relevant results is included in Figure 5.8. All simulations start at 06:00 on 30 May, and have an identical lead time of 60 minutes. The *days ahead*-criterion is not active since the tide is already rising at 06:00. The extra check, as shown in Figure 5.3 impedes discharges ahead of the lead time when the tide is rising for safety reasons. The red bars and green bars show simulations with large outflow rates until 15mm/10min, the blue bars can only discharge a maximal volume of 6mm/10min.
The required number of scenarios to achieve the minimal flood depends largely on one of the addition of the so-called *release-store* scenarios. mentioned earlier in subsection 5.1.2. These very basic steering options only empty the buffer in the first time step, and store water in the subsequent steps. Such scenarios are of course very interesting to consider, but with the random scenario generator, these are not always present. If the *release-store* scenarios are explicitly included, a smaller set of scenarios already suffices to attain optimal reductions.
While the MPC without these basic scenarios needs 200 options to find the minimal flood, the addition of the *release-store* scenarios reduces this to 50. Moreover, if one leaves out these simple scenarios, there is no monotonous relation between the amount of scenarios and the reduction of the flood. The simulation with 150 different possibilities yields higher volumes on the street than the one with 100 scenarios. This means that too few good options are randomly generated.
Another parameter which has a significant impact on the required number of scenarios is the maximal outflow rate of the buffer. This is illustrated by the blue bars. If the buffer's discharge options are limited, the system needs scenarios which evacuate as much as possible in the earliest time steps. The addition of the *release-store* scenarios is also unuseful here, since the buffer should keep emptying for more than one time step to compensate for the low discharge rate. At 200 scenarios, the MPC is still not able to reach the minimal flood. Other conclusions concerning the outflow settings of the system are mentioned later.
In all other simulations, the *release-store* scenarios are taken into account.

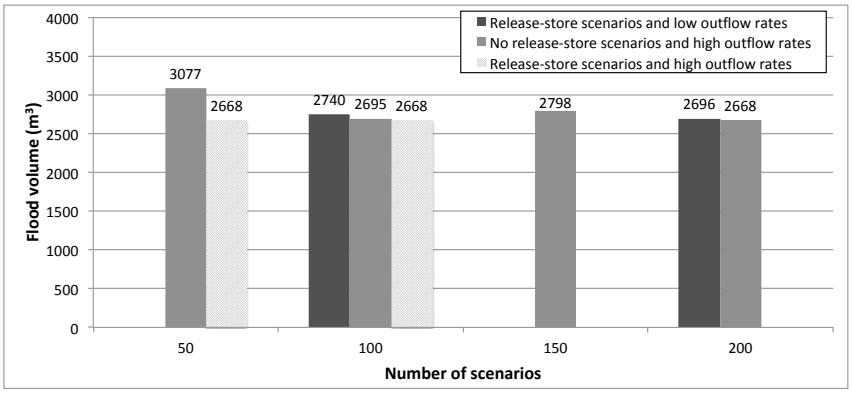

Figure 5.8: Flood volumes in function of the amount of scenarios in MPC. High outflow settings (blue) and basic *release-store* scenarios (red) sharply reduce the amount of scenarios needed for optimal reductions. Such scenarios only discharge in the first time step, after which the buffer stores the remaining water.

Long-term drought forecast

The previous subsection on the required number of scenarios shows that minimal flood volumes can be achieved relying only on short term forecasts of less than one hour. However, in the case of cloudbursts, one may notice the actual storm too late. And even if the heavy rainfall is predicted within the lead time of one hour, it is possible that the buffer contains too much volume to discharge before the rain arrives. Here, the second criterion comes into focus.
If a long term forecast of 24 hours already indicates that quite some rainfall is expected, it can be beneficial to already free up part of the buffer volume. This will not affect the water availability for the plants on the long term, but might be good for flood mitigation. Figure 5.5 already showed how such a simulation looks like.
Two long term simulations are performed and included in Annex D. Table summarizes the most important findings. The first conclusion is that both criteria can operate independently and achieve nearly identical flood reductions. The simulation relying on the *days ahead* criterion forecasts the exact volume of rainfall to come, so the buffer is completely emptied. The *flood* criterion sees the flood one hour in advance and releases just the right amount of water to reach the optimal situation. However, another conclusion follows from the simulations until September. If this *days ahead* criterion receives a perfect prediction of expected volume, it will always create space to accommodate this water. Because the code cannot determine the retention capacity of the soil layer, the buffer releases too much water. This explains the higher amount of dry buffer days. Still, the system improves a lot in reducing floods, with only a slight increase in water stress. Especially for *Sedum*, the extra 1.8 dry buffer days will not pose a problem.
Furthermore, there are two ways to overcome this increased water stress. Firstly, one can consider to install soil moisture sensors, to include this in the calculation of the water balance. Secondly, the control strategy can be adapted. In real-time,

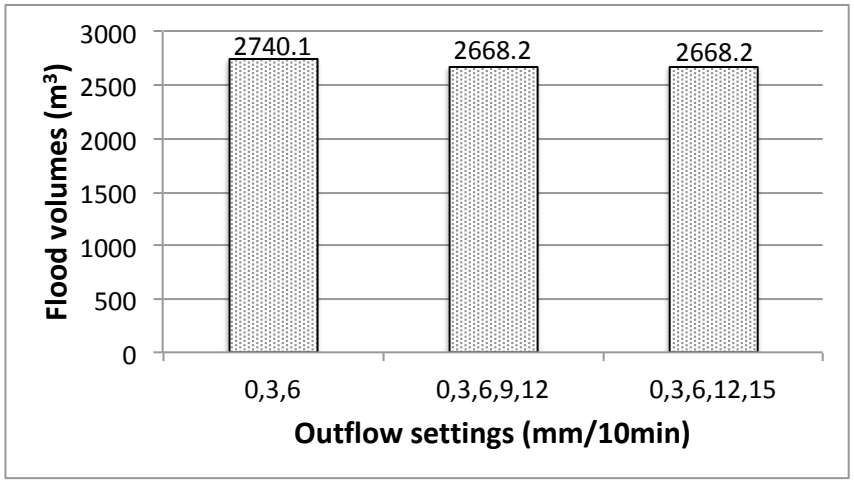

Figure 5.9: *g100* scenarios with lead time 60 minutes, 100 scenarios and no *days ahead*. For this rainfall event, 12mm/10min is the maximal applied discharge rate. Larger rates do not lead to lower flood volumes, and are not chosen by the system.

the code will need to behave differently because of the uncertainty around long term forecasts. Chapter 6 elaborates further on such uncertainties.

Outflow settings

In general, it is expected that the outflow settings are governed by several external rather than internal factors. It is therefore important to try out different options during simulations before implementing this in real-time. The only internal factor is the buffer capacity, whereas the external factors are the rainfall intensity, the sewer characteristics, the lead time and the number of green roofs in the network.
Two different situations are assumed. The first one does not consider the *days ahead*-criterion. Instead, the system always prefers to store water if several scenarios lead to the minimal flood (priority 2b). This situation is equivalent to a real-time system where the extreme rainfall is not predicted outside of the lead time. The results are shown in Figure 5.9. From the outflow rate 12 mm/10min onwards, the system stops selecting the highest possible rate, and no further reduction is realised.

When shifting the water levels in the Scheldt along the time axis, the flood occurs at low tide. This does not only lead to an enormous decrease in the flood volume, it also enables the system to use the higher discharge rate of 15 mm per 10 minutes. This implies that the sewer system is the decisive external factor for this rainfall event. This is a promising result. If more rainfall events are considered, and the sewer system is always the governing factor, one maximal outflow rate can be assigned to all roofs in the city. Another option is that the maximal rate is governed by a combination of rainfall, buffer volume and lead time. This would occur if the expected rainfall exceeds the total buffer capacity. In such a case, the outflow rate needs to be high enough to evacuate the entire buffer before the flood (i.e. within the lead time that revealed the flood). Otherwise, the intelligent control is constrained

and unable to achieve the real optimal flood reduction. In conclusion, a practical rule of thumb for real-time implementation is to check that

$$V_{max} \leq Q_{max} \cdot \Delta t \tag{5.4}$$

with V_max the maximal buffer capacity (L), Q_max the maximal outflow rate (L/min) and Δt the lead time (min). For DUO3, the total volume equals $V = C \cdot H_{b,max} = 0.65L/\text{mm} \cdot 72\text{mm} = 46.8L$. So, with an outflow rate until 15mm/10min, a full buffer is nearly completely empty after half an hour.
In the second situation, the *days ahead*-criterion dictates the optimal steering. Here, the rainfall is already predicted 24 hours in advance, so preventive emptying occurs at a falling tide below 3 m TAW. The *flood* criterion does not come in action, since the buffer is already empty before the flood creation is noticed within the lead time. An example of such a simulation is shown in Figure D.3. The maximal outflow rate that is given to the buffer has little impact on the flood reduction. If a larger value is possible, the system will still release the same volume, only faster.
In conclusion, as long as the outflow options are high enough, the Model Predictive Control is able to achieve the minimal flood based on long term and short term actions. The user does not need to worry that the high outflow rates will cause a larger flood because the sewer model calculates the impact before it moves to action. However, when the buffer follows the *daysahead* criterion, simulations in Tables 5.8 showed that the full buffer evacuation brought more volume in the system, leading to a slight increase in flood volumes (2680 instead of 2668m^3). The next chapter tries to make this second objective more cautious in its release of water.

Calculation time

During the simulations, the duration of every time step is recorded. It is evident that the calculation time increases with an increasing number of scenarios and a longer lead time. The order of magnitude remains quite small if one considers that the MPC only re-evaluates the future every 5 or 10 minutes. For a simulation with 200 scenarios and a lead time of 60 minutes, the calculation itself only takes up 30 seconds for a 10 minute time step and 38.9 seconds for a step of 5 minutes. For 100 scenarios, this becomes 16.5 seconds for a 5 minute step. Reducing the lead time to 30 minutes makes the calculation time 15.1 seconds. This suggests that the length of the lead time has a smaller influence than the number of scenarios because of the speed with which the conceptual model operates.
In any case, the MPC code leaves enough time to collect forecast data such as rainfall or tidal info, and to measure the current state of the sewer network within a time step of 5 minutes.

5.4 Conclusion

This sections treats two types of intelligent control in more detail. On the one hand, a Semi-Intelligent Control strategy is implemented, which only consider rainfall

forecasts. On the other hand, the Model Predictive Control, as described in Chapter 2, is considered. This method selects the optimal scenario, taking into account the current and future state of the sewer network.
Although both systems result in lower floods, the semi-intelligent system shows a lower performance. This is logical, since the buffer volume is managed without calculating the consequences on the urban scale. Still, the SIC achieves a reduction up to 18.6% compared to normal blue-green roofs in the considered flood events, from 2707 to 2203.4m^3.
The chapter concludes with a sensitivity analysis of the parameters in the MPC system. The more outflow settings are added to the system, the better the water is managed. In this event, outflow rates below 12mm/1Omin cause at least an extra 72m^3 water on the streets, roughly equivalent to an additional 720m^2 covered by the flood. This amounts to an increase of 2.7% with respect to the minimal flood found via MPC. For the rainfall event of 30 May 2016, the lead time can be as short as 20 minutes, but this is most likely linked to the speed with which the flood comes up. For such short lead times, the buffer needs to work with outflow rates of at least 12 litres per 10 minutes. As a rule of thumb, it is best to set lead time and maximal outflow rate in such a way that a full evacuation can be conducted within the lead time. For events with a large rainfall depth (i.e. large volume of rainfall), this allows to utilize the entire retention capacity.
The second objective of the MPC can take the long term weather forecasts into account. If enough rain is predicted in the coming day(s), this criterion decides to partly empty the buffer. This precautionary measure can be useful in addition to the short term intelligent control. Simulations of four months only showed an extra 1.8 days where the buffer fell empty, so there is no real increase in water stress.
For all degrees of green roof installation (between 0 and 100% of potential green roof area), the added value of MPC is quite constant. When upgrading all green roofs to MPC, an extra 45-50% of the already removed volume is kept from the streets. In total, intelligent roofs are able to reduce the most recent flood in Antwerp by 37%, resulting in 1.56 hectares saved from water damage. This is achieved by only converting all flat roofs in the centre to intelligent roofs, a mere 9.3% of the inner city surface.
Also, the transition to MPC becomes more efficient than planting another 25% of the potential surface with conventional blue-green roofs.
Blue roofs are also considered, by leaving the vegetation out of the model. A regular blue roof is less efficient than a normal blue-green roof, but via MPC the same minimal flood volume can be achieved. This makes the added value of MPC even greater than 45-50%, to values around 80%.
In anticipation of uncertain rainfall forecasts, the system is given an option to release water without the prospect of a flood within the lead time. The buffer can already discharge some water if long-term forecasts indicate that rain is expected. This option is tested successfully with perfect forecasts of 24 hours. Both the short term (*flood*) and long term (*days ahead*) criterion are tested in the next chapter with uncertain predictions.

Chapter 6

Intelligent control with uncertain weather forecasts

This chapter describes a variation of Model Predictive Control which takes into account uncertainties on the predicted precipitation fields. This variation is called Multiple Model Predictive Control (MMPC), as explained in Chapter 2. Just like in the previous chapter, the rainfall event of 30 May 2016 is considered. The corrected STEPS-BE ensembles, as described in Chapter 3, are used as input. First, the adaptations in the MPC code are explained, followed by the most important results.

6.1 Scenario selection

Compared to the conventional Model Predictive Control, some changes are made. An overview of the entire process of scenario creation and scenario selection is represented in Figure 6.1.
First of all, a set of N possible ensemble members of rainfall is considered. The maximal value for N is 20 in the STEPS-BE data, and the maximal lead time of each member is 120 minutes. Since all N members have an equal chance of occurring, the effect on the sewer network needs to be calculated in all N situations.
Since the power of the MPC lies in the simulation of n possible steering scenarios, this process now has to be repeated for each of the N members. This means that the simulation results now represent nxN possible futures. From this set, the optimal scenario n_{opt} is picked which minimizes the flood risk and the drought risk, in this order of priority.
In this research, the assumption is made that the damage from flood is directly related to the maximal flood volume. Hence, the flood risk R is calculated as follows:

$$R(n_i) = \Sigma(\text{Probability} \cdot \text{Damage}) = \Sigma_{k=1}^{N} \frac{1}{N} \cdot (max(floodvolumes(k, n_i, :))) \quad (6.1)$$

with $floodvolumes$ a (Nxnxt) matrix showing the expected evolution of the flood volume in SC3 and SC4 for each member and each scenario. The dimension t signifies the number of time steps in the lead time of the MMPC. As a consequence, if a

steering scenario $n*$ leads to a flood under one of the considered rainfall members, $R(n*)$ becomes different from zero. As a consequence, the MMPC will select an option that is safer, with a smaller R, preferably equal to zero.
It is interesting to remark that this definition is also valid for the normal MPC. When choosing $N = 1$, the risk calculation for each scenario reduces to

$$R(n_i) = \frac{1}{1} \cdot (max(floodvolumes(1, n_1, :))). \tag{6.2}$$

For each scenario, only one expected evolution of the flood is calculated in the normal MPC. The maximal value of this evolution is taken as the damage, and the probability becomes 1.
The calculation of the drought risk happens in an analogous way. Instead of $floodvolumes$, a matrix $drydays$ is defined with the dimensions (Nxn). Each element (k, i) is equal to 0 when the buffer contains water during the entire time horizon, or equal to $T \cdot 5\text{min}/(60\text{min/h} \cdot 24\text{h/days})$ if the buffer falls empty. T signifies the number of time steps where the buffer volume falls below 1 mm.
After this calculation, it becomes clear which steering scenario minimizes the risk of flooding. If multiple scenarios fulfill this criterion, the same drought criterion as with MPC is applied. If a lot of rain is predicted in the following day(s), preventive emptying is preferred. In this specific sewer network, the preventive emptying can still be halted if the water levels in the river are too high. In other sewer networks, this last check might be unnecessary.
After the selection of the best steering scenario, the actual rainfall is applied to the system, combined with this steering action. The effects are calculated on an urban scale, and the whole process is repeated in the next time step.

6.2 Results

In total, seven MMPC simulations are conducted for the rainfall event of 30 May 2016. The parameter values that are selected for each event are shown in Table 6.1. The time step for the impact model and the MMPC is taken equal to 5 minutes. Simulations 1 and 2 assess the importance of the number of ensemble members and the lead time. Here, the *days ahead*-criterion is able to see the long term forecast of one day, but it will not empty part of the buffer beforehand. This is because the simulation starts at rising tide (at 06:00), and the extra check for a tidal river, as explained in Figure 5.3 in the previous chapter, impedes this risky action.
Simulation 3 is performed to check the consequences of the MMPC actions by simulating up until after the event. The system settings should ensure that enough water remains in the buffer after the rain. Simulation 4 is done to check if the precautionary emptying based on the *days ahead*-criterion is a safer working method.
Simulations 5, 6 and 7 are run to see if an unforeseen cloudburst is handled well by the MMPC. This is achieved by disabling the *days ahead*-criterion, which is based on the exact recordings of the actual event. By disabling this, the entire MMPC strategy counts on the reliability of the ensemble members.

Table 6.1: Parameters and results of MMPC simulations 1-7

	Simulation time (hours)	Lead time (min)	n x N scenarios members	outflow settings (mm/10min)	2nd objective	release-store	max flood (m^3)	dry days	V_{out} (mm)	V_{rain} (mm)	comment
1	0900-1500	30	40 x 10	0,3,6,12,15	days ahead (1 day, 3m TAW)	yes	**2668**	0	27	36.3	no days ahead (tide high)
2	0900-1500	20	40 x 15	0,3,6,12,15	days ahead (1 day, 3m TAW)	yes	**2668**	0	30	36.4	more members and lower lead time
3	0800-2300	60	40 x 10	0,3,6,12,15	days ahead (1 day, 3m TAW)	yes	**2668**	0	60	62.8	less members and longer lead time
4	29/05 0900 - 30/05 1500	30	40 x 10	0,3,6,12,15	days ahead (1 day, 3m TAW)	yes	2690	**0.8**	67.7	40.7	days ahead
5	0900-1500	30	40 x 10	0,3,6,12,15	store water	yes	**2668**	0	15	36.3	emergency evacuation
6	0900-1500	30	40 x 5	0,3,6,12,15	store water	yes	**2668**	0	10.5	36.3	less members
7	0900-1330 (MMPC at 1130)	20	40 x 5	0,3,6,12,15	store water	yes	**2668**	0	10.5	35.3	shorter lead time

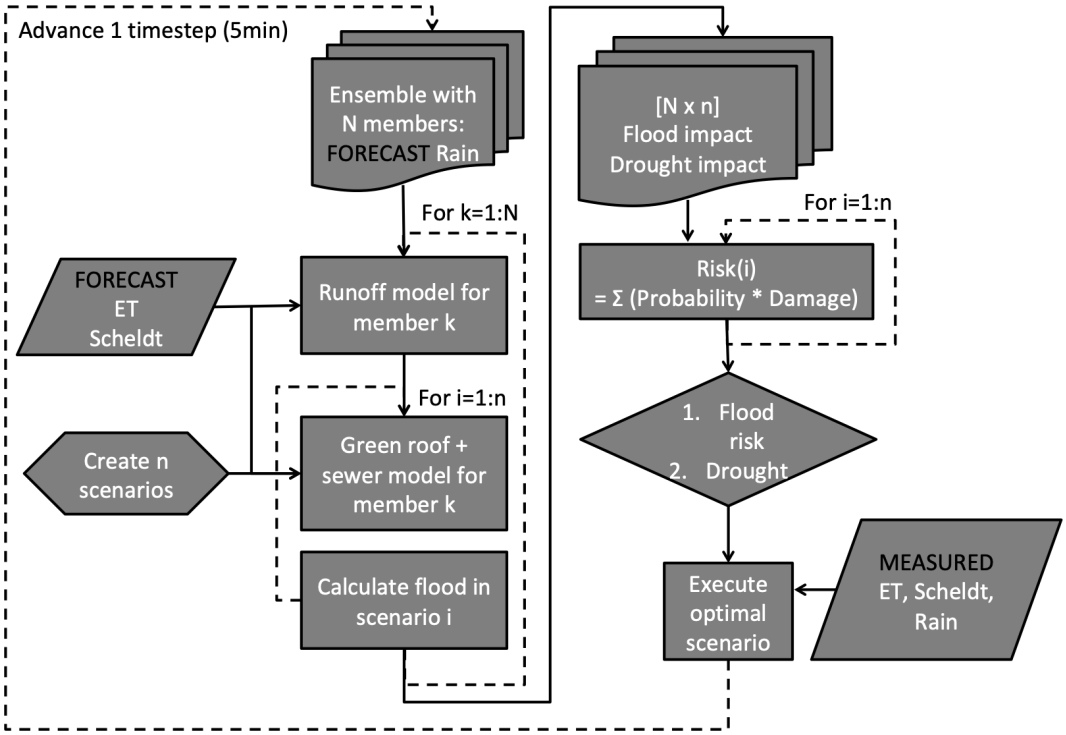

Figure 6.1: Flowchart presenting the process of Multiple Model Predictive Control.

The process of MMPC is illustrated by means of an example. Figure 6.2 gives a step by step execution of MMPC for simulation 6. Concerning the rainfall in the top graph, an upper and lower bound is plotted over the actual rainfall in SC3. The upper and lower bound are continuously updated during the MMPC process. For simulation 6, the MMPC looks 30 minutes ahead at 11:30 and from the N members, the maximal value and minimal value at each time step between 11:30 and 12:00 are updated. In other words, each value in the upper and lower bound is predicted at one certain point in time and in one certain member. The certain point in time is at most one lead time, and at least one time step away from the predicted value. For example, if the lead time is 30 minutes and the number of members is 5 (as in simulation 6), each value in the upper bound is the maximum of $(30\text{min})/(5\text{min/step}) \cdot 5(\text{members/step}) = 30$ maximal predictions. It gives an idea of the expected rainfall intensities during the simulation.
The second plot also contains more information. So-called spaghetti plots represent three possible futures with a lead time of 30 minutes in Figure 6.2. All three consider the worst rainfall member, but differ in the way the buffers are steered. The line *worst case* is the buffer evacuation that results in the worst flood. This line represents an upper limit for the flood expected over the lead time for all members and all steering scenarios. Note that the actual flood can still end up above this line, since the worst case considers the worst rainfall prediction, which is not necessarily higher than the actual rainfall recordings. The *zero case* is the scenario where the buffer

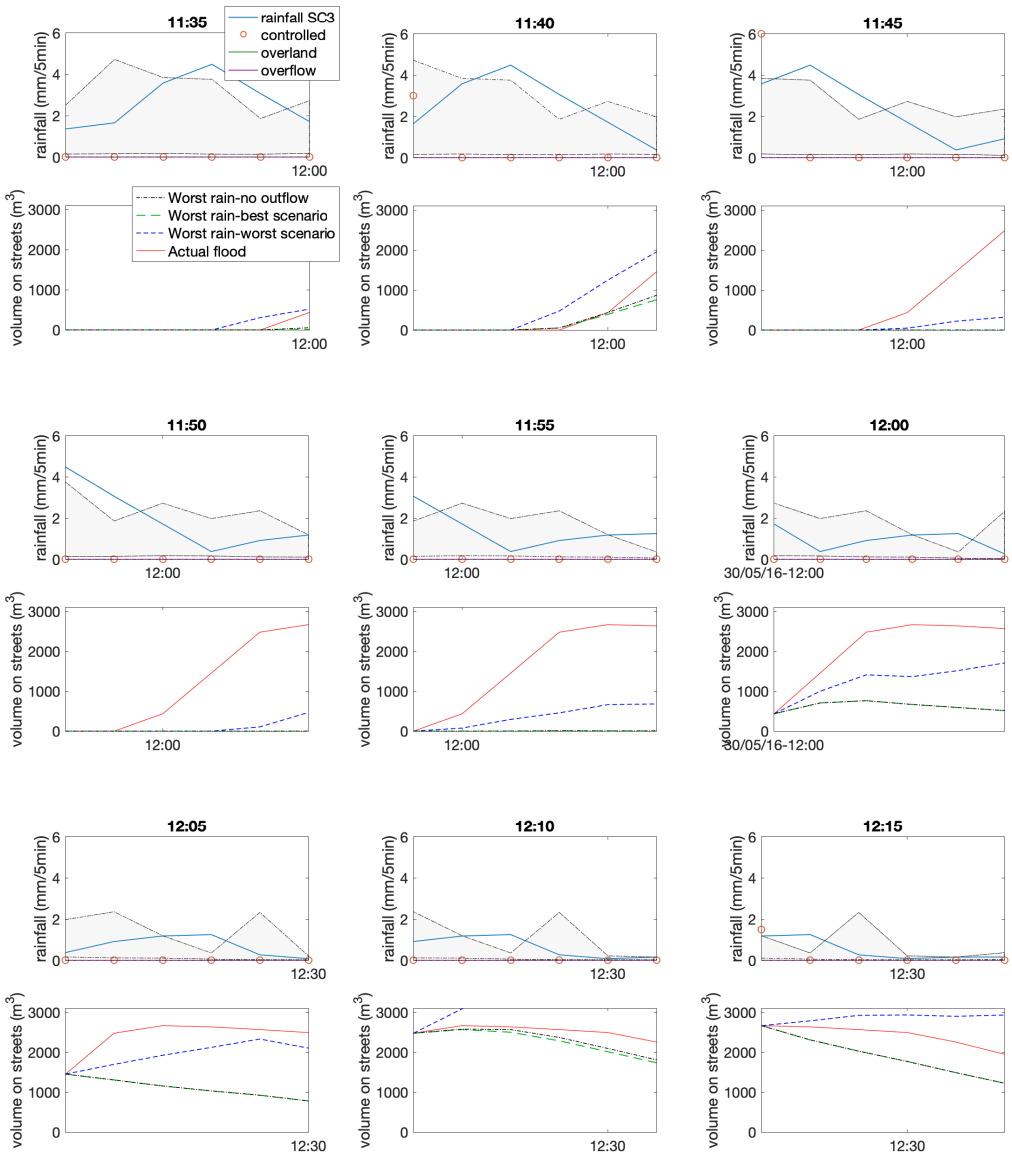

Figure 6.2: Illustration of MMPC with steps of 5 minutes, from 11:35 until 12:15. Every time the green line yields a lower flood than the grey line (11:35, 11:40 and 12:10), the system follows this scenario and discharges in the next time step. The discharge is indicated via a non-zero value for the variable 'controlled' (in orange).

is not emptied by the control system. This case is included because it shows what could happen in the worst member without an action from the MMPC. The last line, *best case*, is the best flood reduction which can be attained under the worst rainfall member. In a lot of the time steps, this coincides perfectly with the *zero case*. Only in cases where a lower flood is attainable by emptying the buffer, one can observe that the MMPC evacuates water in the next time step. On the figures, the orange scatterplot starts with a non-zero value in such cases.

6.3 Discussion

Based on these MMPC simulations, several conclusions can be drawn with respect to the user-defined settings of the intelligent control.

6.3.1 Accuracy

The STEPS-BE extrapolations do not always present a good prediction of the actual rainfall event, as already described in the work of Allaeys [76]. This is confirmed by the flood predictions on Figure 6.2, which systematically underestimate the flood creation. Between 11:40 and 12:05, the worst case flood prediction is always a lot less than the actual flood creation. However, the timing of the flood creation is assessed very precise. Because of this, buffer capacity is made available in time to intercept part of the heavy rainfall.
This suggests that the good performance with uncertain forecasts is mostly due to a good adaptation of the *flood* criterion to a *flood risk* criterion, in combination with a reliable impact model. As shown for simulation 6 at 11:35, the slightest sign of a flood creation already convinces the system to act fast and follow an evacuation scenario.

6.3.2 Number of members

A completely new parameter that needs to be considered is the number of radar extrapolations. Ideally, the system works with all 20 available members to create a more reliable risk assessment. In simulation 5, Matlab already requires 6 minutes to decide which scenario to pick based on 10 members. This is longer than the time step of 5 minutes between each MMPC calculation. So, the code will need to run faster to enable a real-time implementation. This can be done by increasing the time step to 10 minutes, by improving the code performance or by lowering the number of scenarios or members. Changing the lead time only has a limited effect on the calculation time, as discussed in Chapter 5. Luckily, the results from simulations 5, 6 and 7 indicate that running the MMPC with 10 or 5 members is already sufficient to achieve the minimal flood of 2668.2m^3 with *g100*.
It seems that the number of members is not the most governing factor for MMPC during this specific event. Whenever the rainfall event allows for large discharges right before the flood, this low amount of members should be sufficient. If only one of the members predicts enough rainfall to create a flood, the risk calculation will

notice this and act accordingly. So, as long as acceptable extrapolations are provided, the cautious risk assessment aids in keeping the number of members relatively low.

6.3.3 Lead time

Based on the simulations performed, the Multiple Model Predictive Control seems to achieve identical flood reductions compared to the regular MPC. Simulation 7 even suggests that the minimal lead time of 20 minutes from the previous Chapter is still valid. The 5 extrapolated rainfall fields, in combination with the cautious *flood risk* criterion are enough to convince the intelligent control to free up buffer space.
As mentioned in Chapter 5, it is best to provide outflow rates that are high enough to empty the full buffer within the lead time. If a storm occurs with a higher rainfall volume than the capacity of the buffer, it should at least be completely empty to intercept as much as it can. This is also done here, since a lead time of 30 minutes and an outflow rate of 15L/10min can take out 45 litres. For DUO3, the total volume equals $V = C \cdot H_{b,max} = 0.65L/\text{mm} \cdot 72\text{mm} = 46.8L$.

6.3.4 Long term predictions

Although it seems as if the nowcasting is sufficient to minimize the flood in this event, it will presumably not always be the case. The poor predictions of the flood volumes confirm this. Moreover, it is possible that emptying 60 or 30 minutes in advance is too late for some events, regardless of the precision of forecasts. Simulation 4 proves that the *days ahead*-criterion also works, which was already expected based on the results of Chapter 5. It should however be noted that the reduction is slightly less, and the buffer falls dry for almost a full day in this simulation. This dry period is directly linked to the *days ahead*-criterion, which forecasts one day in advance. Because it already sees the full rainfall event, the system completely empties the buffer beforehand.
A critical note to make for simulation 4 that the predictions of the *days ahead*-criterion are not subjected to uncertainties for this simulation. They are exact recordings of rainfall and evaporation. In a real-time application, this criterion would need to operate with a less reliable prediction. For instance, the RMI in Belgium creates rainfall maps, showing the future rainfall over 24 hours. An example of this is shown in Figure 6.3. To quantify the effect of such uncertain forecasts, the *days ahead* criterion is slightly modified. The rainfall forecast of 24 hours is still the summation of exact rainfall data, but the result is rounded down according to the scale of the RMI. This scale is as follows: 0, 0.5, 1, 10, 25, 50, 75mm. So, if the exact recording says 12mm rain fell in 24 hours, the MMPC will round this to 10mm. If this underestimation of the exact rainfall still shows that a lot of water is expected, the buffer will discharge part of its retained volume. A long term simulation of 4 four months is conducted to test the efficiency of this modified *days ahead* criterion. Table 6.2 shows the values from the earlier Table 5.8, but now the extra simulation is added. The lower amount of dry days (3.99) shows that the more cautious *days ahaed* criterion manages the buffer water better. However, the flood reduction decreased

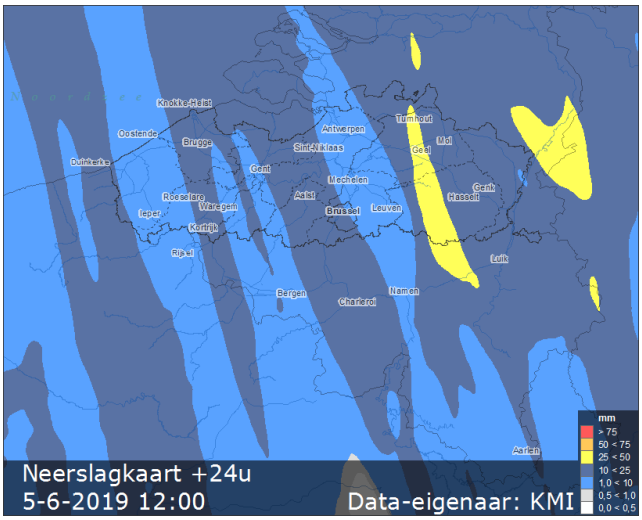

Figure 6.3: A forecast of the future rainfall depth with a time horizon of 24 hours [47]. For Antwerp, this predicts between 1 and 10mm precipitation.

Table 6.2: Flood volumes and water stress for MPC with uncertain long term weather forecasts. The *days ahead* criterion with uncertain long term forecasts leads to less spillage of water.

	Flood volume (m^3)	Dry buffer days
No MPC	3180.2	2.63
MPC using only *flood* criterion	2668.2	2.63
MPC using *days ahead* criterion	2680.0	4.42
MPC with *days ahead* criterion based on uncertain forecasts	2796.0	3.99

because part of the precautionary emptying happened closer to the extreme rainfall event.
These simulation results indicate that further fine-tuning of this *days ahead* criterion might be useful.

6.3.5 Calculation time

A last important factor to consider when investigating the potential benefit of a real-time intelligent control, is the calculation time. In the simulations that are performed here, a the strategy is re-evaluated every 5 minutes. However, the calculation of 10 ensemble members over 40 different scenarios with a lead time of 30 minutes takes around 360 seconds (6 minutes) in the current Matlab code. Considering that a real-time system also needs to collect its data at the start of a new time step, this code is not fit for real-time implementation yet. The tidal info needs to be downloaded, the rainfall ensemble needs to be calculated, the temperature and humidity can be used for an evaporation estimation and the water levels can be read

to update the system state in the model.
One option is to lower the parameters even more, which worked for this rainfall event. With a lead time of 20 minutes and with only 5 rainfall members, the same reductions are achieved. The calculation time is then around 88.6 seconds.
Another option is to convert the Matlab code into a faster model. This will probably yield the largest effect. However, this falls outside of the scope of this thesis research.

6.4 Conclusion

This chapter formulates an answer to the last objective of this thesis. Building on the MPC code from Chapter 5, a Multiple Model Predictive Control strategy is developed. The model still calculates the impact of n different steering scenarios, but repeats this process for N future extrapolations of the rainfall field. The selection of the optimal scenario now happens in a probabilistic way. For every scenario n_i, the flood risk is calculated instead of the flood in MPC.
Next, the results of seven simulations are analysed. Using only 5 of the 20 members, the model still ends up with the minimal flood volume. This is a promising result, because this lower amount of possible futures sharply reduces the computational effort for the system. Another way to increase the safety can be to select the rainfall members which predict the largest volume over the lead time.
Concerning the lead time of the MMPC, the same conclusion as Chapter 5 is valid. Up to 20 minutes in advance, the intelligent control is able to steer the buffer towards a maximal reduction. This is again an interesting result. Of course, more rainfall events need to be tested out to confirm or discard this lower bound of around 20 minutes. In any case, calculating only 20 minutes in advance yields a system that is almost to operate within 5 minutes.
In conclusion, the simulations suggest that the *flood risk* criterion is a good first objective for intelligent control with uncertain forecasts.
Still, the simulations also indicated that flood calculations based on the radar extrapolations can still end up with underestimations. To anticipate on this, the second objective from Chapter 5 is also tested here. An almost similar flood reduction is achieved via this objective, by emptying one day in advance based on perfect long term forecasts.
Lastly, the long term forecasts are rounded down to mimic an incorrect long term forecast where the rainfall depth is underestimated. Consequently, the *days ahead* criterion spills less water, but no longer reaches the minimal flood volume. Therefore, this second objective would need further fine-tuning if it is to be implemented in a real application.

Chapter 7

Conclusion

7.1 Objectives of this research

7.1.1 Construction and calibration of new green roof model

In order to solve the main research objective, a green roof model was developed to simulate a green roof's runoff given rainfall and evapotranspiration. The model structure was chosen based on available literature, and calibration is done based on the measurements from the test site in Antwerp. Automatic calibration, which chooses parameter values to minimize the error function between simulated and measured data, proved to be difficult. The algorithm was too limiting, and the amount of parameters to configure was too large. To further improve the parameter values that followed from this approach, inspiration is found in literature and manual calibration is conducted.
Two of the three green roof types are validated with measurements from two different test sites in France. The third roof type (blue-green roof with a static buffer) has no identical experimental set-up in France, so validation is done with another dataset from the same test site in Antwerp. Overall, the model performs reasonable but recalibration is advised when a larger dataset is available. The dry summer of 2018, along with the absence of the winter months gave only very few runoff data. Especially the substrate parameters for the blue-green roof with 20cm of soil and the surface infiltration rates need to be reconsidered.

7.1.2 Long term simulations

On an individual scale, the different green roof types are compared to each other. Long term simulations give a more reliable image. Two key performance indicators are considered: the water balance and the vegetation stress. Contrarily to what the calibration period showed, the long term water balances of the three different roof types are quite close together on the long term. This is because the calibration period gives a skew image without wet winter months and with a very dry summer. Overall, the blue-green roof that continuously discharges a small volume creates the

lowest amount of runoff (49.3% of all rainfall). With a static buffer, the substrate and buffer restore their retention capacity much slower, resulting in more runoff (52% of all rainfall). The conventional green roof creates even more runoff (54.3% of all rainfall) because its retention capacity is lower.
Concerning drought resistance, the static buffer is the best option. On a yearly basis, the substrate is only expected to dry out for a duration of 8.1 days, compared to 44.9 days for a discharging buffer. The conventional green roof is even worse, with 61.0 days in an average year. This is one sixth of the total year, putting a considerable stress on the plants.
On an urban scale, the hydrological performance of each roof type is quantified. Simulations of 100 year show that the blue-green roof with a continuously emptying buffer is most reliable in flood mitigation. If all flat roofs in Antwerp are equipped with such blue-green roofs, the T20 flood can reduce by 28.5%.

7.1.3 Intelligent control of buffers

Looking at the long term simulations, it is clear that a discharging buffer has the advantage of retaining more water during a heavy rainfall, whereas a static buffer is more beneficial for the health of the vegetation. Intelligent control aims to find the best compromise between both.
At first, a rudimentary control system is tested. Here, the buffers release a certain amount of water based on the predicted rainfall. Because the user can only define the lead time and outflow rate, the control strategy does not necessarily perform the right action in every situation of rainfall. Still, long term simulations indicate that the T20 flood can reduce by 37% with this system, if all flat roofs have an intelligent blue-green roof with a 20cm soil layer. Such thin installations can be easily placed on roofs without major structural adjustments to the building.
Next, Model Predictive Control is tried out for two single rainfall events. This control strategy assumes several possible actions that can be done with the buffer and calculates the impact that these actions have on an urban scale. The scenario which yields the lowest flood volume is then picked from this set. This MPC clearly outperforms the rudimentary system of early evacuation. In one of the two considered rainfall events, the simple control mechanism only reduced the flood by 0.14%. The MPC achieved reductions of 5.6%. In the second event, the reduction were 18.6 and 20.8%. The key to this higher flood mitigation is the fact that MPC always operates within the boundaries of the sewer network, because the impact of each scenario is calculated before one is executed.
Based on 50 simulations of the rainfall event of 30 May 2016 which caused a flood in Antwerp, a sensitivity analysis is conducted for MPC. For this recent storm, the simulations indicate that MPC can manage the buffer towards a minimal flood. This already happens for a time horizon as low as 20 minutes and a number of control scenarios as low as 50. The user should give outflow rates that are high enough for a complete evacuation of the buffer within the lead time. This high outflow rate is not chosen by the MPC for the rainfall event of 30 May 2016, but this is because the sewer network would not be able to process this volume at high tide.

Indeed, for simulations at low tide, the MPC immediately picked this outflow rate as the one leading to the minimal flood. This upper limit for the outflow rates is however still open for further investigation. Other MPC simulations from several weeks revealed that such MPC system does not gravely jeopardize the vegetation health on individual green roofs. Over the course of four months, MPC only created 4.42 days where the buffer falls dry, compared to 2.63 without intelligent control.
Three important conclusions are drawn from these simulations. First and foremost, upgrading all green roofs to MPC keeps an extra 45-50% of the already removed volume from the streets. This result is valid for all degrees of urban green roof installation that are tested. Furthermore, filling 50% of the potential green roof area in Antwerp with intelligent blue-green roofs outperforms 75% of the potential area covered with conventional blue-green roofs. The same conclusion is also valid when comparing 75% of the area with intelligent and 100% of the area with conventional blue-green roofs. Lastly, intelligent roofs could have reduced the most recent flood in Antwerp by 37%, by only converting all flat roofs in the centre, a mere 9.3% of the inner city surface. This 37% is roughly equivalent to a reduction of 1.56 hectares.
These results are especially interesting for policy makers, as the flood mitigation via green roofs turns more efficient without asking an extra effort from the citizens. A blue-green roof that is already installed can be converted to an intelligent system at any time. Most local governments in Flanders already promote the installation of green roofs financially. If further research confirms the potential of this intelligent control, these subsidies make even more sense.

7.1.4 Intelligent control of buffers with uncertain weather forecasts

The previous objective was to investigate if and how intelligent control can be feasible in theory. The last objective of this thesis is to assess if such control strategies can work in a real-time application. This is done by introducing uncertainties in the rainfall forecasts. Based on the actual radar observations of that day, extrapolations are made by the Royal Meteorological Institute that function as uncertain forecasts for this event.
Similarly to normal MPC, the code calculates the impact of different discharge actions. Now, the impact of every action is calculated multiple times, considering the different possible rainfall inputs. The optimal scenario is the one that has the lowest overall risk of flooding, with risk the product of damage and probability.
The general conclusion is that the shift from MPC to MMPC does not affect the efficiency of the intelligent control. A step by step analysis of the MMPC process showed that the flood creation is generally underestimated because of the uncertain rainfall forecasts. However, the timing of the flood creation is precise, and together with the cautious risk assessment, this results in good actions from the MMPC. Considering only 5 of the 20 possible extrapolations, the minimal flood is still attained on 30 May 2016. The lead time of 20 minutes is also still manageable, and the lower limit of scenarios is even pushed from 50 in Chapter 5 to 40.
In case the heavy rainfall is poorly predicted over the short term for other rainfall

events, a second objective is tested as extra safety measure. For instance, this objective is activated in the absence of a flood. If enough rainfall is predicted over the long term of 24 hours (or more), this objective will try and restore part of the buffer capacity by discharging water. To cope with uncertainty on the long term forecasts, the objective is modified to release less water beforehand. This modification proved to lower the water stress in long simulations of several months. However, the flood reductions via this criterion are suboptimal, so further investigation of the possibilities is advised.

7.2 Recommendations for future research

By defining a set of objectives for a thesis research, one inevitably leaves a few interesting elements outside of the scope. Such shortcomings, simplifications and assumptions are listed here. Linked to that, some recommendations for future research are given to the reader.

Models First and foremost, a recalibration of the current green roof model would be interesting with a larger set of measurements. The dry summer and the absence of winter months are the most notable shortcomings in the current calibration.
The most important assumptions that need to be reconsidered during recalibration are the infiltration rate and the description of the substrate layer. If the infiltration rate is not correctly determined, the system fails to predict overland runoff on the green roof and the intelligent control might make the wrong choices. Separate tests on the infiltration rate of the soil can be a good way to overcome this first issue. Soil moisture measurements might be a good way to analyse the operation of the substrate layer.
For the Model Predictive Control, the main improvement would be to consider uncertain long term forecasts next to the uncertain short term radar extrapolations. The calculation time is also an obstacle to overcome. This might be done via a faster coding language.
Another topic for future research is the conceptual model for the city of Antwerp. Although this already performs quite well, a critical analysis of its structure is not included in this research.

Other sewer networks Linked to this, the feasibility study for intelligent blue-green roofs can also be extended to other cities and conceptual models. Since the use of such an impact model is the key to success for MPC, the functioning with other sewer models is an interesting topic for further research. The most interesting addition would be the study of a gravitational sewer network. In such a system, the downstream conditions will no longer be a tidal river or pump station, but bottlenecks in the pipe network. Such a case study is able to ascertain the added value of intelligent roofs more directly, since the pluvial flooding would not be governed by a river boundary. Also, different MPC options might become possible,

when the sewer is only limited by pipe capacity and not by other downstream boundaries.

Other rainfall events Next, the current case study can be expanded by considering a heterogeneous set of rainfall events. For instance, for high peak intensities, the MPC might be unable to act because overland runoff is created. In such cases, blue buffers probably outperform blue-green solutions. For slower flood creations, a lead time of 20 minutes is also expected to hinder a timely intelligent control.
However, the most important thing to consider in future research are long simulations with continuously updating short term forecasts. This will provide a better similarity to a real-time implementation. It is also a more certain way to determine if the water is always managed in a smart way under the current MPC.

Pilot project After a solid proof of concept, a pilot project can be started. This enables the researchers to expose the challenges of a real-time system. The last hurdles to be taken here are the calculation speed of the MMPC code, together with the data collection each time step. Every 5 or 10 minutes, new long term and short term forecasts need to be downloaded or calculated, and sensor data needs to be collected and analysed.

Costs and benefits Lastly, the economic aspect should come into focus. For governments, a cost-benefit analysis could demonstrate if the total cost outweighs the expected saving on flood damage. On top of that, the analysis needs to incorporate the other beneficial effects listed in Chapter 2. The total cost encompasses the installation and maintenance, as well as the conversion to an intelligent system via sensors.
Financial or legal means could convince the public opinion of the added value of intelligent water management. Linking the buffers to household applications (washing cars, flushing toilets...) might help here. Apart from that, if companies are reassured that there is a market for such products and services, this would benefit the development phase.

Appendices

Appendix A

Extra information regarding the calibration and validation of the green roof model

A.1 Waterbalances from calibration period

See Figure A.1 and Table A.1.

A.2 Interaction between buffer and substrate layer

Figure A.2 illustrates the interaction that takes place between the buffer and substrate layer. A simulation with a DUO3 roof type is taken as example. The controlled outflow is normally not possible with DUO3, but is added here to show different hydrological regimes. The dashed blue arrows indicate the flow of water from substrate to buffer or vice versa. The blue words indicate the processes that occur in the buffer, whereas the green words explain the substrate processes.
Whenever precipitation brings the relative moisture content in the substrate above the Field Capacity (black dashed line), percolation occurs and the buffer level increases. Between 5 June and 12 June, the substrate content fluctuates in a pattern. The evaporation is extracting water from the substrate layer while the buffer is supplying the substrate with new water. Because the capillary irrigation is of a smaller order of

Table A.1: Overview of the hydrological performance of each green roof type during the calibration period.

	DUO1	DUO2	DUO3	
Rainfall	0.43	0.43	0.43	m^3
Runoff	0.20	0.15	0.16	m^3
ET	0.23	0.29	0.28	m^3
Efficiency	53.5	66.3	65.1	%

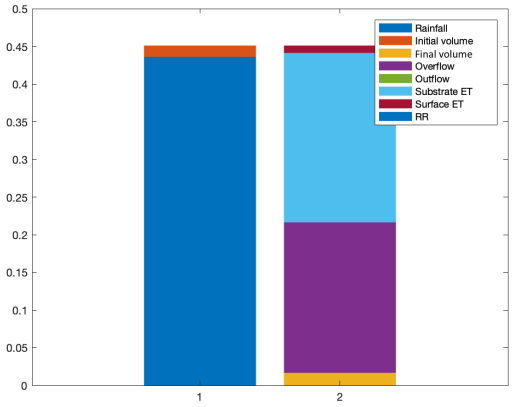

(a) Conventional green roof (DUO1)

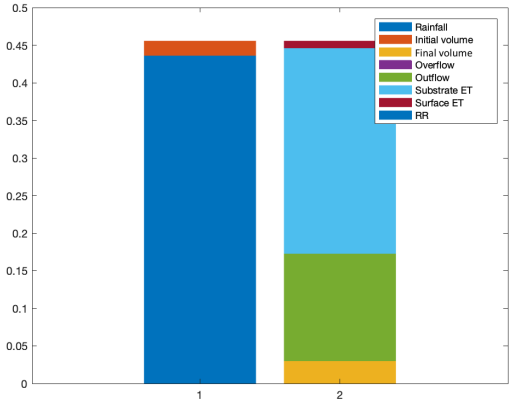

(b) Blue-green roof with outflow (DUO2)

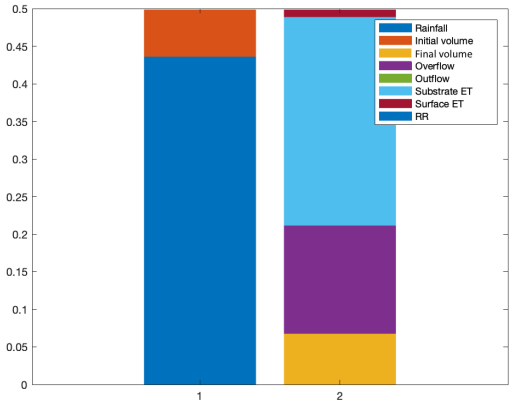

(c) Blue-green roof with static buffer (DUO3)

Figure A.1: Water balance for three roof types over the calibration period in m^3. Input: rainfall (dark blue) and initial volume (orange). Output: evaporation (light blue and red), runoff (light green and purple) and final volume (yellow).

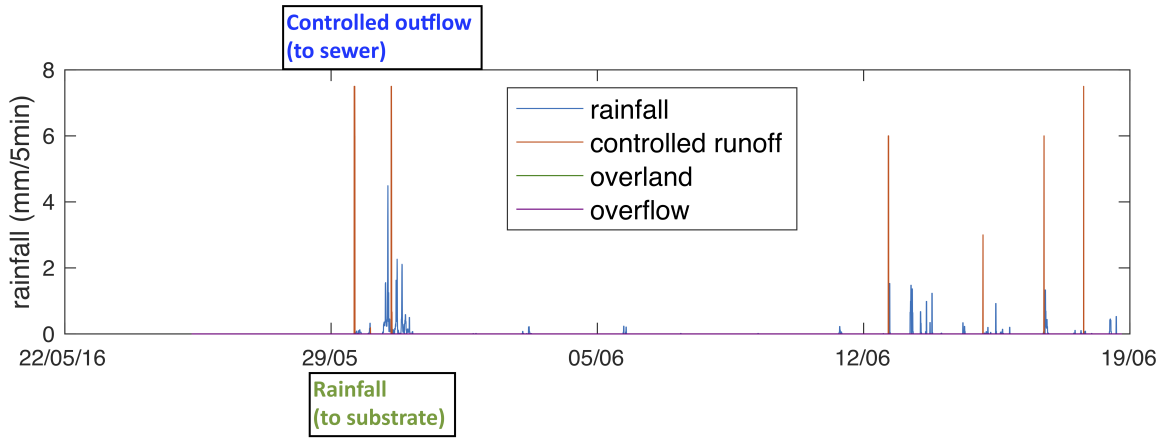

(a) Rainfall and controlled outflow

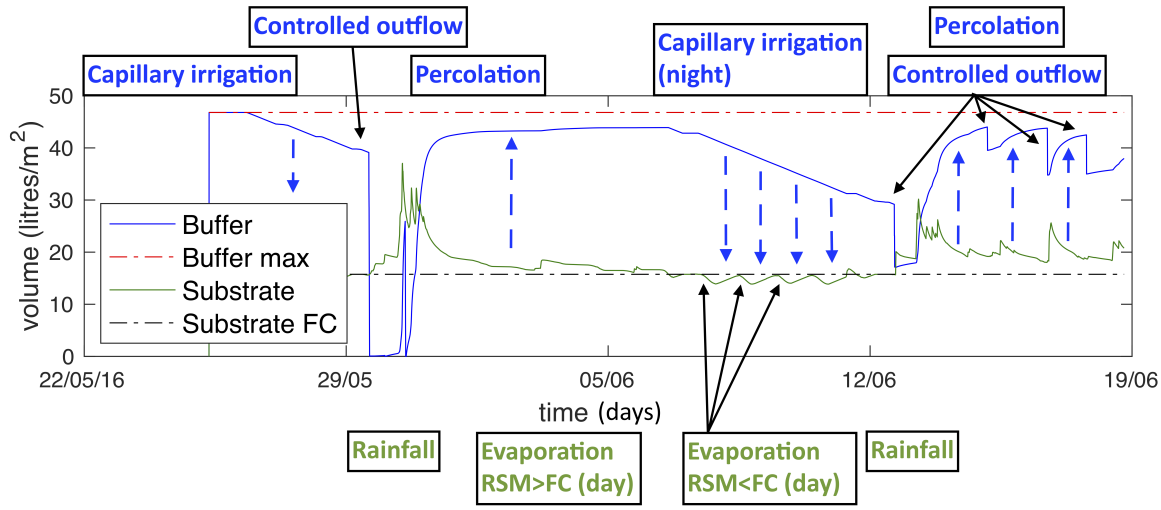

(b) Simulation of the buffer and substrate layer for a DUO3 roof. The buffer content varies between 0 and 46.8 litres, whereas the substrate content fluctuates less and stays around its Field Capacity.

Figure A.2: An illustration of the interaction between substrate and buffer for a DUO3 green roof.

magnitude, the substrate becomes drier during the day. However, in the evening and the night the evaporation turns to values close to zero, and the capillary irrigation manages to bring the RSM back to the Field Capacity. At this point, the capillary irrigation stops until the substrate is dry again. This behaviour will always occur in long periods without rain and with a filled buffer.

Appendix B

Long term simulations for the city of Antwerp considering several green roof configurations

B.1 Flood volumes in Antwerp according to simulations of 100 years

Figures B.1, B.2 and B.3 are the result of long term simulations with the conceptual sewer model for Antwerp. The dots in colour scale and the diamonds in grey scale show the peak volumes for two different roof types, allowing a comparative analysis. Several degrees of urban green roof installation are considered from *basis* (no green roofs) to *g100* (100% of potential green roof surface area utilised). The time scale indicates 5,259,600 timesteps of 10 minutes, which equals 100 years. The flood volumes are used to determine the values in Table 4.6.

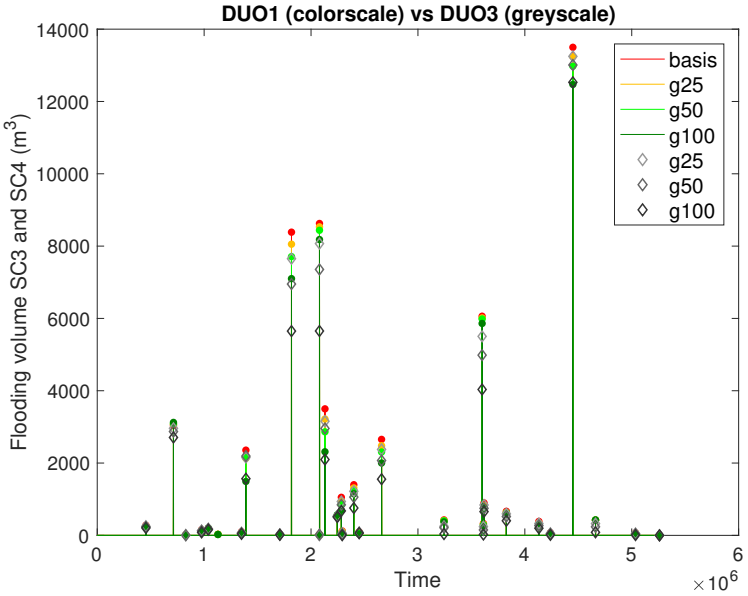

Figure B.1: Flood volumes in SC3 and SC4 for a 100 year simulation with DUO1 roofs (colour) versus DUO3 roofs (grey).

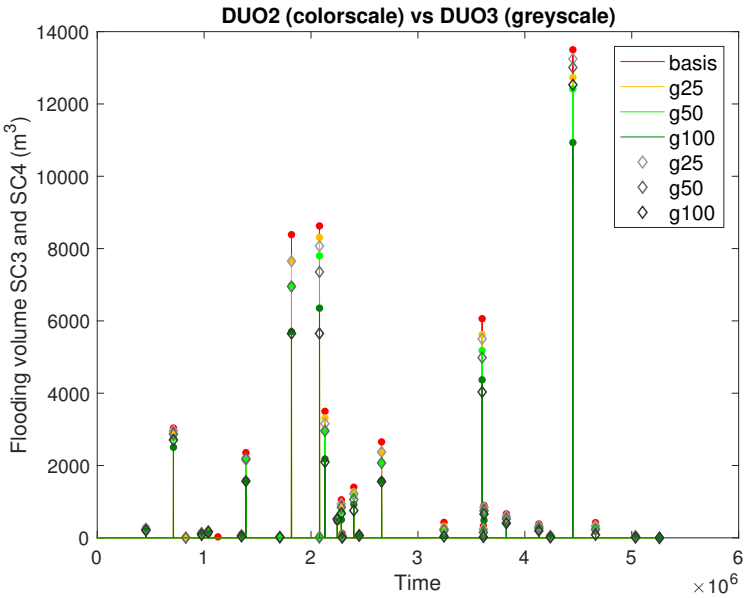

Figure B.2: Flood volumes in SC3 and SC4 for a 100 year simulation with DUO2 roofs (colour) versus DUO3 roofs (grey).

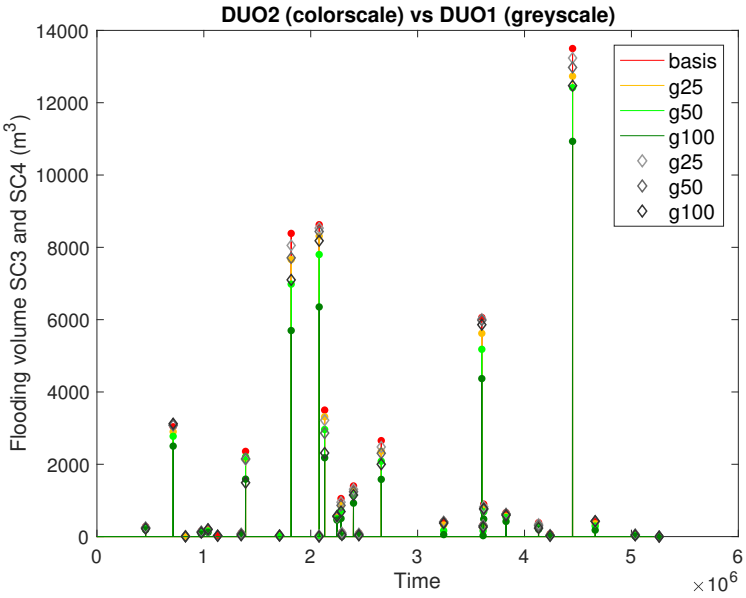

Figure B.3: Flood volumes in SC3 and SC4 for a 100 year simulation with DUO2 roofs (colour) versus DUO1 roofs (grey).

Appendix C

Simulation results for Semi-Intelligent Control

C.1 Long term simulations with SIC

For a Semi-Intelligent Control system, long term simulations of 100 years are performed on the scale of a single roof and on an urban scale.

C.1.1 SIC with constant outflow

For SIC with a constant outflow of 0.2mm/10min and a lead time of 24 hours, the water stress in an average year is illustrated in Figure C.1. Compared to the results in Chapter 4, this intelligent control gives less water stress for a DUO2 system and slightly more water stress for the DUO3 type, which normally has a static buffer.

C.1.2 SIC with variable outflow

For SIC with a variable outflow and a lead time of 24 hours, the flood reductions are illustrated in Figures C.2. The intelligent control gives better reductions for both roof types, but DUO3 becomes the best type for flood mitigation.

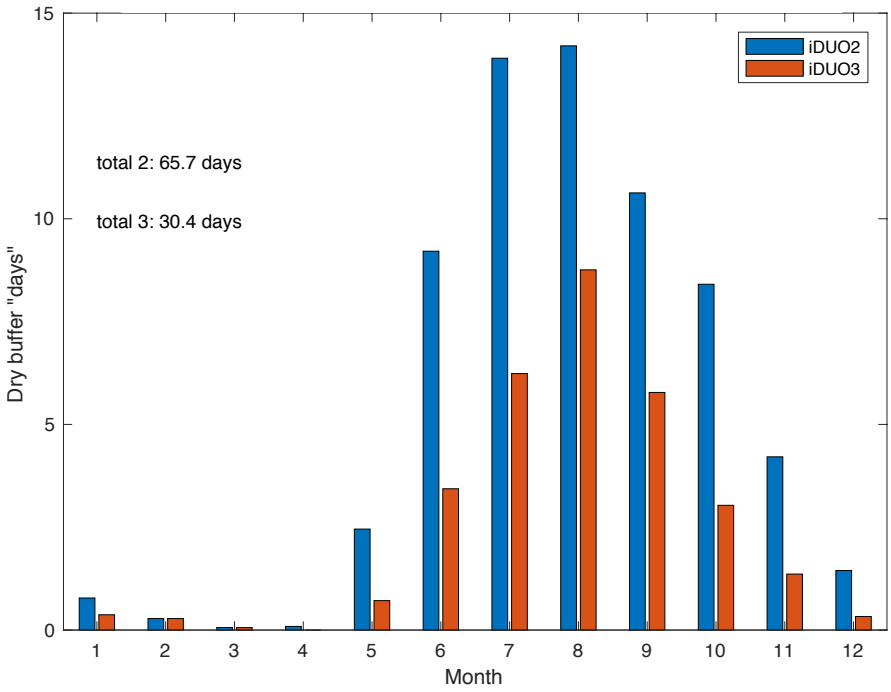

(a) Buffer

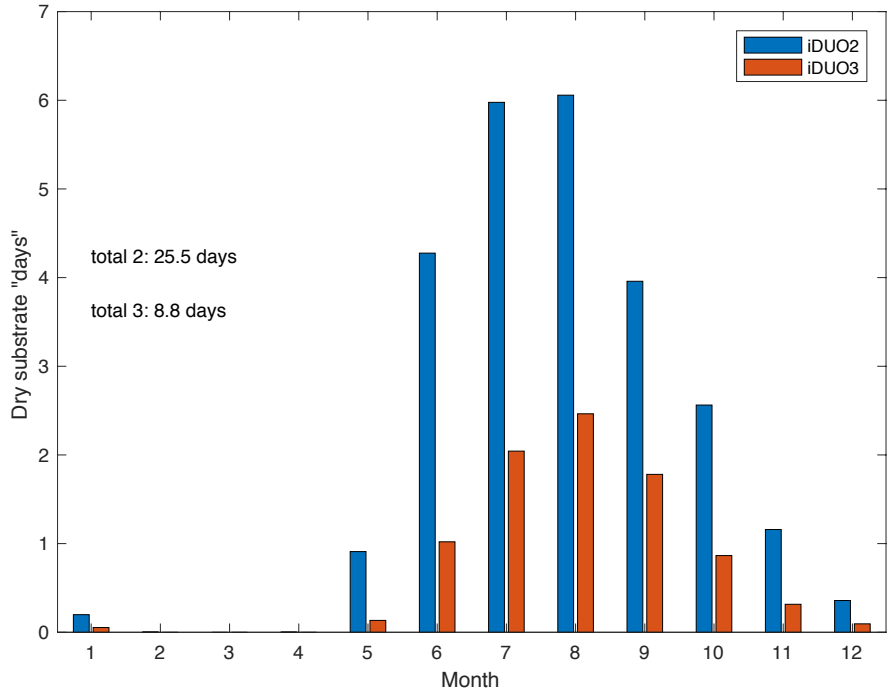

(b) Substrate

Figure C.1: Duration of water scarcity in an average year with intelligent control, expressed as days per month.

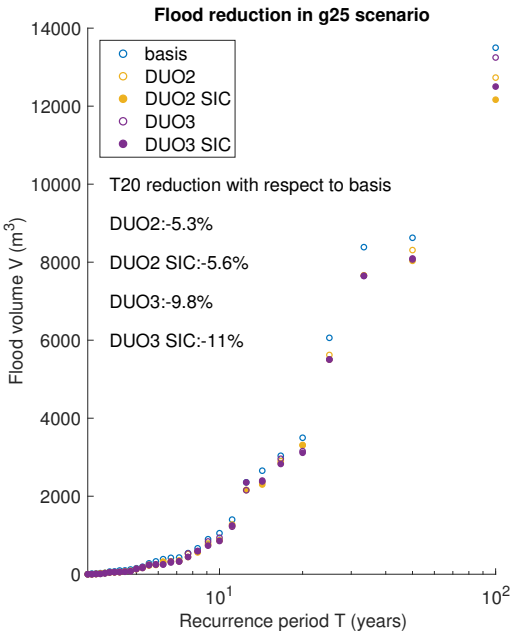

(a) 25% of potential green roof area used.

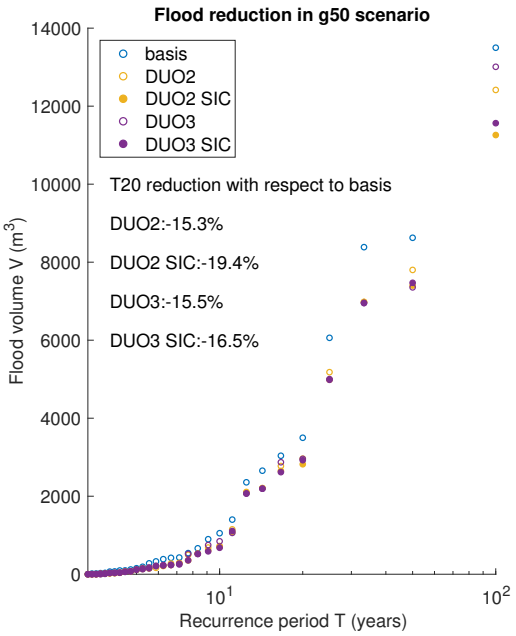

(b) 50% of potential green roof area used.

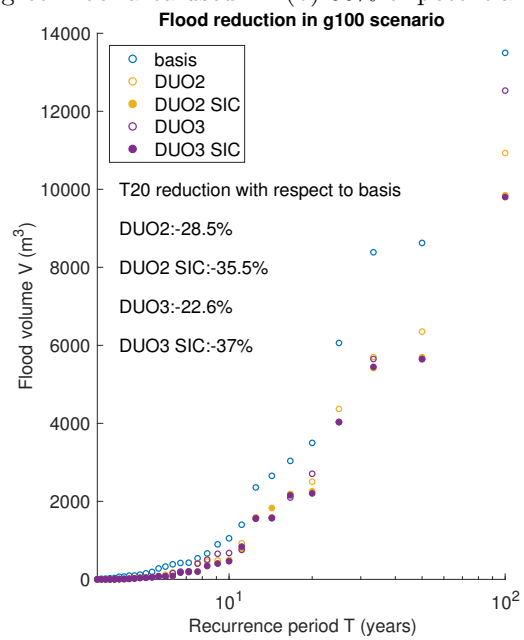

(c) 100% of potential green roof area used.

Figure C.2: Graphs showing the flood volumes (m^3) for events T100 until T3, assuming different degrees of green roof installation in Antwerp. The solid markers represent the results for Semi-Intelligent Control of DUO2 or DUO3. The T20 reductions are expressed in percentages with respect to the original T20 flood.

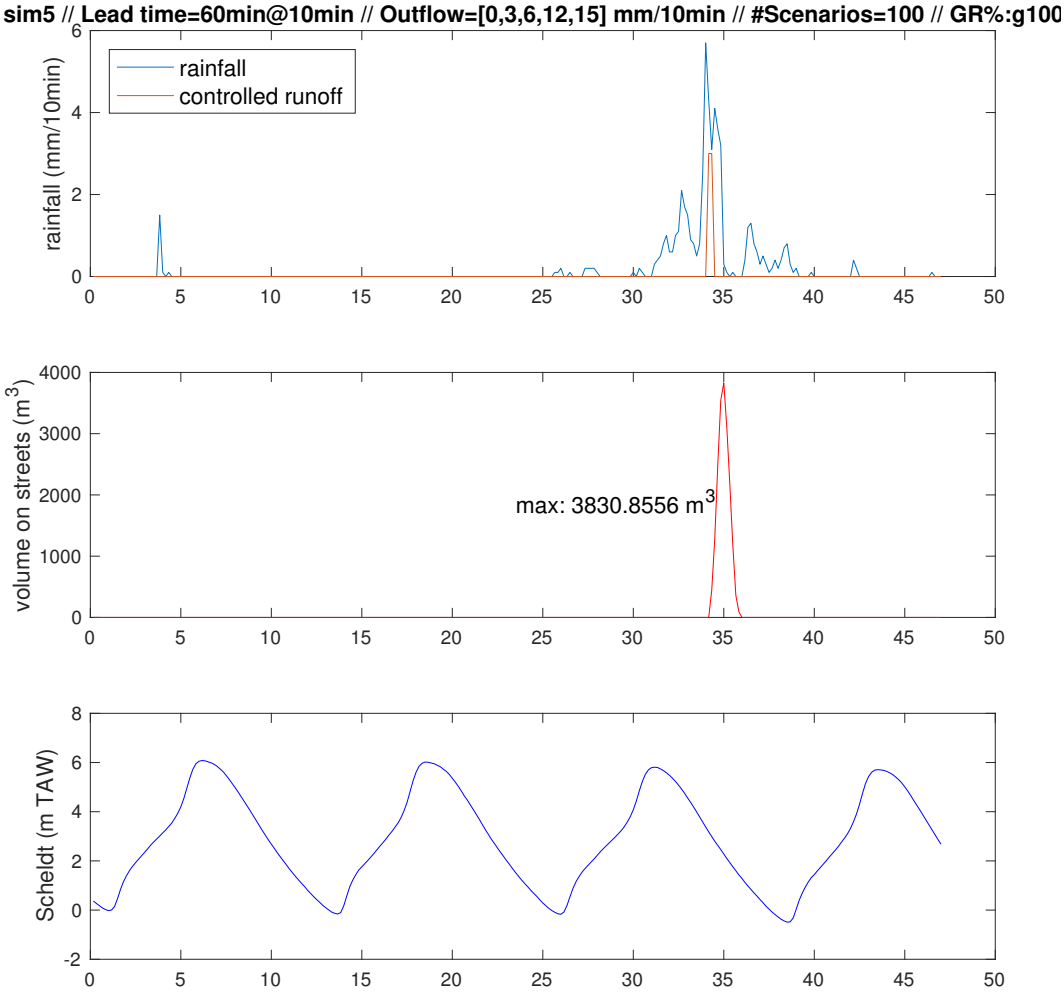

Figure C.3: Overview of the simulation with Model Predictive Control for event 1 with DUO3. First graph shows the rainfall and buffer discharge rates, the second one the flood volumes and the third one the water levels in the tidal river.

C.2 Comparison of SIC and MPC

C.2.1 Rainfall event 1

See Figures C.3 for the results with MPC and C.4 for the results with SIC. These volumes are used to construct Table 5.4. The title above the MPC results indicate the parameters used for the intelligent control (lead time, outflow rates, number of scenarios and degree of green roof installation).

C.2.2 Rainfall event 2

See Figures C.5 for the results with MPC and C.6 for the results with SIC. These volumes are used to construct Table 5.4.

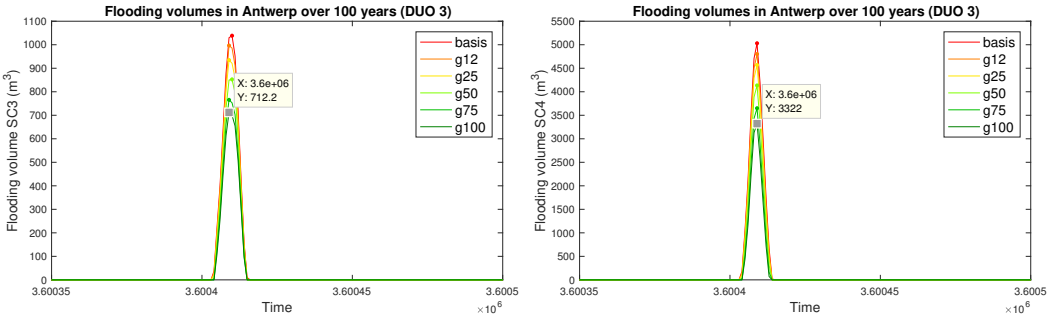

(a) Subcatchment 3 (max 712.2 m^3)

(b) Subcatchment 4 (max 3322 m^3)

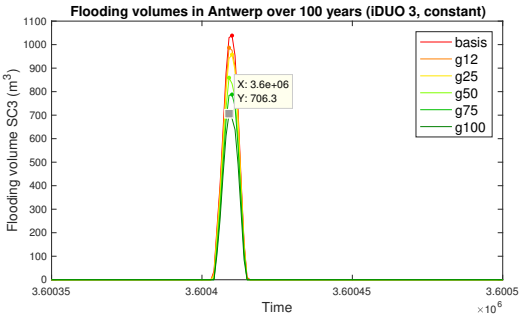

(c) Subcatchment 3 (max 706.3 m^3)

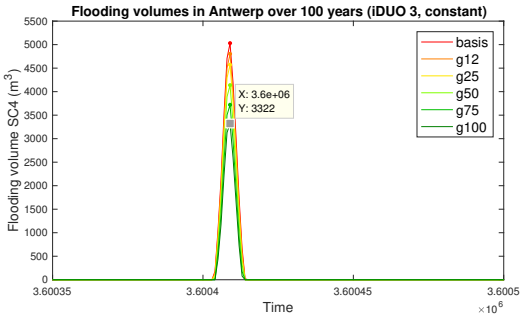

(d) Subcatchment 4 (max 3322 m^3)

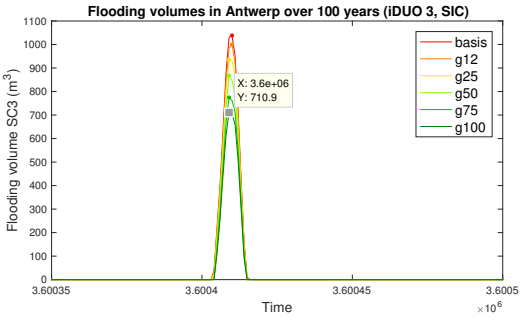

(e) Subcatchment 3 (max 710.9 m^3)

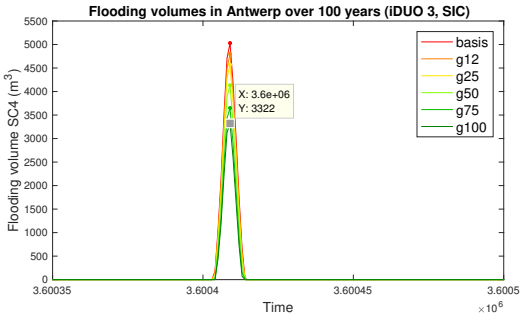

(f) Subcatchment 4 (max 3322 m^3)

Figure C.4: Flood volumes for event 1 with roof type DUO3: (a-b) normal, (c-d) SIC constant and (e-f) SIC variable.

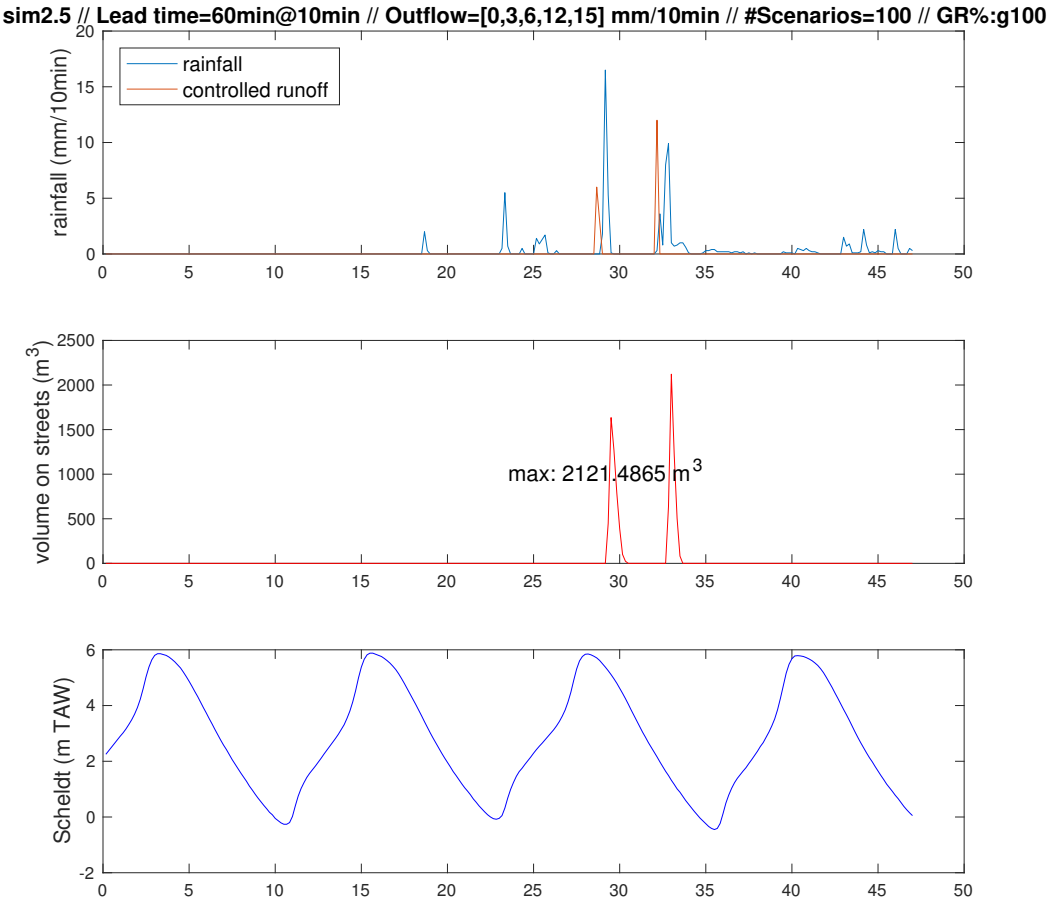

Figure C.5: Overview of the simulation with Model Predictive Control for event 2 with DUO3. First graph shows the rainfall and buffer discharge rates, the second one the flood volumes and the third one the water levels in the tidal river.

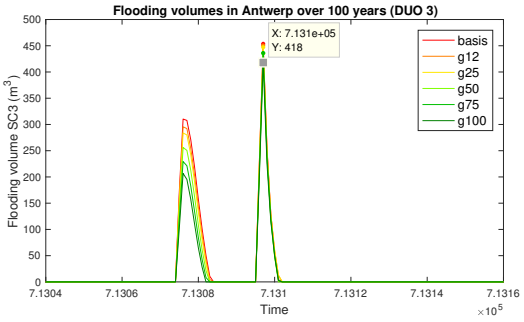

(a) Subcatchment 3 (max 418 m^3)

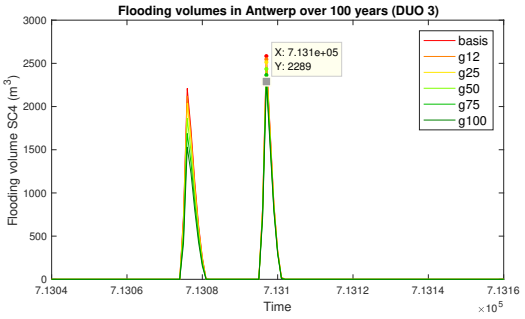

(b) Subcatchment 4 (max 2289 m^3)

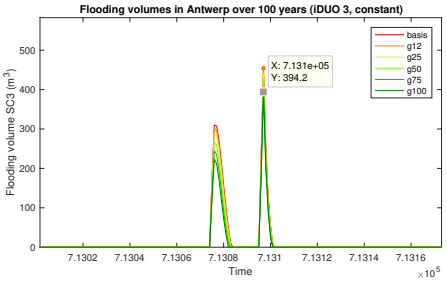

(c) Subcatchment 3 (max 394.2 m^3)

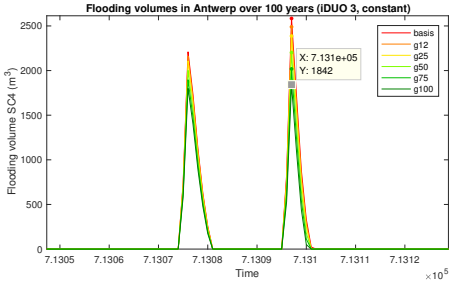

(d) Subcatchment 4 (max 1842 m^3)

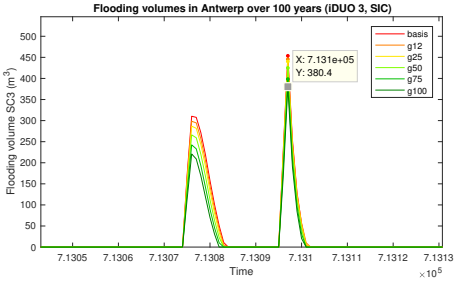

(e) Subcatchment 3 (max 380.4 m^3)

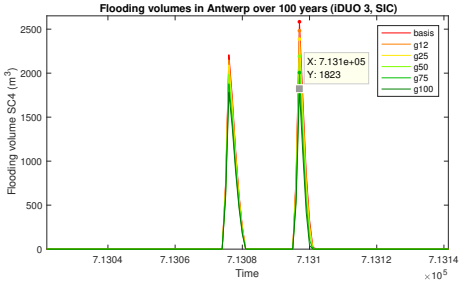

(f) Subcatchment 4 (max 1823 m^3)

Figure C.6: Flood volumes for event 2 with roof type DUO3: (a-b) normal, (c-d) SIC constant and (e-f) SIC variable).

Appendix D

Model Predictive Control for 30 May 2016

Figure D.1 shows how the intelligent control behaves for short term perfect forecasts. The parameter values are indicated in the title of the plot. The flood volume 2668.2m^3 is the minimal flood event in this case.
Figures D.2 and D.3 show long term simulations, respectively with and without intelligent control. The *days ahead* criterion cause precautionary evacuation of buffer water one day before rainfall predictions, causing more water stress.

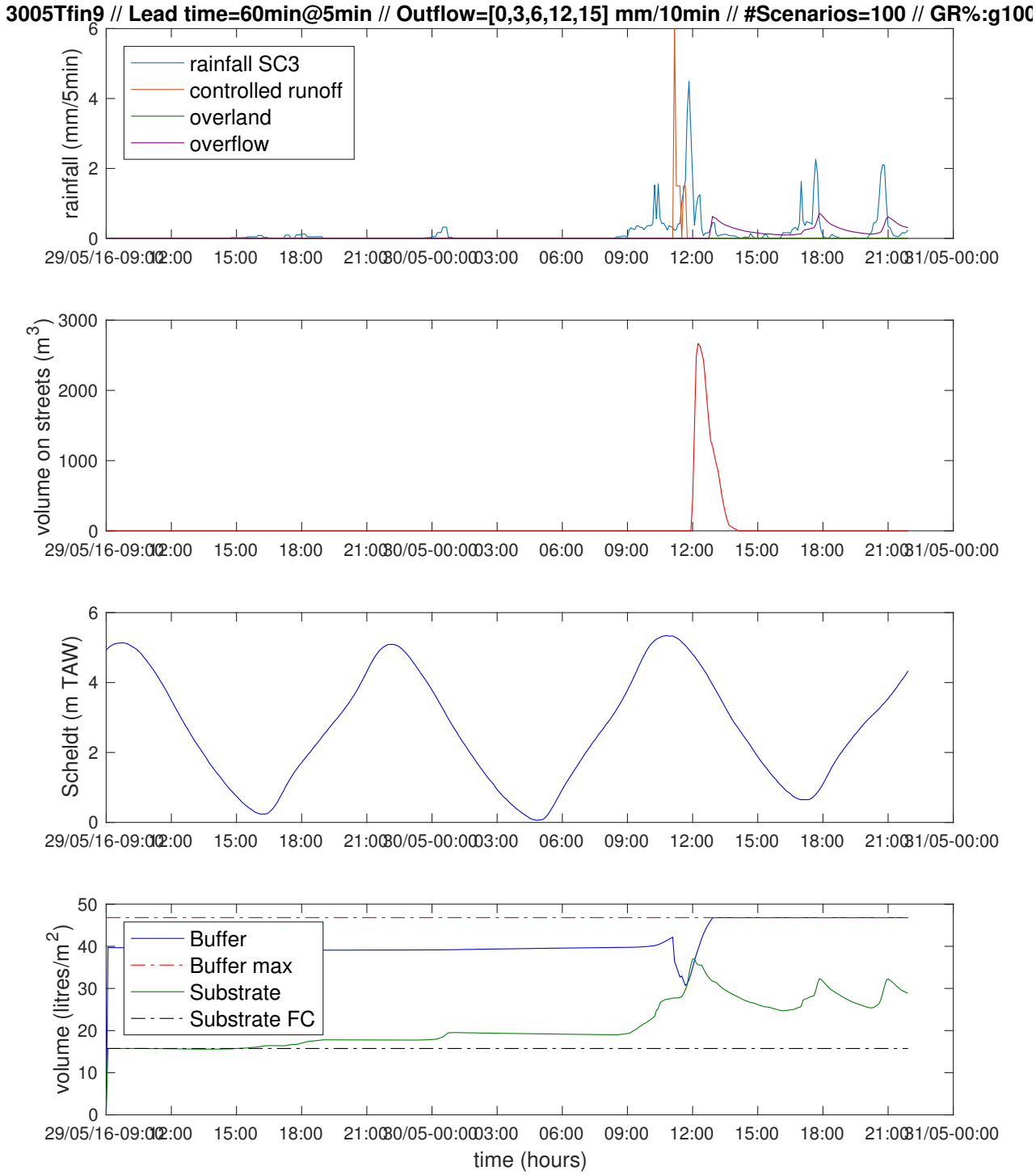

Figure D.1: An MPC simulation for DUO3 on 30 May 2016. The minimal flood of 2668.2m^3 is achieved.

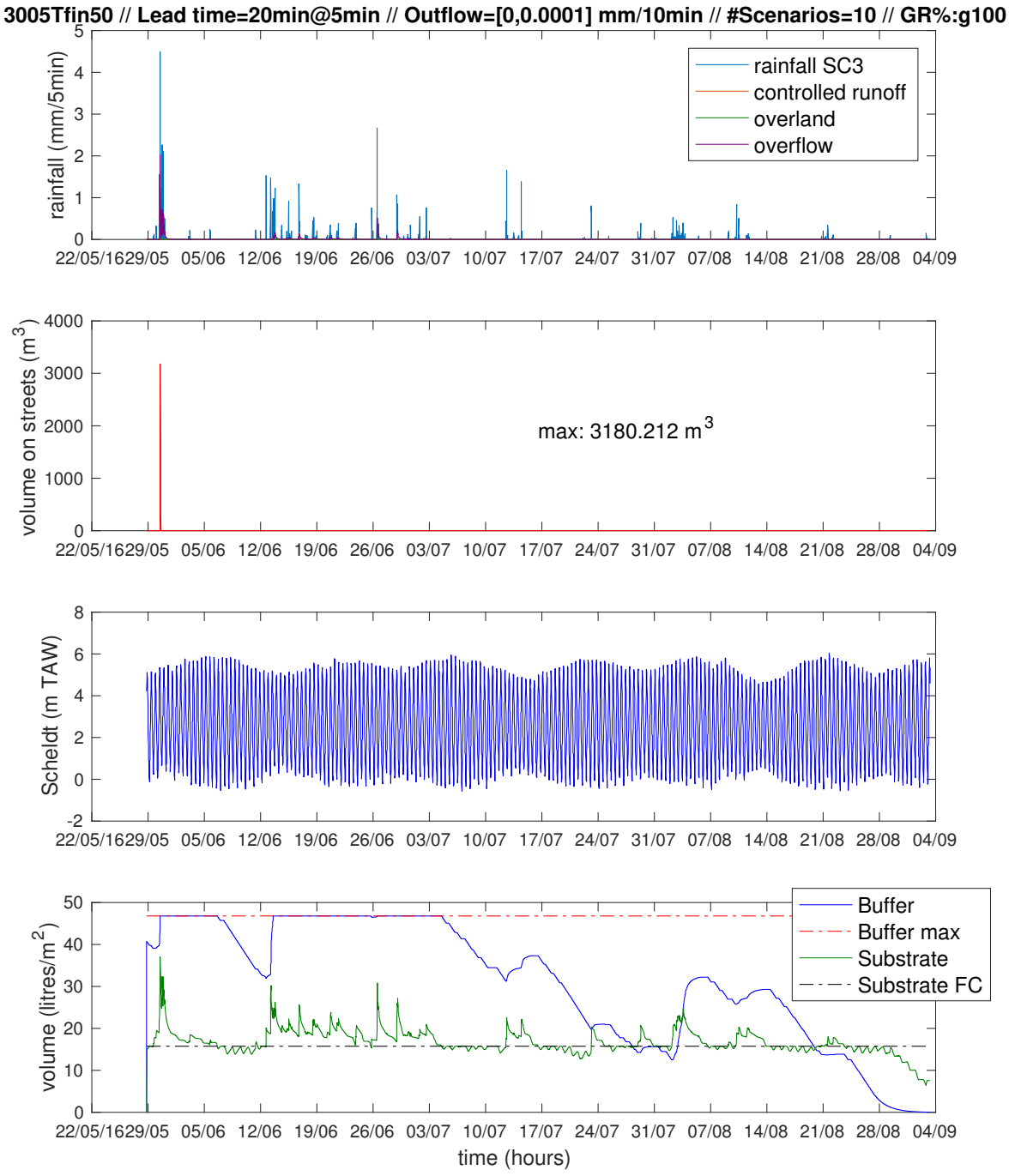

Figure D.2: A long term simulation without any type of intelligent control. The total number of dry days is 2.63.

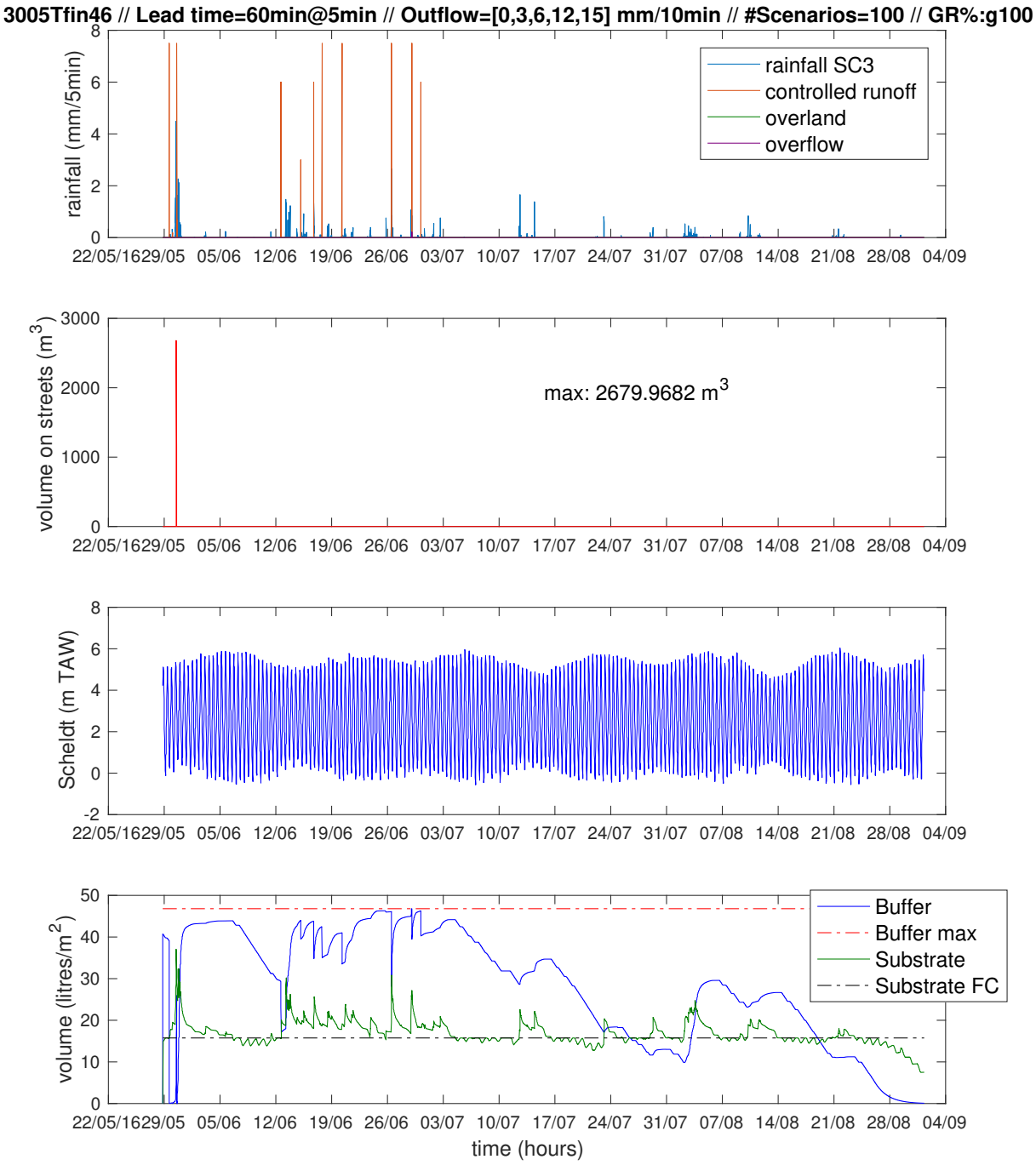

Figure D.3: A long term simulation with MPC. The total number of dry days is 4.42, of which 0.83 days right before the heavy rainfall event on 30 May 2016.

Bibliography

[1] M. Antrop. Landscape change and the urbanization process in Europe. *Landscape and Urban Planning*, 67(1-4):9–26, 2004.

[2] H. Qin, Z. Li, and G. Fu. The effects of low impact development on urban flooding under different rainfall characteristics. *Journal of environmental management*, 129:577–585, 2013.

[3] V. Veach, A. Moilanen, and E. Di Minin. Threats from urban expansion, agricultural transformation and forest loss on global conservation priority areas. *PloS one*, 12(11), 2017.

[4] X. Xu, Y. Xie, K. Qi, Z. Luo, and X. Wang. Detecting the response of bird communities and biodiversity to habitat loss and fragmentation due to urbanization. *Science of the Total Environment*, 624:1561–1576, 2018.

[5] A. Mohajerani, J. Bakaric, and T. Jeffrey-Bailey. The urban heat island effect, its causes, and mitigation, with reference to the thermal properties of asphalt concrete. *Journal of Environmental Management*, 197:522–538, 2017.

[6] J.M. Shepherd. A review of current investigations of urban-induced rainfall and recommendations for the future. *Earth Interactions*, 9(12):1–27, 2005.

[7] J. Han, J. Baik, and H. Lee. Urban impacts on precipitation. *Asia-Pacific Journal of Atmospheric Sciences*, 50(1):17–30, 2014.

[8] P. Willems, V. Ntegeka, P. Baguis, and E. Roulin. Climate change impacts on hydrological extremes along rivers and urban drainage systems in Belgium, 2010.

[9] J. De Niel, H. Tabari, and P. Willems. Modellering en beleidsaanbevelingen ten aanzien van neerslag in antwerpen–samenvatting en beleidsaanbevelingen, 2015.

[10] P. Willems and M. Vrac. Statistical precipitation downscaling for small-scale hydrological impact investigations of climate change. *Journal of Hydrology*, 402(3-4):193–205, 2011.

[11] L. Van Ootegem, K. Van Herck, T. Creten, E. Verhofstadt, L. Foresti, E. Goudenhoofdt, M. Reyniers, L. Delobbe, D. Murla Tuyls, and P. Willems. Exploring the potential of multivariate depth-damage and rainfall-damage models. *Journal of Flood Risk Management*, 11:S916–S929, 2018.

[12] P. Willems. Evaluatie en actualisatie van de IDF-neerslagstatistieken te Ukkel, 2011.

[13] P. Willems. De effecten van verdroging als gevolg van de klimaatwijziging en urbanisatie op oppervlaktewater (slides online). URL: `https://www.kuleuven.be/hydr/cci/reports/Waterforum2014-PWillems.pdf`, last checked on 2010-01-17.

[14] L. Poelmans, A. Van Rompaey, and O. Batelaan. Coupling urban expansion models and hydrological models: How important are spatial patterns? *Land Use Policy*, 27(3):965–975, 2010.

[15] G.A. Meehl and C. Tebaldi. More Intense, More Frequent, and Longer Lasting Heat Waves in the 21st Century. *Science*, 305(5686):994–997, 2004.

[16] H. Wouters and et al. Heat stress increase under climate change twice as large in cities as in rural areas: A study for a densely populated midlatitude maritime region. *Geophysical Research Letters*, 44(17):8997–9007, 2017.

[17] United Nations. Sustainable development goals: clean water and sanitation. URL: `https://www.un.org/sustainabledevelopment/water-and-sanitation/`, last checked on 2010-01-14.

[18] J. De Waegemaeker, M. Van Acker, E. Kerselaers, and E. Rogge. Shifting climate, reshaping urban landscapes: Designing for drought in the Campine landscape. *Journal of Landscape Architecture*, 11(3):72–83, 2016.

[19] G. Ziervogel, M. Shale, and M. Du. Climate change adaptation in a developing country context: The case of urban water supply in Cape Town. *Climate and Development*, 2(2):94–110, 2010.

[20] J. Viljoen. Cape Town Drought Highlights Water Scarcity Risk to Vulnerable Cities Globally: UBS. *Insurance Journal*, 2018.

[21] I. Khalid, A. Mukhtar, and Z. Ahmed. Water Scarcity in South Asia: A Potential Conflict of Future Decades. *Journal of Political Studies*, 21(1):259–280, 2014.

[22] R. Cameron and T. Katzschner. Every last drop: the role of spatial planning in enhancing integrated urban water management in the City of Cape Town. *South African Geographical Journal*, 99(2):196–216, 2017.

[23] B. Dvorak and A. Volder. Green roof vegetation for North American ecoregions: A literature review. *Landscape and Urban Planning*, 96(4):197–213, 2010.

[24] N. Dunnet and N. Kingsbury. Planting green roofs and living walls, 2d ed. *Scitech Book News*, 32(3), 2008.

[25] S. Konasova and R. Vagner Da Silveira. Green roofs: roof system reducing heating and cooling costs. *Business & IT*, 6(1):60–65, 2016.

[26] Y. Toparlar, B. Blocken, B. Maiheu, and G. J.F. van Heijst. The effect of an urban park on the microclimate in its vicinity: a case study for Antwerp, Belgium. *International Journal of Climatology*, 38(December 2017):e303–e322, 2018.

[27] T. Susca, S. R. Gaffin, and G. R. Dell'Osso. Positive effects of vegetation: Urban heat island and green roofs. *Environmental Pollution*, 159(8-9):2119–2126, 2011.

[28] D.B. Rowe. Green roofs as a means of pollution abatement. *Environmental Pollution*, 159(8-9):2100–2110, 2011.

[29] V. Stovin, S. Poë, S. De-Ville, and C. Berretta. The influence of substrate and vegetation configuration on green roof hydrological performance. *Ecological Engineering*, 85(C):159–172, 2015.

[30] L. De Roeck. *Slim omgaan met regenwater*. Coördinatiecommissie Integraal Waterbeleid en Ruimte Vlaanderen, 2013.

[31] Y. Qiu, A. Ichiba, I. Tchiguirinskaia, and D. Schertzer. Evaluation of nature-based solutions for storm water management with a fully distributed model in semi-urban catchment. *11th International Workshop on Precipitation in Urban Areas (UrbanRain18)*, 2018.

[32] E. Vanuytrecht, C. Van Mechelen, K. Van Meerbeek, P. Willems, M. Hermy, and D. Raes. Runoff and vegetation stress of green roofs under different climate change scenarios. *Landscape and Urban Planning*, 122(C):68–77, 2014.

[33] D.G. Cirkel, B.R. Voortman, T. van Veen, and R.P. Bartholomeus. Evaporation from (Blue-)Green Roofs: Assessing the benefits of a storage and capillary irrigation system based on measurements and modeling. *Water (Switzerland)*, 10(9):1–21, 2018.

[34] K. Broks and H. van Luijtelaar. Groene daken nader beschouwd, 2015.

[35] D. Bertels and L. Janssen. Duurzame maatregelen tegen wateroverlast in de stedelijke omgeving, casestudie Antwerpen, 2018.

[36] K.L. Getter, D.B. Rowe, and J.A. Andresen. Quantifying the effect of slope on extensive green roof stormwater retention. *Ecological Engineering*, 31(4):225–231, 2007.

[37] C. De Pauw. *Technische voorlichting 229: Groendaken*. Wetenschappelijk en Technisch Centrum voor het Bouwbedrijf (WTCB), 2006. ISSN 0577-4880.

[38] Vegetal i.D. OASIS: La toiture hydroactive multimodale, 2018.

[39] R. Castiglia Feitosa and S. Wilkinson. Modelling green roof stormwater response for different soil depths. *Landscape and Urban Planning*, 153:170–179, 2016.

[40] N. Vanwoert, J. Andresen, and C. Rugh. Green roof stormwater retention: Effects of roof surface, slope, and media depth. *Journal of Environmental Quality*, 34(3):1036–44, 2005.

[41] M.A. Monterusso, D.B. Rowe, C.L. Rugh, and D.K. Russell. Runoff water quantity and quality from green roof systems. In *Acta Horticulturae*, pages 369–376. International Society for Horticultural Science, 2004.

[42] H. Liesecke. The retention capacity of green roofs. *German Horticulture*, 47:46–53, 1998.

[43] C. Van Mechelen. Nature as a template for a new concept of extensive green roofs, 2015.

[44] L. Locatelli, O. Mark, P.S. Mikkelsen, K. Arnbjerg-Nielsen, M. Bergen Jensen, and P.J. Binning. Modelling of green roof hydrological performance for urban drainage applications. *Journal of Hydrology*, 519(PD):3237–3248, 2014.

[45] A. Palla and L.G. Gnecco, I.and Lanza. Hydrologic Restoration in the Urban Environment Using Green Roofs. *Water*, 2(2):140–154, 2010.

[46] S. De-Ville, M. Menon, and V. Stovin. Temporal variations in the potential hydrological performance of extensive green roof systems. *Journal of Hydrology*, 558:564–578, 2018.

[47] Flemish Environment Agency (VMM). Waterinfo.be, 2018.

[48] H.S. Yang, J. Kang, and M.S. Choi. Acoustic effects of green roof systems on a low-profiled structure at street level. *Building and Environment*, 50(C):44–55, 2012.

[49] A.L.S. Chan and T.T. Chow. Energy and economic performance of green roof system under future climatic conditions in Hong Kong. *Energy and Buildings*, 64:182–198, 2013.

[50] V.W.Y. Tam, J. Wang, and K.N. Le. Thermal insulation and cost effectiveness of green-roof systems: An empirical study in Hong Kong. *Building and Environment*, 110:46–54, 2016.

[51] G. Heidarinejad and A. Esmaili. Numerical simulation of the dual effect of green roof thermal performance. *Energy Conversion and Management*, 106:1418–1425, 2015.

[52] M. Alshayeb and J.D. Chang. Photovoltaic Energy Variations Due to Roofing Choice. *Procedia Engineering*, 145:1104–1109, 2016.

[53] H. Ogaili and D. Sailor. Measuring the Effect of Vegetated Roofs on the Performance of Photovoltaic Panels in a Combined System. *Journal Of Solar Energy Engineering-Transactions Of The Asme*, 138(6), 2016.

[54] A. Jahanfar, J. Drake, B. Sleep, and L. Margolis. Evaluating the shading effect of photovoltaic panels on green roof discharge reduction and plant growth. *Journal of Hydrology*, 568:919–928, 2019.

[55] F. Mayrand and P. Clergeau. Green roofs and greenwalls for biodiversity conservation: A contribution to urban connectivity? *Sustainability (Switzerland)*, 10(4), 2018.

[56] N.S.G. Williams, J. Lundholm, and J. Scott Macivor. Do green roofs help urban biodiversity conservation? *Journal of Applied Ecology*, 51(6):1643–1649, 2014.

[57] A.F. Speak, J.J. Rothwell, S.J. Lindley, and C.L. Smith. Urban particulate pollution reduction by four species of green roof vegetation in a UK city. *Atmospheric Environment*, 61:283–293, 2012.

[58] Q. Zhang, L. Miao, X. Wang, D. Liu, L. Zhu, B. Zhou, J. Sun, and J. Liu. The capacity of greening roof to reduce stormwater runoff and pollution. *Landscape and Urban Planning*, 144:142–150, 2015.

[59] Assessing methods for predicting green roof rainfall capture: A comparison between full-scale observations and four hydrologic models, 2017.

[60] R. Cronshey. Urban hydrology for small watersheds. Technical report, US Dept. of Agriculture, Soil Conservation Service, Engineering Division, 1986.

[61] H. Kasmin, V.R. Stovin, and E.A. Hathway. Towards a generic rainfall-runoff model for green roofs. *Water Science and Technology*, 62(4):898–905, 2010.

[62] G. Vesuviano, F. Sonnenwald, and V. Stovin. A two-stage storage routing model for green roof runoff detention. *Water science and technology : a journal of the International Association on Water Pollution Research*, 69(6), 2014.

[63] G. Vesuviano and V. Stovin. A generic hydrological model for a green roof drainage layer. *Water science and technology : a journal of the International Association on Water Pollution Research*, 68(4), 2013.

[64] D.J. Van Luijtelaar. RAINTOOLS SOFTWARE DEVELOPMENT. Oulu University of Applied Sciences: Information Technology, 2015.

[65] United States Environmental Protection Agency. Storm water management model: Application that helps predict the quantity and quality of runoff within urban areas. URL: `https://www.epa.gov/water-research/storm-water-management-model-swmm`, last checked on 2019-01-16.

[66] S.S. Cipolla, M. Maglionico, and I. Stojkov. A long-term hydrological modelling of an extensive green roof by means of SWMM. *Ecological Engineering*, 95:876–887, 2016.

[67] United States Environmental Protection Agency. Hydrologic evaluation of landfill performance (help) model. URL: `https://www.epa.gov/land-research/hydrologic-evaluation-landfill-performance-help-model`, last checked on 2019-01-16.

[68] Innovyze. Infoworks icm. URL: `https://www.innovyze.com/en-us/products/infoworks-icm?`, last checked on 2019-01-13.

[69] V. Wolfs. Conceptual Model Structure Identification and Calibration for River and Sewer Systems, 2016.

[70] T. Barjas Blanco and B.L.R. De Moor. *Flood prevention of the Demer River using model predictive control*, volume 17. IFAC, 2008.

[71] A.K.V. Falk, C. MacKay, H. Madsen, and P.N. Godiksen. Model Predictive Control of a Large-scale River Network. *Procedia Engineering*, 154:80–87, 2016.

[72] E. Vermuyten, P. Meert, V. Wolfs, and P. Willems. Combining Model Predictive Control with a Reduced Genetic Algorithm for Real-Time Flood Control. *Journal of Water Resources Planning and Management*, 144(2):04017083, 2018.

[73] M. Wendt, P. Li, and G. Wozny. Nonlinear chance-constrained process optimization under uncertainty. *Industrial & Engineering Chemistry Research*, 41(15):3621–3629, 2002.

[74] T.B. Blanco, P. Willems, P.-K. Chiang, K. Cauwenberghs, B. De Moor, and J. Berlamont. *Flood Regulation by Means of Model Predictive Control*, pages 407–437. Springer Netherlands, Dordrecht, 2010.

[75] T. Barjas Blanco, P. Willems, P.K. Chiang, N. Haverbeke, J. Berlamont, and B. De Moor. Flood regulation using nonlinear model predictive control. *Control Engineering Practice*, 18(10):1147–1157, 2010.

[76] M. Allaeys. Nowcasting and fine-scale flood modelling in urban areas, 2018.

[77] L. Foresti, M. Reyniers, A. Seed, and L. Delobbe. Development and verification of a real-time stochastic precipitation nowcasting system for urban hydrology in Belgium. *Hydrology and Earth System Sciences*, 20(1), 2016.

[78] P. Willems, L. De Cruz, L. Delobbe, M. Reyniers, L. Van Ootegem, G. Mahy, X. Li, C. Muñoz Lopez, D. Murlà Tuyls, L. Wang, V. Ntegeka, V. Wolfs, L. Foresti, J. Lebeau, J. Marechal, J. Bogaert, K. Van Herck, T. Creten, and K. Van Balen. Plurisk - forecasting and management of extreme rainfall induced risks in the urban environment, 2017.

[79] P.-J. van Overloop, S. Weijs, and S. Dijkstra. Multiple Model Predictive Control on a drainage canal system, 2008.

[80] E. Vermuyten, P. Meert, V. Wolfs, and P. Willems. Dealing with rainfall forecast uncertainties in real-time flood control along the Demer river. *E3S Web of Conferences*, 7:4–11, 2016.

[81] KMI (Royal Meteorological Institute). Klimaatstatistieken van de belgische gemeenten: Antwerpen (nis 11002). URL: `http://www.meteo.be/resources/climateCity/pdf/climate_INS11002_ANTWERPEN_nl.pdf` , last checked on 2019-01-13.

[82] Port of Antwerp. Publications: Annual reports. URL: `https://www.portofantwerp.com/en/publications/annual-report`, last checked on 2019-01-20.

[83] Stad Antwerpen. Stad in cijfers: Demografie sint-andries versus stad antwerpen (pdf). URL: `https://stadincijfers.antwerpen.be/dashboard/Demografie--c635848223015539581`, last checked on 2019-01-20.

[84] Stad Antwerpen. Wateroverlast na hevige regen. URL: `https://www.antwerpen.be/nl/info/574a9d91b2a8a764538b4577/stormweer`, last checked on 2019-01-20.

[85] Het Parool. Doden door hevige wateroverlast in belgië. URL: `https://www.parool.nl/buitenland/doden-door-hevige-wateroverlast-in-belgie~a1051034/`, last checked on 2019-01-20.

[86] European Union. Brigaid: Bridging the gap for innovations in disaster resilience. URL: `https://brigaid.eu`, last checked on 2019-01-20.

[87] Ijinus. Ijinus: L'instrumentation connectee - capteurs de niveau. URL: `https://www.ijinus.com/categorie-produit/capteurs/niveau/`, last checked on 2019-01-09.

[88] VRT NWS. Droogte van zomer 2018 wordt erkend als landbouwramp. URL: `https://www.vrt.be/vrtnws/nl/2018/10/26/droogte-van-zomer-2018-wordt-erkend-als-landbouwramp/`, last checked on 2019-01-20.

[89] VRT NWS. Hittegolf in aantocht. URL: `https://www.vrt.be/vrtnws/nl/2018/07/22/hittegolf-in-aantocht/`, last checked on 2019-01-20.

[90] Météo France. Fiche climatologique (paris - montsouris). URL: `https://donneespubliques.meteofrance.fr/FichesClim/FICHECLIM_75114001.pdf`, last checked on 2019-01-26.

[91] Météo France. Fiche climatologique (lyon - bron). URL:https://donneespubliques.meteofrance.fr/FichesClim/FICHECLIM_69029001.pdf , last checked on 2019-01-26.

[92] L.-P. Wang, S. Ochoa-Rodriguez, C. Onof, and P. Willems. Singularity-sensitive gauge-based radar rainfall adjustment methods for urban hydrological applications. *Hydrology and Earth System Sciences*, 19(9), 2015.

[93] A. Wang, K.Y. Li, and D.P. Lettenmaier. Integration of the variable infiltration capacity model soil hydrology scheme into the community land model, 2008.

[94] J. Zonta, M.A. Martinez, F. Pruski, D.D. Da Silva, and M. Dos Santos. Effect of successive rainfall with different patterns on soil water infiltration rate. *Revista Brasileira De Ciencia Do Solo*, 36(2):377–387, 2012.

[95] D.J. Watson. Comparative physiological studies on the growth of field crops: I. variation in net assimilation rate and leaf area between species and varieties, and within and between years. *Annals of botany*, 11(41):41–76, 1947.

[96] European Soil Data Centre (ESDAC). "focus surface water scenarios in the eu evaluation process under 91/414/eec". report of the focus working group on surface water scenarios, ec document reference sanco/4802/2001-rev.2. 245 pp. (appendix c and d). URL: https://esdac.jrc.ec.europa.eu/projects/surface-water, last checked on 2019-02-01, 2001.

[97] M. Gabrych, D.J. Kotze, and S. Lehvavirta. Substrate depth and roof age strongly affect plant abundances on sedum-moss and meadow green roofs in Helsinki , Finland, 2016.

[98] N.D. VanWoert, D.B. Rowe, J. a Andresen, C.L. Rugh, R.T. Fernandez, and L. Xiao. Green roof stormwater retention: effects of roof surface, slope, and media depth. *Journal of environmental quality*, 34(3):1036–1044, 2015.

[99] N. Dunnett, A. Nagase, and A. Hallam. The dynamics of planted and colonising species on a green roof over six growing seasons 2001-2006 : influence of substrate depth, 2008.

[100] L.R. Costello. *WUCOLS, water use classification of landscape species: a guide to the water needs of landscape plants*. California Department of Water Resources, 1994.